AFFDL-TM-77-4

# TEST REPORT ON VIBRATION MEASUREMENTS ON A LIGHTWEIGHT MHD GENERATOR CHANNEL

**Jerome Pearson**
**Roger E. Thaller**
**David L. Banazak**

**Structural Vibration and Acoustics Branch**
**Structures and Dynamics Division**
**Flight Dynamics Laboratory**
**Wright-Patterson AFB, OH 45433**

**March 1978**

**Final Report for April 1977 – September 1977**

**APPROVED FOR PUBLIC RELEASE; DISTRIBUTION UNLIMITED**



**FLIGHT DYNAMICS LABORATORY**
**AIR FORCE SYSTEMS COMMAND**
**WRIGHT-PATTERSON AIR FORCE BASE, OH 45433-7542**

# REPORT DOCUMENTATION PAGE

*Form Approved*
*OMB No. 0704-0188*



| 1. REPORT DATE *(DD-MM-YYYY)* | 2. REPORT TYPE | 3. DATES COVERED *(From - To)* |
|---|---|---|
| MARCH 1978 | FINAL | April 1977 – September 1977 |

**4. TITLE AND SUBTITLE**

TEST REPORT ON VIBRATION MEASUREMENTS ON A LIGHTWEIGHT MHD GENERATOR CHANNEL

**5a. CONTRACT NUMBER**

**5b. GRANT NUMBER**

**5c. PROGRAM ELEMENT NUMBER**

**6. AUTHOR(S)**

Jerome Pearson, Roger E. Thaller, and David L. Banaszak

**5d. PRO**

**5e. TASK NUMBER**

**5f. WORK UNIT NUMBER**

**7. PERFORMING ORGANIZATION NAME(S) AND ADDRESS(ES)**

Structural Vibration and Acoustics Branch
Structures and Dynamics Division
Flight Dynamics Laboratory
Wright-Patterson AFB, OH 45433

**8. PERFORMING ORGANIZATION REPORT NUMBER**

**9. SPONSORING / MONITORING AGENCY NAME(S) AND ADDRESS(ES)**

Structural Vibration and Acoustics Branch
Structures and Dynamics Division
Flight Dynamics Laboratory
Wright-Patterson AFB, OH 45433

**10. SPONSOR/MONITOR'S ACRONYM(S)**

Now: AFRL/VASM

**11. SPONSOR/MONITOR'S REPORT NUMBER(S)**

AFFDL-TM-77-4

**12. DISTRIBUTION / AVAILABILITY STATEMENT**

Approved for Public Release; Distribution Unlimited

**13. SUPPLEMENTARY NOTES**

**14. ABSTRACT**

This test report presents data which define the vibration environment of a lightweight magnetohydrodynamic (MHD) generator channel. These data were needed to determine the vibration responses of the MHD channel during rocket engine operation.

Descriptions of the MHD test channel, instrumentation, test procedure, data analysis, and a discussion of the test results are presented in Appendix A. Figures, tables, and photographs are presented in Appendix B.

**15. SUBJECT TERMS**

MHD Generator; magnetohydrodynamic

| 16. SECURITY CLASSIFICATION OF: | | | 17. LIMITATION OF ABSTRACT | 18. NUMBER OF PAGES | 19a. NAME OF RESPONSIBLE PERSON |
|---|---|---|---|---|---|
| a. REPORT | b. ABSTRACT | c. THIS PAGE | | | David Banaszak |
| UNCLASSIFIED | UNCLASSIFIED | UNCLASSIFIED | SAR | 101 | 19b. TELEPHONE NUMBER *(include area code)* 937-904-6859 |

**Standard Form 298 (Rev. 8-98)**
**Prescribed by ANSI Std. 239.18**

AIR FORCE FLIGHT DYNAMICS LABORATORY

AIR FORCE SYSTEMS COMMAND

WRIGHT-PATTERSON AIR FORCE BASE, OHIO

STRUCTURAL MECHANICS DIVISION

# TEST REPORT

# ON

# VIBRATION MEASUREMENTS ON A LIGHTWEIGHT MHD GENERATOR CHANNEL

REPORT NO: AFFDL/FBG-77-4 DATE: March 1978

PROJECT NO: 31455000 PROJECT ORDER: WAL74012P

TYPE OF TEST: Measurement of Vibratory Environment

REQUESTED BY: AFAPL/POD-1

## I. PURPOSE

This test report presents data which define the vibration environment of a lightweight magnetohydrodynamic (MHD) generator channel. These data were needed to determine the vibration responses of the MHD channel during rocket engine operation.

## II. BACKGROUND

The Air Force Aero Propulsion Laboratory has been considering the generation of MHD power for short-term, high-power airborne applications. In order to minimize the weight of the system, a new lightweight generator channel was designed, which carries the exhaust gases of a small rocket engine. The rocket exhaust is made conductive by

injecting cesium and then is carried through the 106 cm (41-5/8 inch) long MHD channel to a diffuser. An electrical power output of up to 200 KW is obtained from electrodes along the sides of the channel when an external magnetic field of 23 kilogauss is applied to the moving, electrically conducting gas. One problem was to determine the vibration responses of the new lightweight MHD channel during rocket engine operation and to evaluate these responses in terms of structural integrity, fatigue, and deterioration resulting from repeated firings.

On 30 March 1977 AFAPL requested the Field Test and Evaluation Branch of the Air Force Flight Dynamics Laboratory to make vibration and voltage output measurements on the MHD channel during a series of rocket firings at the AFAPL MHD Test Facility. Personnel of the Structural Mechanics Division prepared a test plan on 7 April 1977 which was approved by the AFAPL. The AFFDL provided and installed all instrumentation, wiring, and data recording equipment for the tests, which were performed between April and September 1977. The data were analyzed in the facility of the Flight Dynamics Laboratory.

Descriptions of the MHD test channel, instrumentation, test procedure, data analysis, and a discussion of the test results are presented in Appendix A. Figures, tables, and photographs are presented in Appendix B.

## III. SUMMARY OF RESULTS

The MHD channel vibrations during steady-state firings were normally in the range of 0.01 $g^2$/Hz, with occasional peaks of 0.05 to 0.1 $g^2$/Hz. On one firing an accelerometer nearest the rocket nozzle showed a peak of 1 $g^2$/Hz at a frequency of 4500 Hz. The same sensor showed the highest measured overall rms acceleration during steady-state firing, 7.11 g rms summed over the frequency range of zero to 10 kHz. During the starting transients, peak values of instantaneous acceleration as high as 75 g were recorded.

This vibratory environment would be considered severe for electronic equipment; however, for the MHD channel structure this vibration is not expected to be a limiting factor in operation. As sample calculations of the channel vibratory stress levels showed an expected fatigue life of 31 minutes to 105 hours, being very dependent on the value of Young's modulus, E, for the glass fibers. A laboratory measurement of the fiberglass modulus, which was not available from the channel manufacturer, could reduce this uncertainty.

A frequency analysis of the voltage output of the MHD generator showed a broadband signal with a distinct roll-off to 6 kHz and a flat spectrum from 6 kHz to 20 kHz, with no prominent frequency spikes.

PREPARED BY:

Jerome Pearson
JEROME PEARSON

Roger E. Thaller
ROGER E. THALLER

David L. Banazak
DAVID L. BANAZAK

COORDINATION:

Earl N. Bingman
R. N. BINGMAN

John T. Ach
J. T. ACH

PUBLICATION REVIEW

This test report has been reviewed and is approved.

Charles E. Thomas
CHARLES E. THOMAS
Acting Chief, Field Test & Evaluation Br.
Structural Mechanics Division

DISTRIBUTION:

AFAPL/POD (10)
AFFDL/FB ( 3 )
AFFDL/FBG (12)

## APPENDIX A

Test Description, Data Analysis, and Results (Refer to Appendix B for Tables and Illustrations).

### Test Configuration

The lightweight MHD generator channel is shown schematically in Figure 1 and in the operating condition in Photograph 1. The channel is constructed of a series of hollow copper coolant tubes which serve as electrodes, separated by ceramic insulation and covered by a layer of 2 cm (3/4") thick fiberglass. The coolant tubes are connected externally by plastic tubing to complete the water flow system. The inside dimensions of the channel vary from 2.5 x 10 cm (1 x 4") at the rocket exhaust inlet to 7.3 x 13.6 cm (2 7/8 x 5 3/8") at the diffuser; the channel length is 106 cm (41 5/8"). The channel has flanges at the ends which are bolted to the nozzle and to the exit diffuser. After the conductive rocket exhaust has travelled the length of the MHD channel, it is slowed in the diffuser and exhausted to the atmosphere. The channel is clamped at the flanges to vertical beams mounted on the false floor of the test stand. The 96.5-cm long diffuser is likewise supported by a beam 180 cm from the exit flange of the MHD channel. During power generation the large magnet faces are rolled into position around the channel, as shown in Photograph 2.

### Instrumentation

Accelerometers were chosen to measure the channel dynamic responses because of their simplicity and accuracy. The channel acceleration responses can be readily evaluated in terms of the severity of vibration, and the vibratory displacements can be derived from a double integration of the accelerometer outputs. Strain gages could be used to provide a direct readout of vibratory strain, but would prove very difficult to mount and calibrate on the irregular fiberglass channel.

The MHD channel wall accelerations were sensed by the 12 Columbia Research Laboratories Model 902H accelerometers numbered as shown in Figure 1. The odd numbered accelerometers were used to determine the channel transverse vibration in the horizontal plane and, by using the differences in response between 1 and 3, 5 and 7, and 9 and 11, to determine the horizontal breathing modes of the walls. Similarly, the even numbered accelerometers were used to determine the channel transverse and breathing vibrations in the vertical plane.

After MHD run number LWC 13 (using the AFAPL numbering system), three of the 902H accelerometers were moved to a mounting block on the combustor flange. These accelerometers, labelled x, y, and z in Figure 1, were used to measure the longitudinal, transverse, and vertical accelerations, respectively, of the combustor flange.

The accelerometer outputs were conditioned by Intech Model A2318 automatic-gain-controlled amplifiers and recorded in a portable instrument package by a Leach Model 3200A FM tape recorder. Photograph 3 shows a picture of the data acquisition system. A Datametrics Type SP105 time-code generator provided a 1000-Hz, amplitude-modulated, IRIG B time code which was recorded on the tape. A voice signal was also recorded during each of the MHD runs. The instrument package was configured for 115 VAC power, which was available in the control room. A block diagram of the data acquisition system is shown in Figure 2.

MHD run number LWC 24 was the last record on which vibration data were collected. During the remaining runs, a signal proportional to the voltage generated by the MHD channel was recorded on track 7 of the recorder. This signal was obtained from one of the voltage divider networks in the MHD test facility. At run number LWC 68 the recorder speed was increased to 60 ips to obtain a bandpass flat within 3 dB from zero to 20 kHz. The bandpass at 30 ips was 10 kHz.

## Test Procedures

Accelerations were recorded on 16 MHD test runs during May-July of 1977, as shown in Table I. Each record was approximately 30 seconds long, so that the actual MHD firing time of 3-6 seconds could be recorded with certainty. Fuel and oxidizer mass flow rates and other data will be provided in a separate report by the AFAPL. The nominal propellant flow rate was 0.6 kg/s of toluene and gaseous oxygen. The signal proportional to the MHD-generated voltage was recorded during 14 runs, as shown in Table I.

In order to properly record starting transients during the first 0.1 second, the amplifiers were locked into pre-calculated gain settings during the last 15 test runs. Between tests, the accelerometers remained on the channel and the instrument package remained in the MHD facility control room. During MHD electrical power testing, however, all the accelerometers were disconnected from the Intech amplifiers.

## Data Reduction

Magnetic tapes recorded during the tests were returned to the Air Force Flight Dynamics Laboratory for analysis and retention. A block diagram of the analysis system is shown in Figure 3. The data were played back on a laboratory recorder meeting IRIG Standard #106-72

and converted to digital form. These digitized data were used for time histories with 24 microsecond resolution. Using the Fast Fourier Transform, power spectral densities of all accelerometer signals were computed from zero to 500 Hz with a resolution of 1.22 Hz and from zero to 10 kHz with a resolution of 6.79 Hz.

## Test Results

Time histories of the accelerometer responses were first played back through an oscillograph to determine the character of the signals. Examples of these time histories are shown for run number LWC 13 in Figures 4-14. Accelerometer number 4 responses were not obtained on this run because of electronic problems.

The typical MHD run is characterized by an abrupt, high-amplitude transient lasting about 0.02 second as the mainburner is turned on, followed by a steady-state firing period of several seconds, and climaxed by a cutoff transient of about 0.05 second. In these time histories, most of the steady-state firing response is deleted in order to show the details of the starting and ending transients. The pilot burner was turned on before these records begin. For all the plots, the overall rms acceleration of the plotted portion is shown in the upper right-hand corner in g rms, summed over the frequency range of zero to 10 kHz. The time resolution of these computer-generated plots is 24 microseconds. During the starting and ending transients, instantaneous accelerations as high as 75 g were recorded. The acceleration peaks during steady-state firing were normally in the 15 g range. The rms values range from 2.5 to 10 g rms for the various accelerometers.

These time histories are random signals which are non-stationary, especially at the beginning and at the end. The steady-state portion of the firing, however, is nearly stationary and can be analyzed spectrally. All the spectra presented in this report represent the steady-state portion of the MHD firings. Examples of frequency spectra for the individual accelerometers are shown for run number LWC 13 in Figures 15-25 for the full frequency range of the instrumentation. The frequency resolution of these acceleration spectral densities is 6.787 Hz. Because the accelerometers have a flat frequency response to 6 kHz and the tape recorder is 3 dB down at 10 kHz, the decrease in response above 5 kHz is apparently a characteristic of the rocket exhaust excitation.

These acceleration responses were normally in the range of 0.01 $g^2/Hz$ except for narrow peaks at 2-3 kHz which reach 0.05 - 0.1 $g^2/Hz$. The highest spectrum measured was accelerometer number 11 for run LWC 13 (Figure 24). This accelerometer, on the side of the channel nearest the rocket nozzle, showed a peak of 1 $g^2/Hz$ at a frequency of 4500 Hz. A measure of the overall energy in the response is the rms acceleration

in g's, which is shown for each accelerometer in the upper right corner. The highest overall acceleration recorded was by accelerometer number 11 during run number LWC 13, 7.11 g rms summed over the frequency range of zero to 10 kHz.

In order to determine the effects of continued firings on the vibration responses, data were analyzed at selected runs over a long series of firings. The firing numbers and durations are shown in Table I. An expected change due to deterioration of the channel walls would be a change in the damping of the vibration modes. These modes may be identified with individual response peaks in the lower frequency range of the acceleration responses. By measuring any change in the widths of these response peaks over a series of runs, a change in damping of the mode would be observable. An increase in damping could be caused, for example, by the development of cracks in the material.

In order to show the lower frequency modes more clearly, accelerometer responses were analyzed from zero to 500 Hz. The results for run number LWC 3 are shown in Figures 26-34, those for run number LWC 13 in Figures 35-44, and those for run number LWC 23 in Figures 45-56. Accelerometers 1, 2, and 4 are missing from run LWC 3, and accelerometers 2 and 4 are missing from run LWC 13. For run LWC 23, accelerometers 2, 8, and 11 were replaced by accelerometers x, y, and z on the combustor flange.

These responses showed little indication of any change in damping with wear on the channel. Although the random character of the rocket exhaust excitation results in fluctuations in the relative amplitudes at different frequencies from run to run, distinct modes can be identified. Accelerometer number 3, for example, on the side of the channel near the diffuser end, showed a prominent mode at 53 Hz. The width of this mode during run LWC 3 (Figure 26) showed a Q of 18, from the relation $Q = f/\Delta f$, where $\Delta f$ is the frequency bandwidth at the half-power points. This same response peak at 53 Hz during run LWC 13 (Figure 36) and during run LWC 23 (Figure 46) had the same bandwidth, to within the accuracy of the 1.22 Hz frequency resolution, indicating little or no change in damping for this mode over 20 firings. Similar results were obtained for the mode at 43 Hz. This method, however, is limited to detecting gross damping changes because of the 1.22 Hz frequency resolution. The resolution is limited by the amount of data available during one firing.

The responses from a single firing were also analyzed with respect to accelerometer position along the channel, to determine any change in character of the excitation along the channel length. No clear pattern of distinct differences was found, either in the overall rms accelerations or in the frequency content, between the diffuser end and the rocket end of the channel.

The responses from different firings show different overall amplitudes, which may be due to differences in the propellant flow rates and combustion temperatures. The rms responses of firing numbers LWC 3 and LWC 23 can be compared directly. The rms responses for firing number LWC 13 were not obtained.

The individual accelerometer frequency responses show several peaks which might be interpreted as overall vibration modes of the channel. In order to distinguish between bending and breathing modes, the accelerometer signals on opposite sides were combined by both adding and subtracting the signals. These responses are shown for run LWC 13 in Figures 57-66. The results showed no correlation between the motion of opposite sides of the channel. Apparently the modes of the structure were so highly damped by the visco-elastic fiberglass coating that the four sides moved independently.

The fatigue life of the MHD channel can be estimated as follows. The MHD channel is approximated as a beam with pinned ends of height h and length L, as shown in Figure 67. The transverse deflection of the wall vibrating in the nth mode is

$$y_n(x,t) = y_o \mathrm{Sin}\left(\frac{n\pi x}{L}\right) \sin \omega_n t \qquad (1)$$

where $y_o$ is the peak deflection. The moment M at any point is given by the relation $M = EI\frac{d^2y}{dx^2}$, where E is Young's modulus of the material, I is the moment of inertia of the beam cross-section ($I = bh^3/12$), and b and h are the width and height of the beam, respectively. The maximum stress occurs at the surface of the beam and is given by $\sigma = Mh/2I$.

From these relations we derive

$$\sigma_{rms} = y_{rms} \left(\frac{Eh}{2}\right) \left(\frac{n\pi}{L}\right)^2 \qquad (2)$$

In order to find the actual displacements of the MHD channel walls from the accelerometer frequency responses, the latter were transformed by $1/\omega^2$ and converted to rms displacement. These results of wall deflections for runs LWC 12 and LWC 13 are shown in Table II. These deflections can be used to estimate the stress levels and thus the expected fatigue life of the structure. The maximum deflections observed during these runs is seen to be 0.00431 meters rms for accelerometer 12.

To evaluate the rms stress produced by this response peak, refer to Figure 57, which is typical. This particular plot is an average of accelerometers 1 and 3, near one end of the beam. From this and the other figures the peak at 17.3 Hz appears to be the first mode, so the 53 Hz peak may be identified as the third mode, n = 3.

From the channel wall geometry, L is 1 meter, h is 0.6 cm, and we may assume E = 3 to 5 million PSI (2.1-3.5 x $10^{10}$ $N/m^2$), from measurements on similar fiberglass. From AFFDL-TR-74-112, page 514, data are given for the $\sigma$-N curves (N cycles to failure at stress level $\sigma$) for 181-S Type III glass fabric. Applying these values gives the following results:

| E, $10^{10}$ $N/m^2$ ($10^6$ PSI) | $\sigma$, $10^7$ $N/m^2$ ($10^3$ PSI) | Lifetime |
|---|---|---|
| 2.07 (3.0) | 2.4 (3.48) | 105 hrs |
| 2.76 (4.0) | 3.2 (4.64) | 7.9 hrs |
| 3.45 (5.0) | 4.0 (5.80) | 31 min |

These results show that the fatigue life is so strongly dependent on the value of E that no reliable prediction can be made. A more refined estimate could be obtained by directly measuring the modulus of the material in a laboratory force-deflection test, and then measuring the stress levels during firing with strain gages.

A final point of interest is the form of the electrical output from the MHD generator. During several runs the voltage output of the generator was sampled and analyzed by a spectral analyzer. Sample results are shown in Figure 68 on a linear scale from zero to 20 kHz in frequency and on a logarithmic scale in voltage output. The voltage output is broadband, with no significant energy at discrete frequencies.

APPENDIX B

TABLE I. DATA RECORDED DURING MHD CHANNEL TESTS

| Date 1977 | MHD Run # | MHD Firing Time (Sec) | Data Recorded | Comments |
|---|---|---|---|---|
| May | | | | |
| 4 | 001 | 3.5(est) | Accel #1-12 | #4 bad |
| 6 | 002 | 1.7(est) | #1-12 | #4 bad |
| 6 | 003 | 3.5(est) | #1-12 | #4 bad |
| June | | | | |
| 10 | 012 | 4 (est) | #1-12 | #4 bad |
| 10 | 013 | 4.5(est) | #1-12 | #4 bad |
| July | | | | |
| 26 | 014 | 6.9 | Accel's #1, 3-7, 9, 10, 12, x, y, z | |
| 26 | 015 | 5.6 | " | |
| 27 | 016 | 3.2 | " | |
| 27 | 017 | 3.3 | " | |
| 27 | 018 | 5.6 | " | |
| 27 | 019 | 5.7 | " | |
| 27 | 020 | 5.8 | " | |
| 28 | 021 | 5.6 | " | |
| 28 | 022 | 5.6 | " | |
| 28 | 023 | 5.6 | " | |
| 28 | 024 | 5.6 | " | |
| Sep | (SEP 19, 1977 ACCELEROMETERS REMOVED & WIRES DISCONNECTED) | | | |
| 20 | 052 | 5.3 | MHD Output Voltage | Recorder @ 30 ips |
| 20 | 053 | 5.7 | MHD Output Voltage | Recorder @ 30 ips |

TABLE I CONTINUED

| Date 1977 | MHD Run # | MHD Firing Time (Sec) | Data Recorded | Comments |
|---|---|---|---|---|
| 20 | 054 | 5.3 | MHD Output Voltage | Recorder @ 30 ips |
| 20 | 055 | 4.8 | MHD Output Voltage | Recorder @ 30 ips |
| 20 | 056 | 5.6 | MHD Output Voltage | Recorder @ 30 ips |
| 20 | 057 | 5.7 | MHD Output Voltage | Recorder @ 30 ips |
| 20 | 058 | 6.4 | MHD Output Voltage | Recorder @ 30 ips |
| 29 | 068 | 4.5 | MHD Output Voltage | Recorder @ 60 ips |
| 29 | 069 | 5.7 | MHD Output Voltage | Recorder @ 60 ips |
| 29 | 070 | 5.0 | MHD Output Voltage | Recorder @ 60 ips |
| 29 | 074 | 4.5 | MHD Output Voltage | Recorder @ 60 ips |
| 29 | 075 | 5.3 | MHD Output Voltage | Recorder @ 60 ips |
| 29 | 076 | 5.8 | MHD Output Voltage | Recorder @ 60 ips |
| 29 | 077 | 5.8 | MHD Output Voltage | Recorder @ 60 ips |

TABLE II. CALCULATED MHD CHANNEL rms DISPLACEMENTS

| LWC RUN NUMBER | ACCELEROMETER | DISPLACEMENT (m) |
|---|---|---|
| 12 | 1 | .00459 |
| 12 | 3 | .00263 |
| 12 | 5 | .00352 |
| 12 | 7 | .00334 |
| 12 | 6 | .00123 |
| 12 | 8 | .00392 |
| 12 | 9 | .00407 |
| 12 | 11 | .00404 |
| 12 | 10 | .00123 |
| 12 | 12 | .00431 |
| 13 | 1 | .00395 |
| 13 | 3 | .00280 |
| 13 | 5 | .00286 |
| 13 | 7 | .00283 |
| 13 | 6 | .00124 |
| 13 | 8 | .00366 |
| 13 | 9 | .00354 |
| 13 | 11 | .00399 |
| 13 | 10 | .00104 |
| 13 | 12 | .00365 |

| ACCEL NO. | X(in) | RECTRK | ACCEL NO. | X | RECTRK | ACCEL NO. | X | TRK |
|---|---|---|---|---|---|---|---|---|
| 1 | 28 3/4 | 1 | 6 | 19 1/2 | 6 | 11 | 10 3/8 | 11 |
| 2 | 28 5/8 | 2 | 7 | 19 3/4 | 7 | 12 | 10 3/4 | 12 |
| 3 | 28 1/2 | 3 | 8 | 19 1/2 | 8 | x | --- | 8 |
| 4 | 28 1/4 | 4 | 9 | 10 1/2 | 9 | y | --- | 11 |
| 5 | 19 3/4 | 5 | 10 | 10 3/8 | 10 | z | --- | 2 |

x - Distance from combustor end to center of accelerometer

Columbia Model 902H Accelerometers

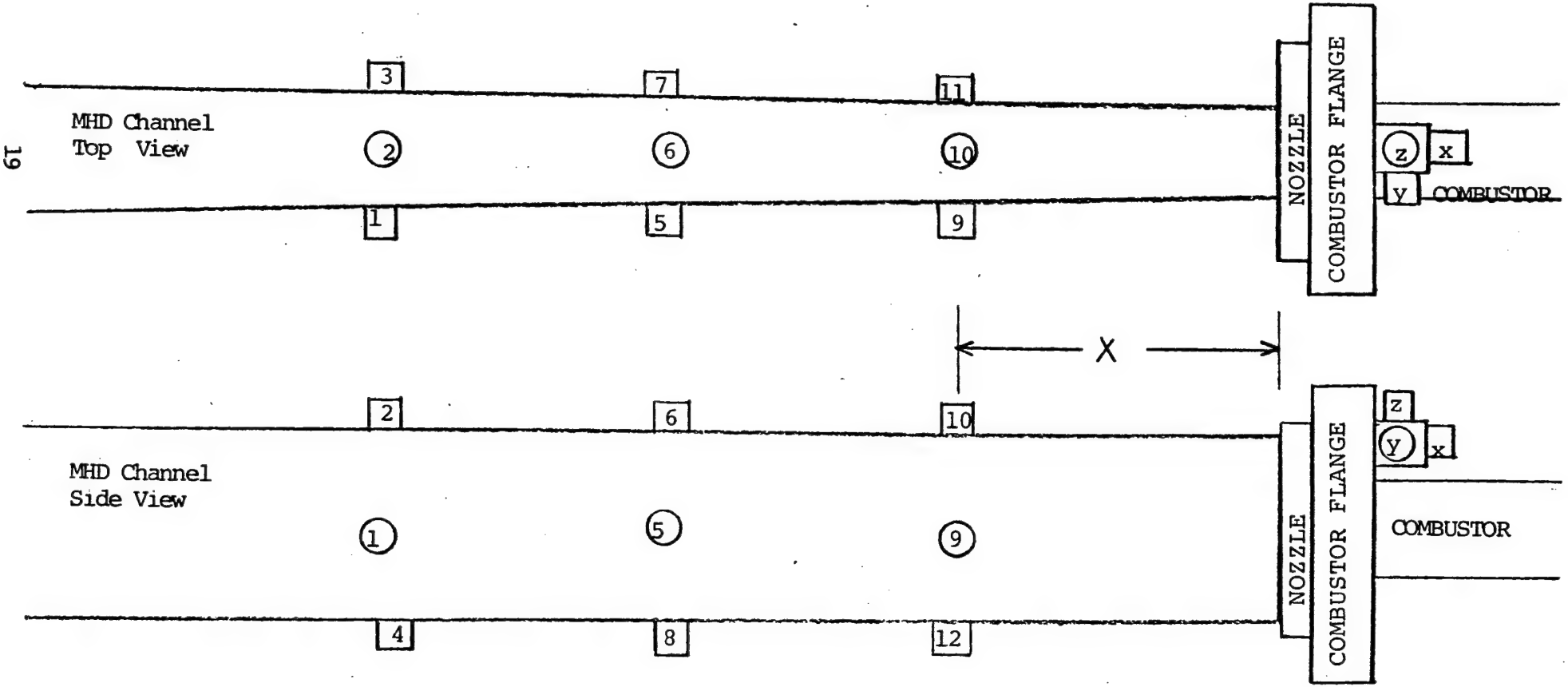


Figure 1. Accelerometer Locations on MHD Channel

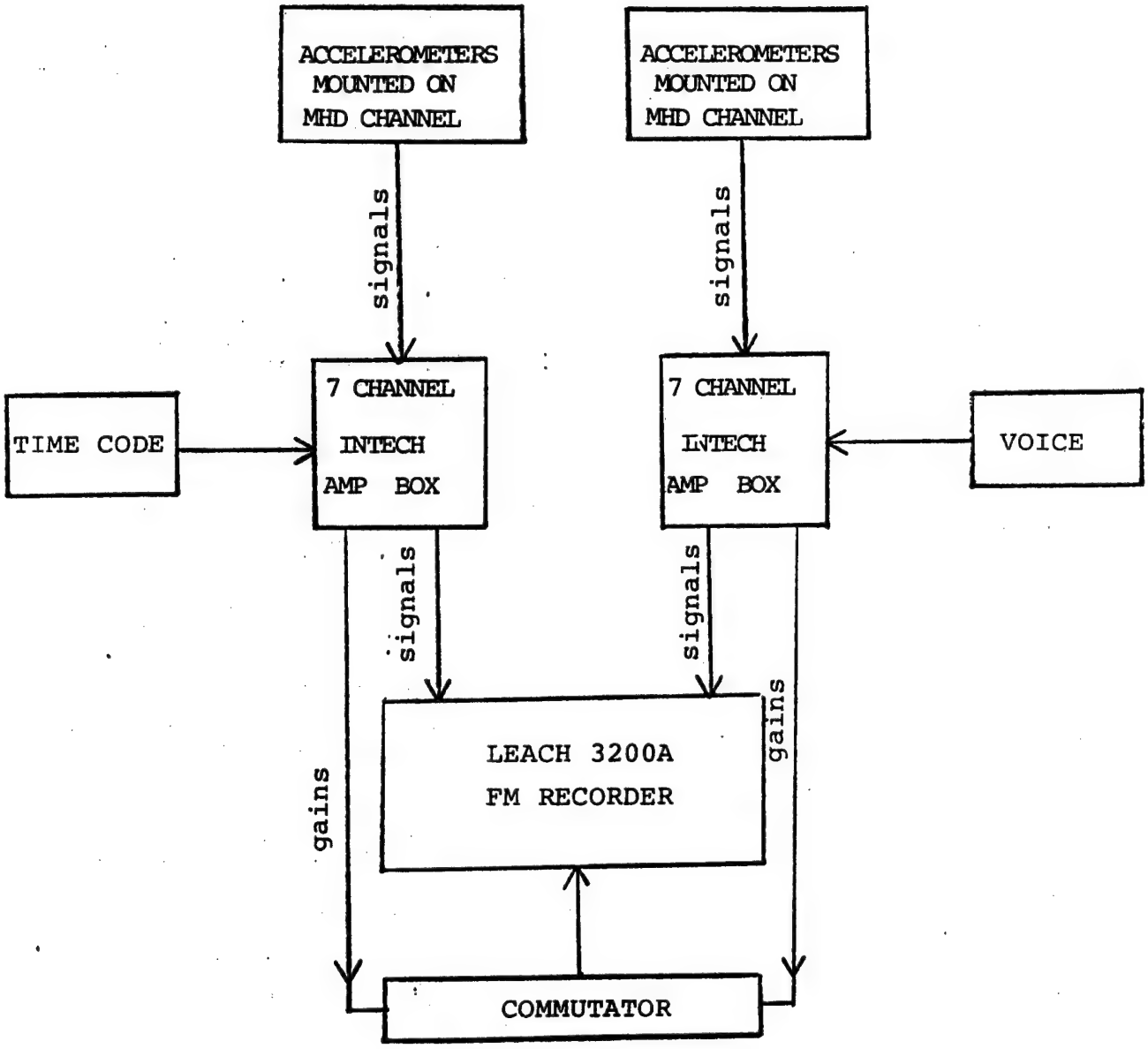


Figure 2. Block Diagram of Data Recording Package.

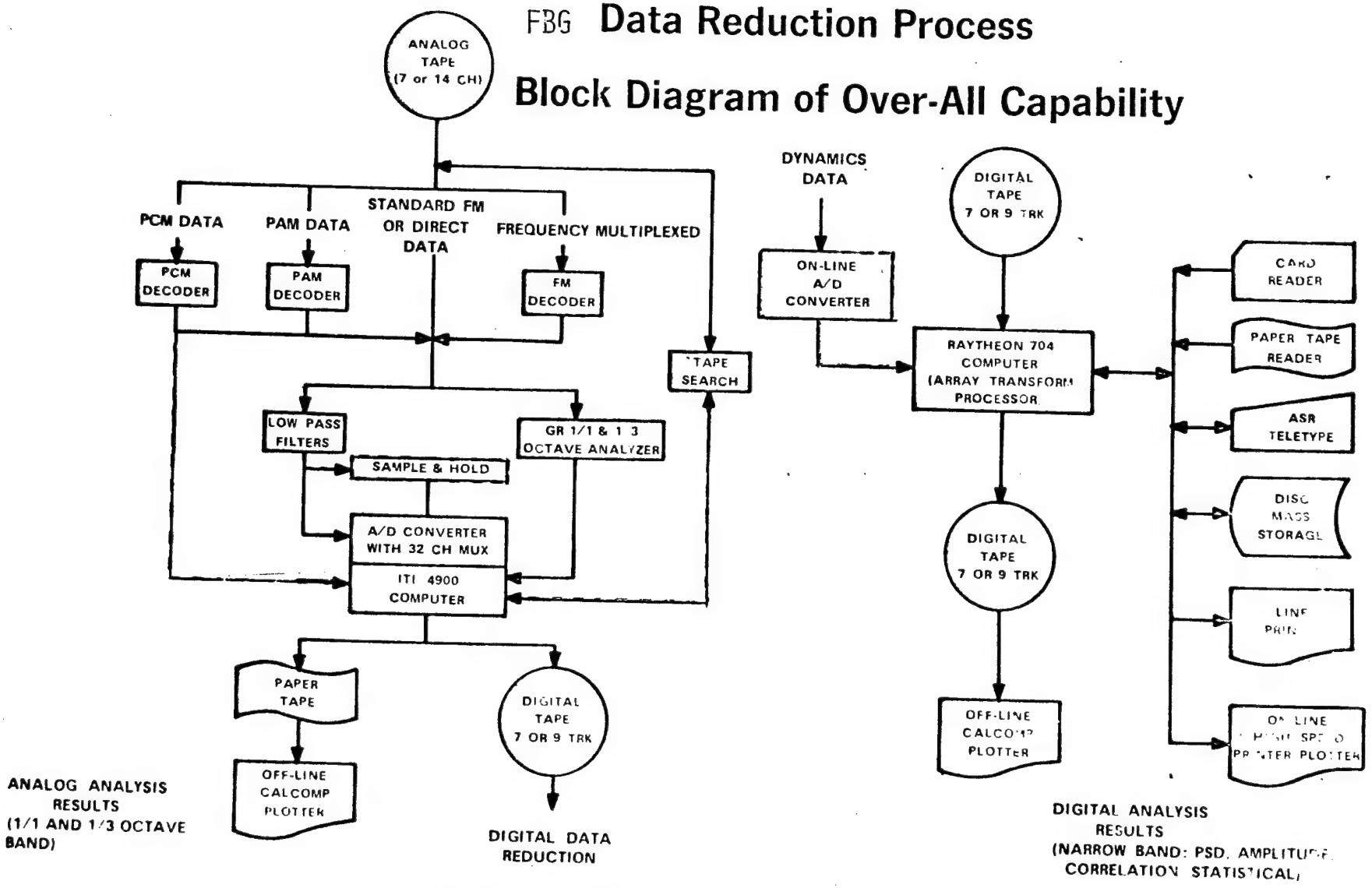


Figure 3. Block Diagram of Data Analysis System.

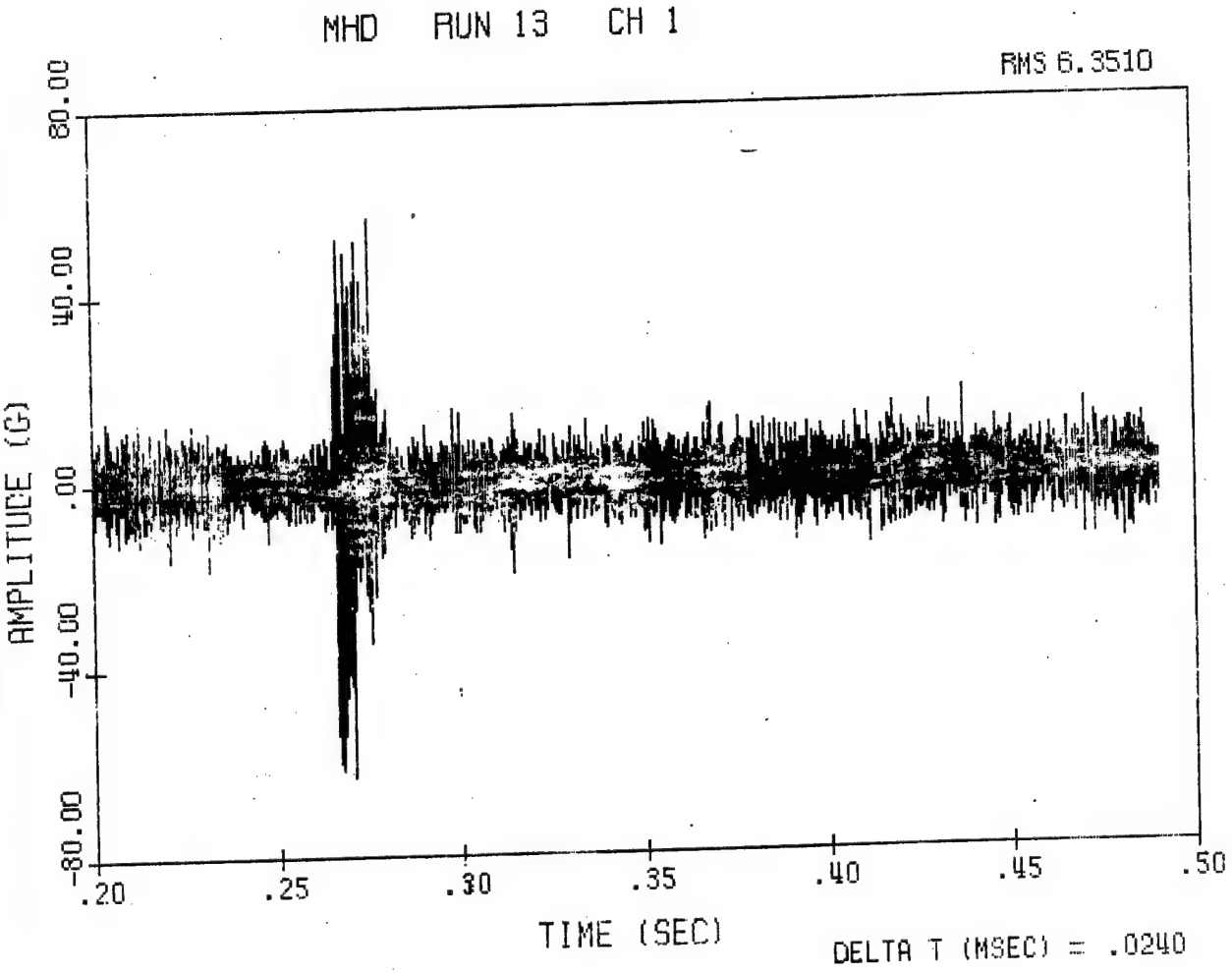


Figure 4a. Time History of Accelerometer 1 During Run LWC 13 Starting Transient.

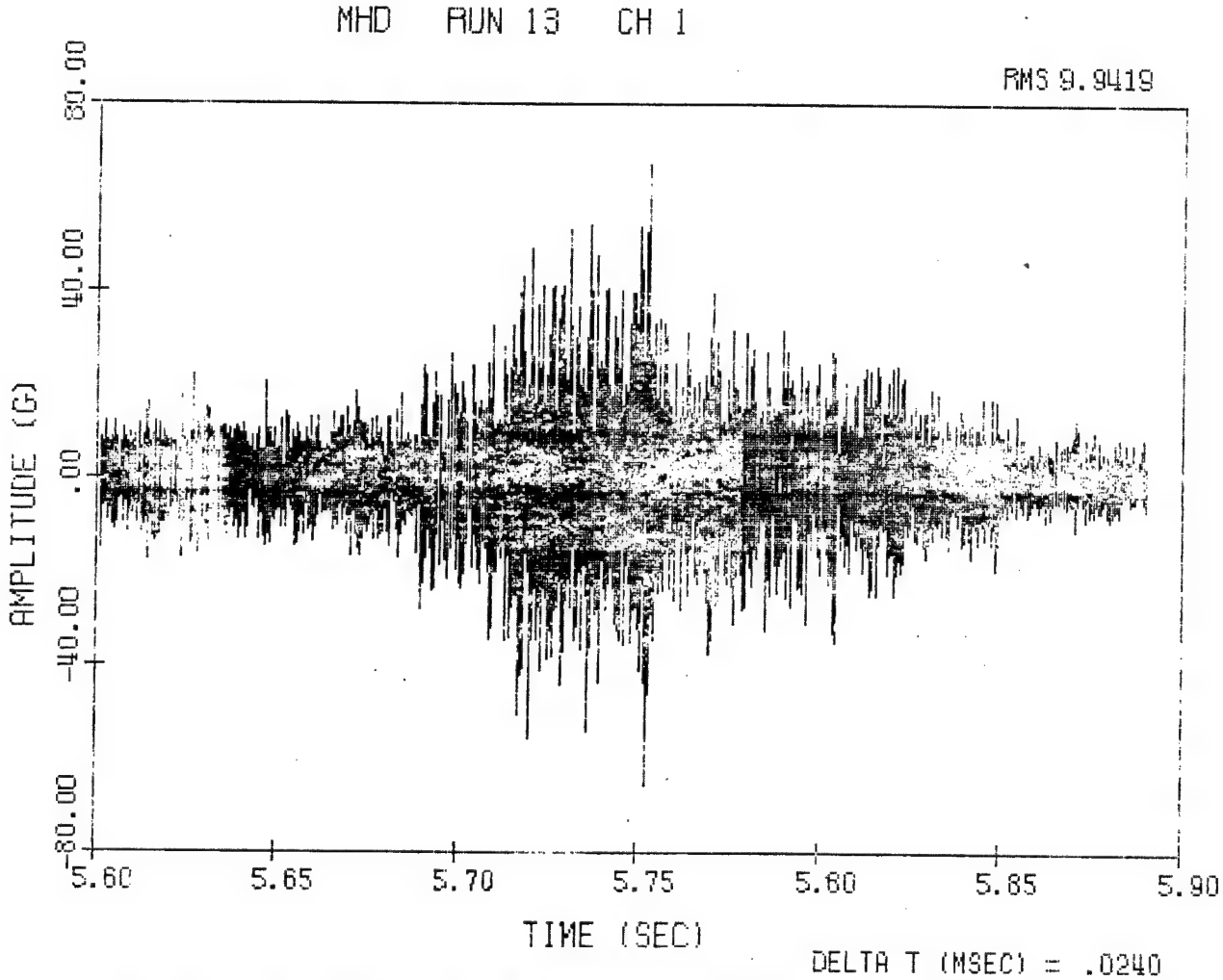


Figure 4b. Time History of Accelerometer 1 During Run LWC 13 Ending Transient.

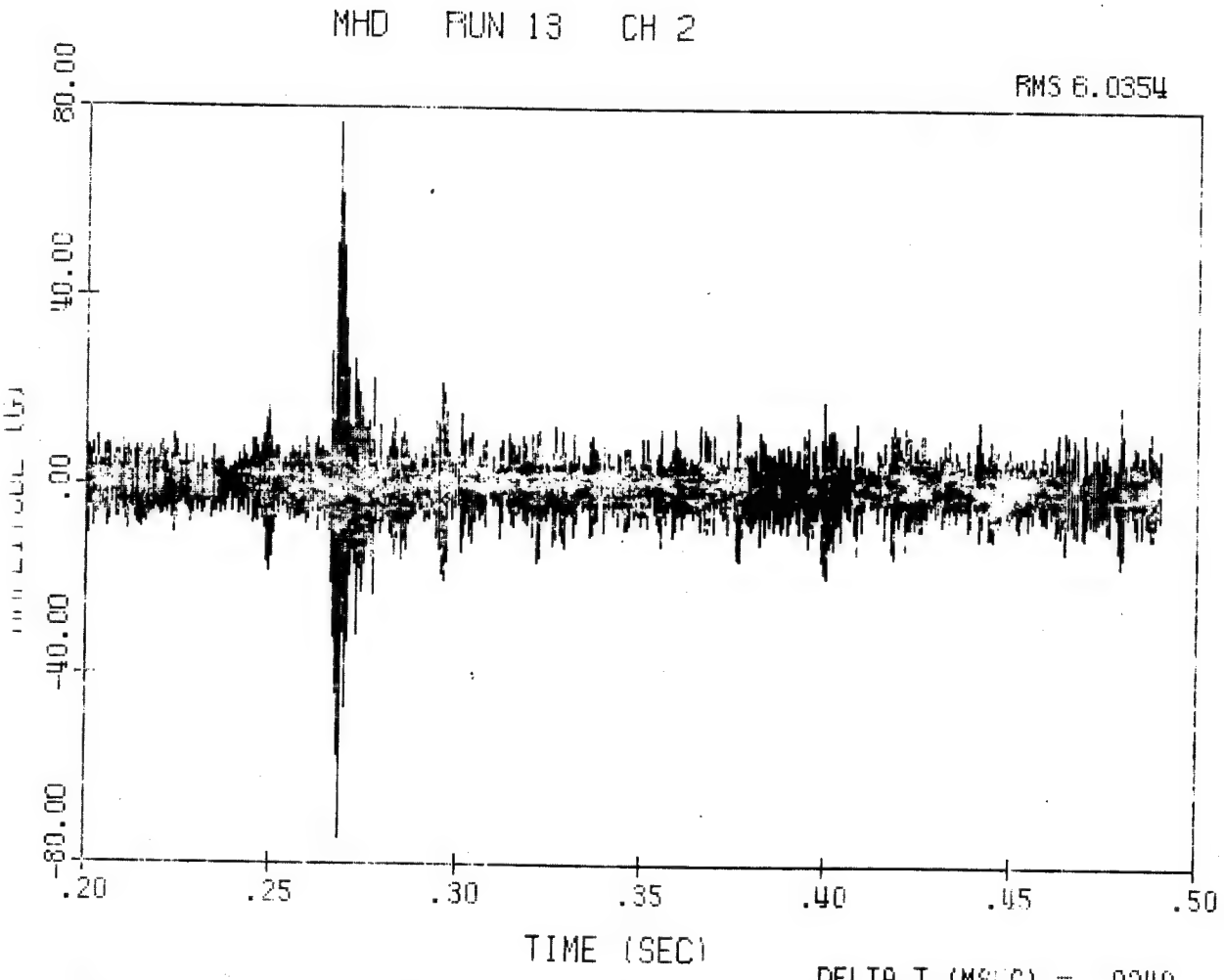


Figure 5a. Time History of Accelerometer 2 During Run LWC 13 Starting Transient.

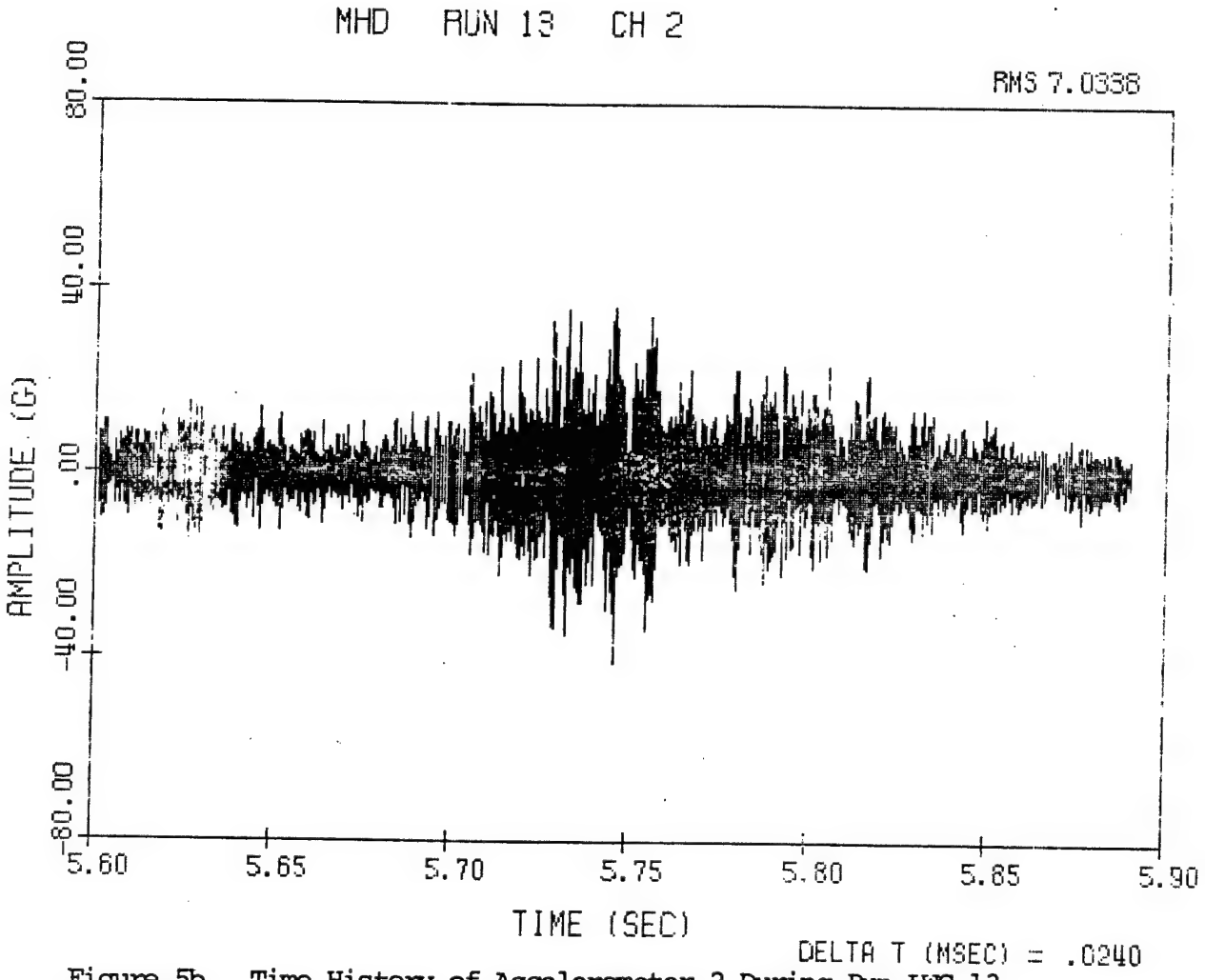


Figure 5b. Time History of Accelerometer 2 During Run LWC 13 Ending Transient.

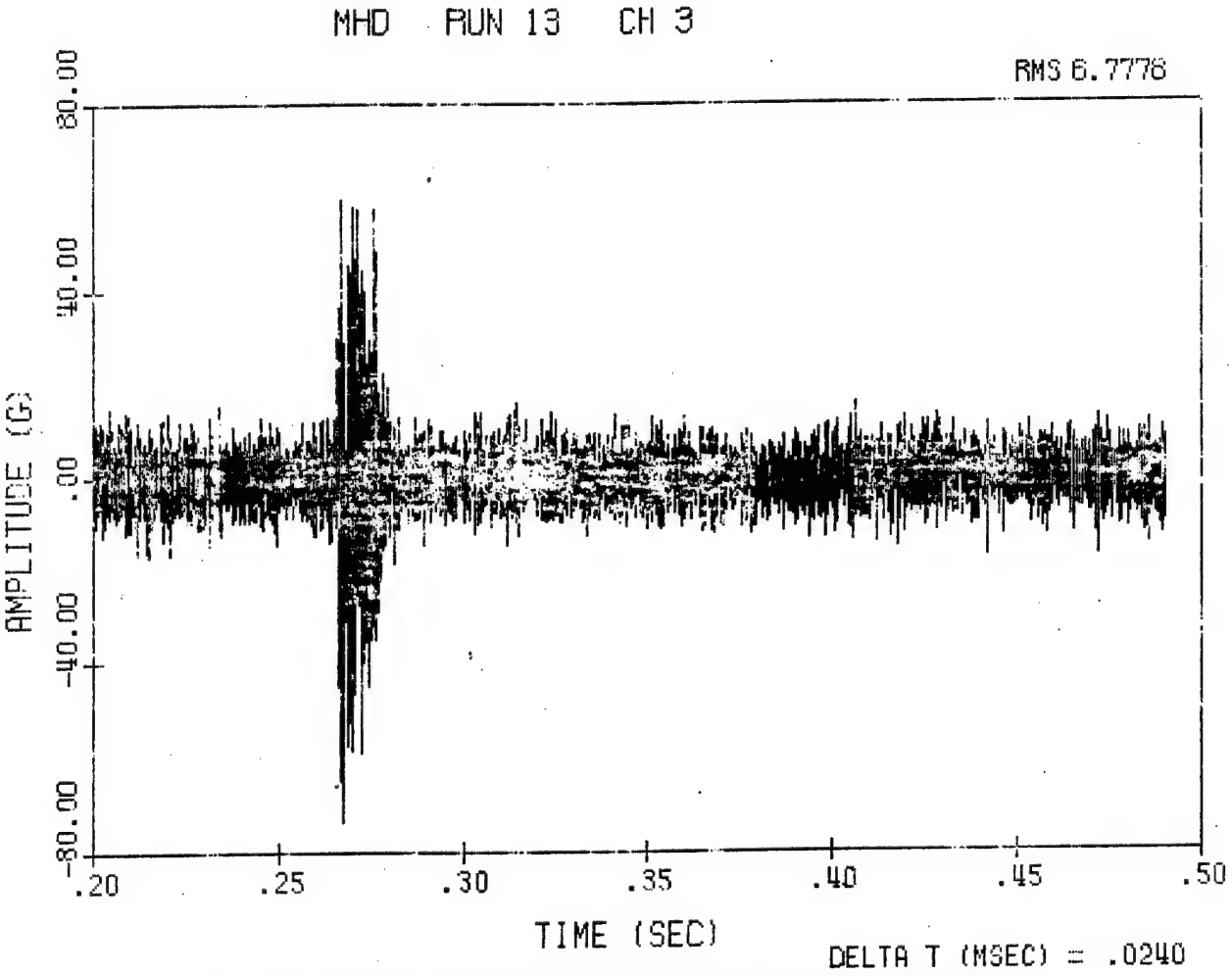


Figure 6a. Time History of Accelerometer 3 During Run LWC 13 Starting Transient.

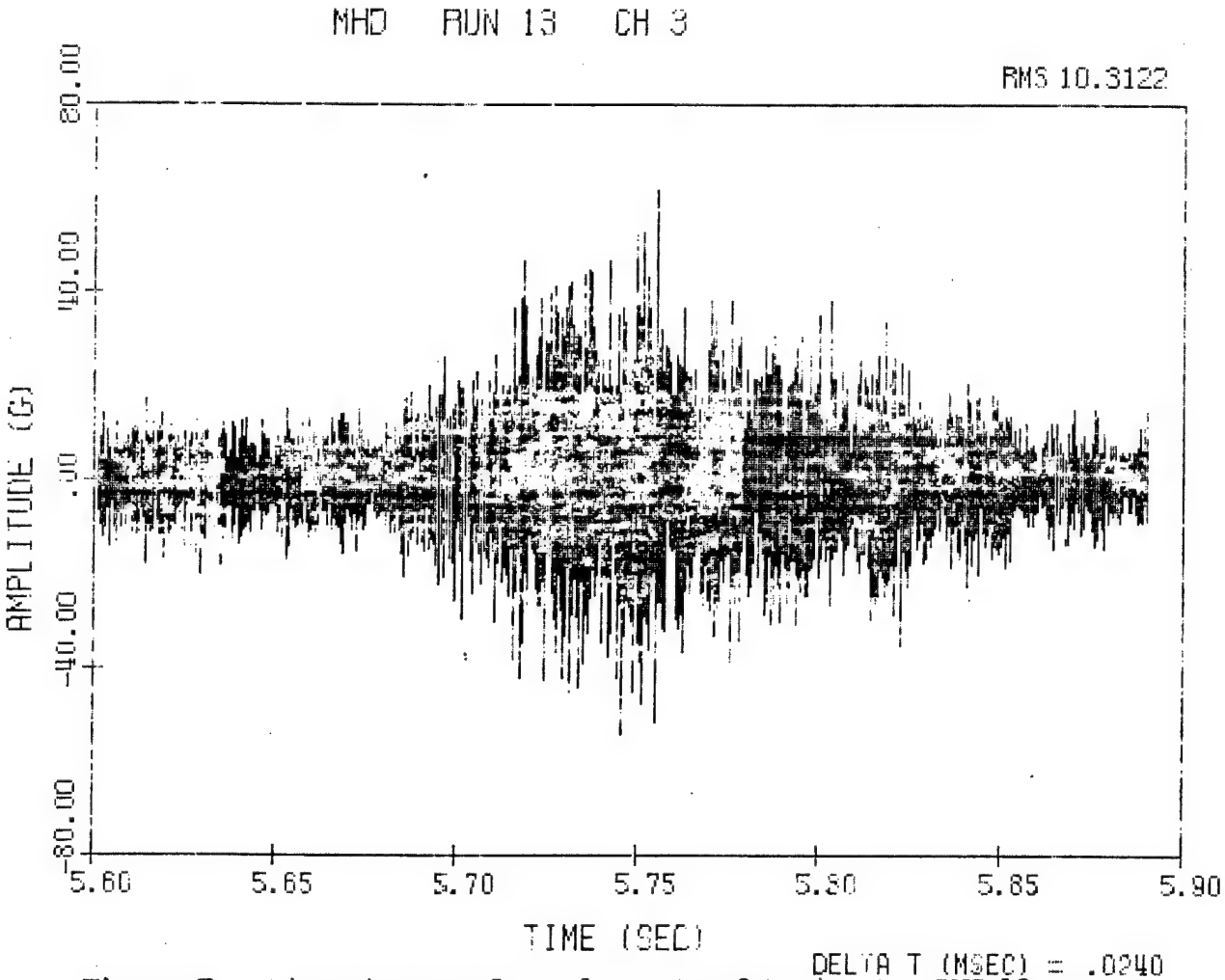


Figure 6b. Time History of Accelerometer 3 During Run LWC 13 Ending Transient.

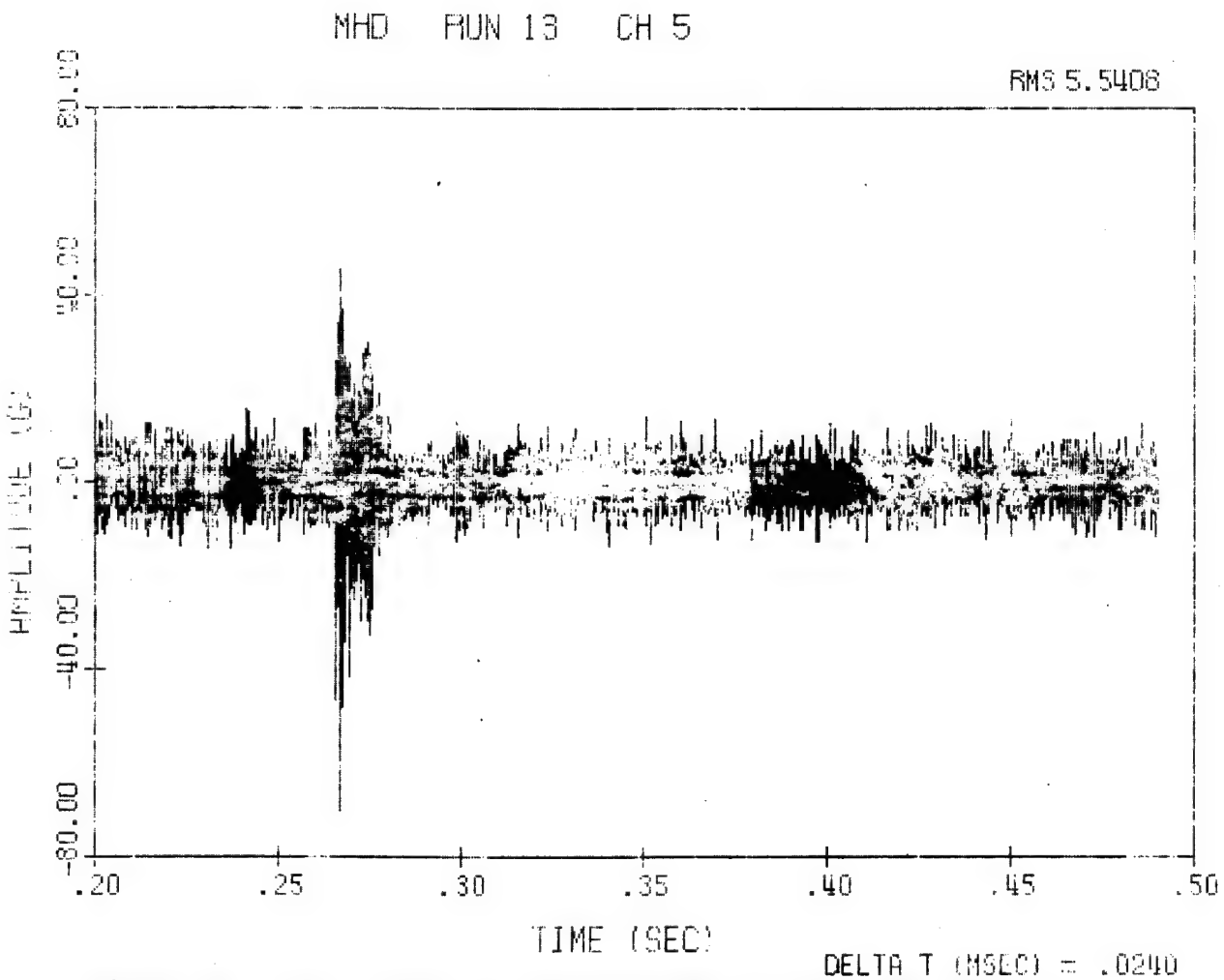


Figure 7a. Time History of Accelerometer 5 During Run LWC 13 Starting Transient.

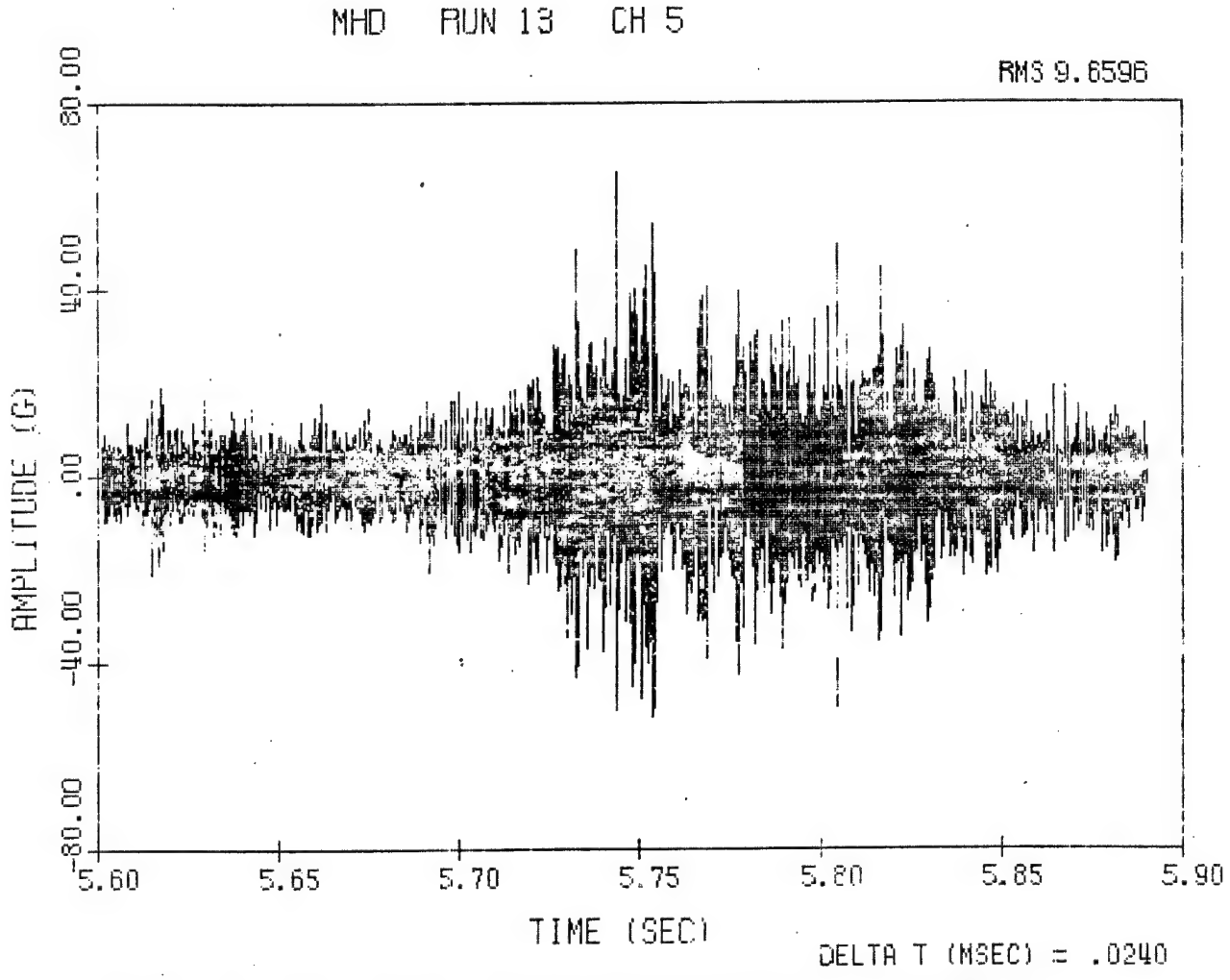


Figure 7b. Time History of Accelerometer 5 During Run LWC 13 Ending Transient.

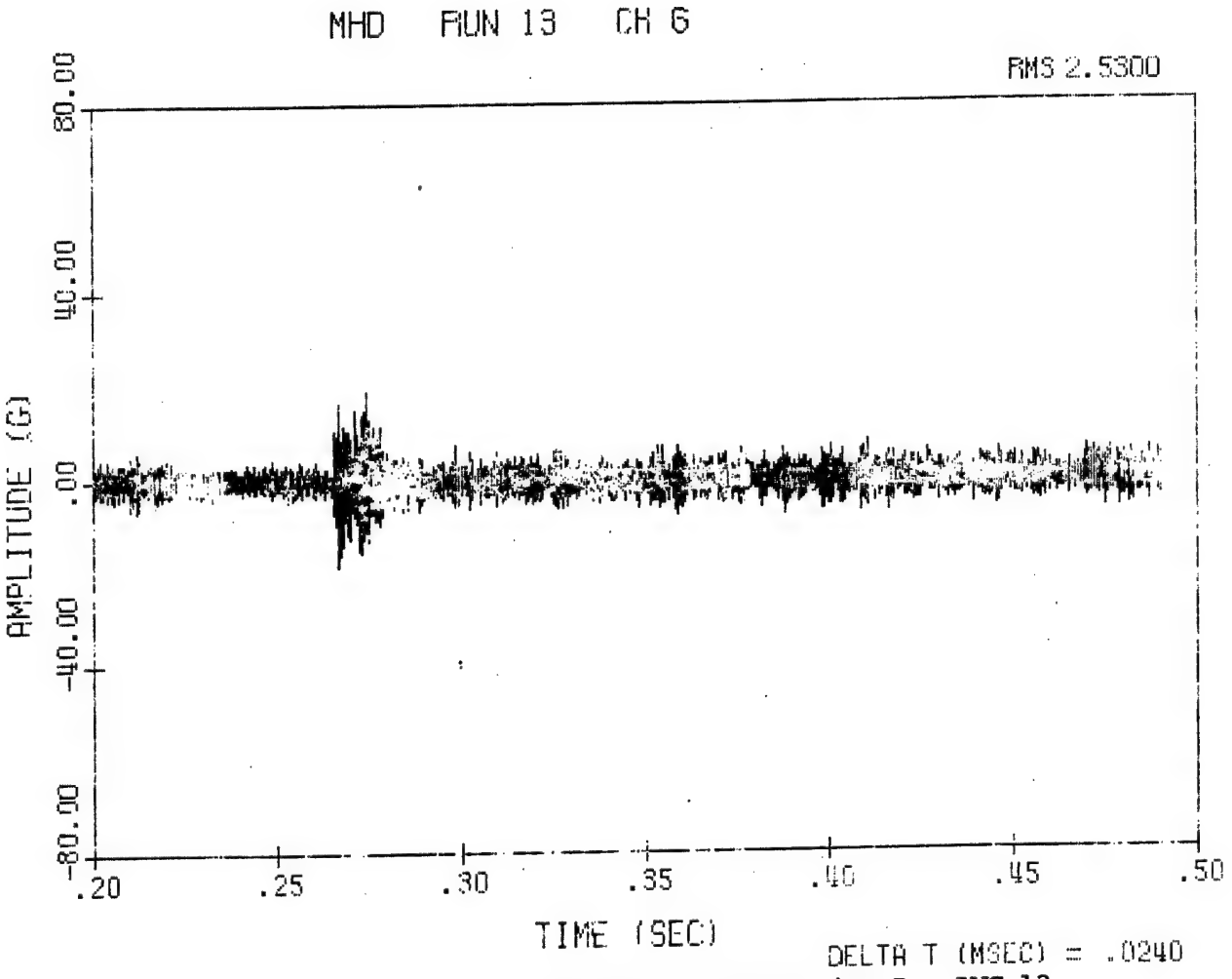


Figure 8a. Time History of Accelerometer 6 During Run LWC 13 Starting Transient.

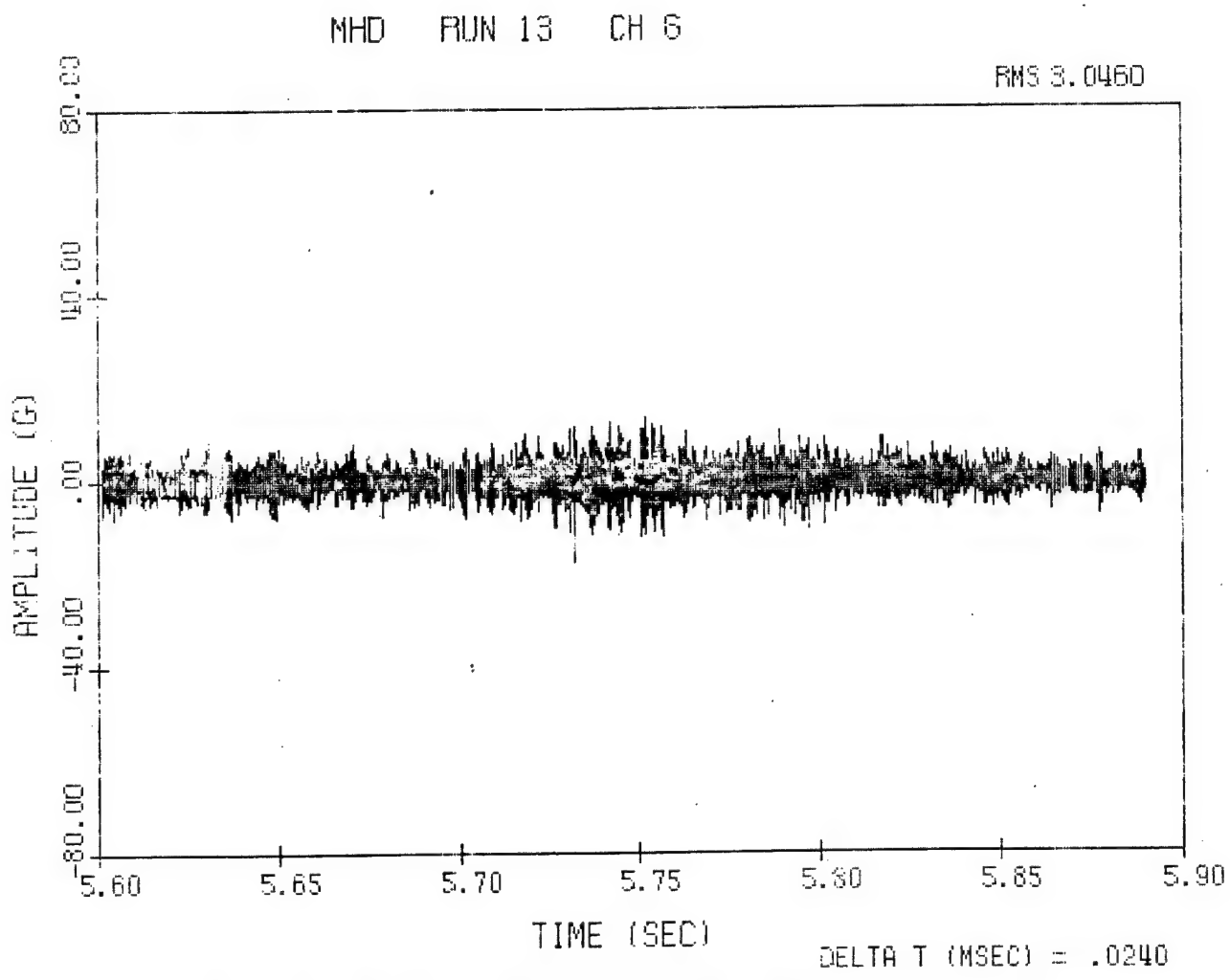


Figure 8b. Time History of Accelerometer 6 During Run LWC 13 Ending Transient.

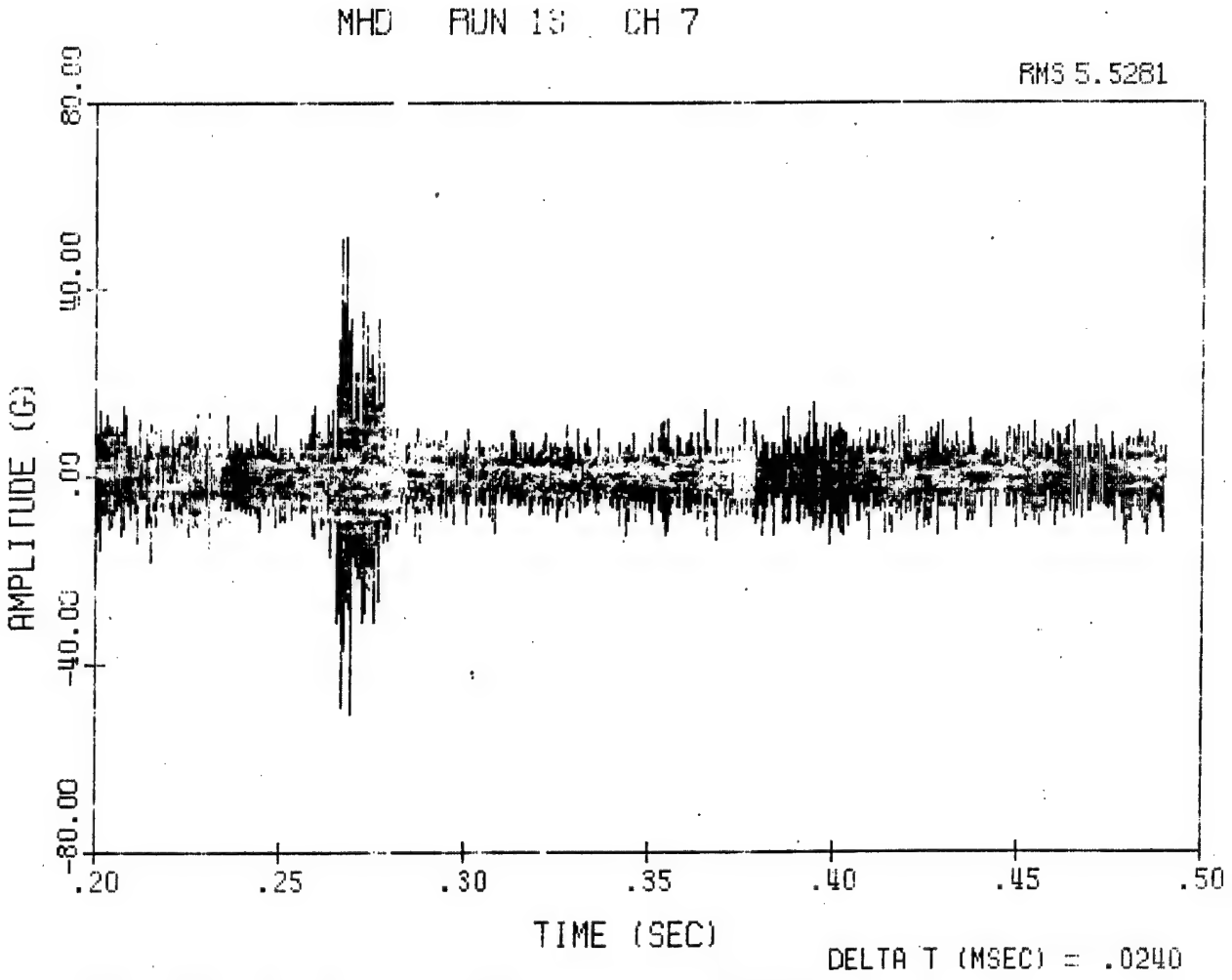


Figure 9a. Time History of Accelerometer 7 During Run LWC 13 Starting Transient.

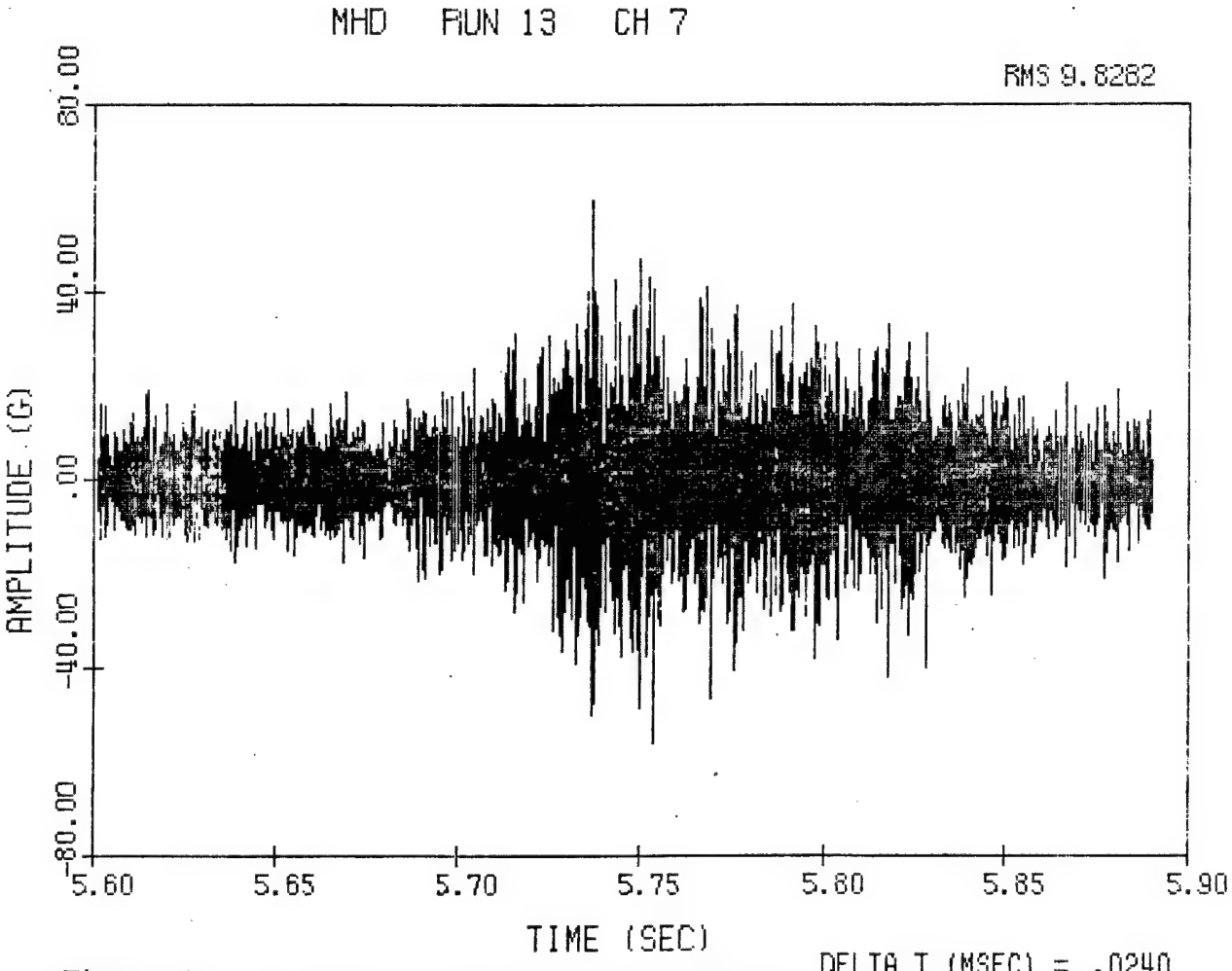


Figure 9b. Time History of Accelerometer 7 During Run LWC 13 Ending Transient.

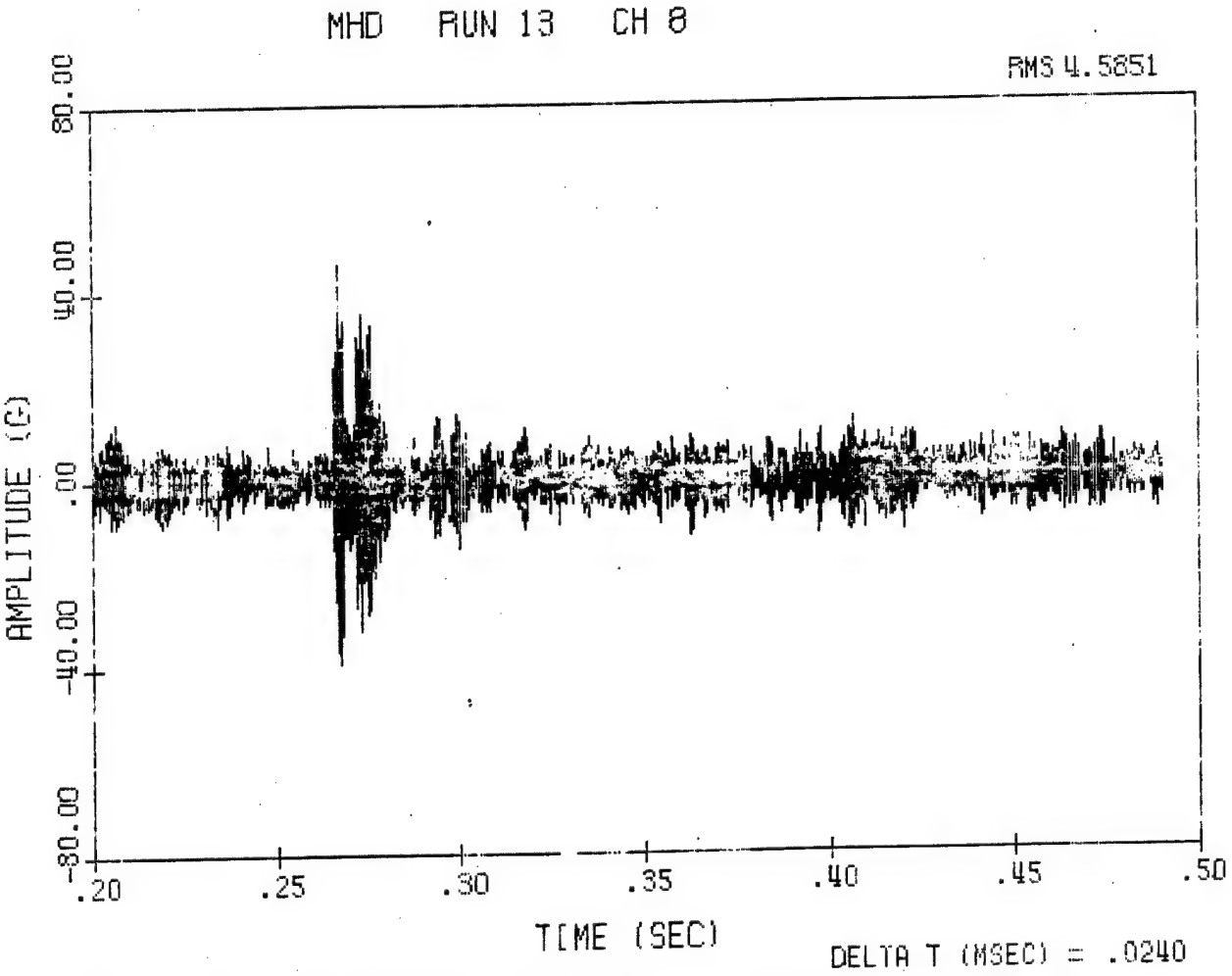


Figure 10a. Time History of Accelerometer 8 During Run LWC 13 Starting Transient.

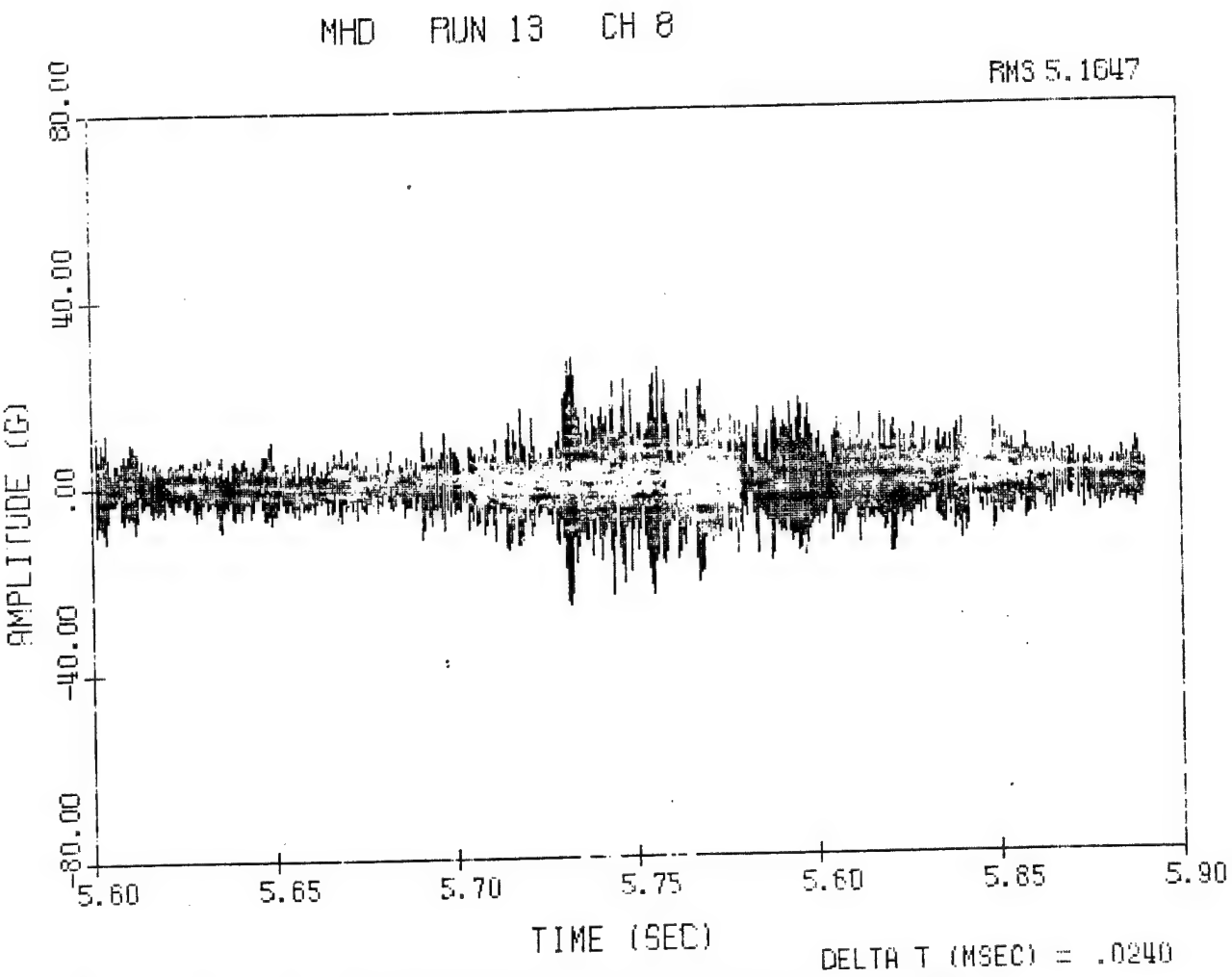


Figure 10b. Time History of Accelerometer 8 During Run LWC 13 Ending Transient.

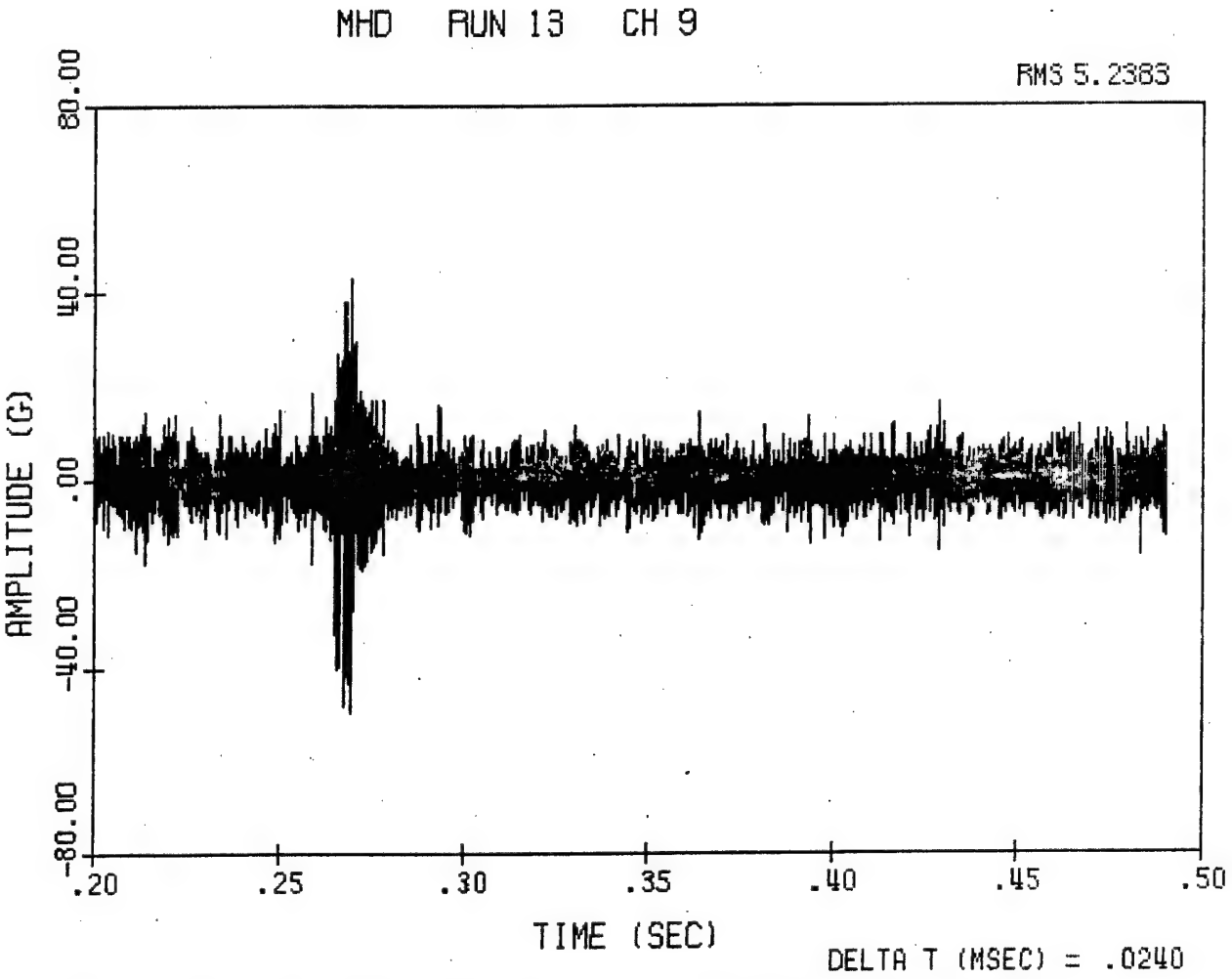


**Figure 11a.** Time History of Accelerometer 9 During Run LWC 13 Starting Transient.

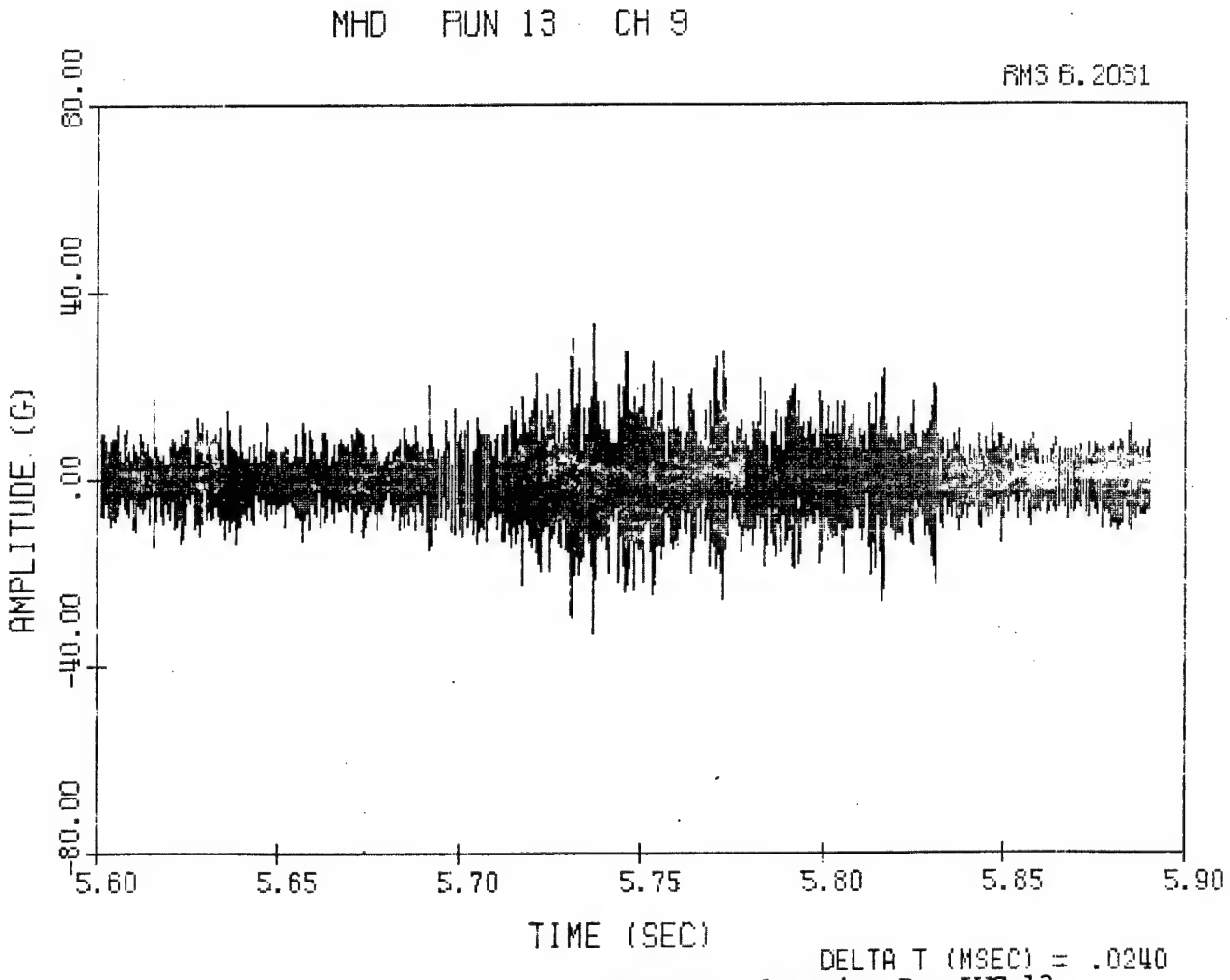


Figure 11b. Time History of Accelerometer 9 During Run LWC 13 Ending Transient.

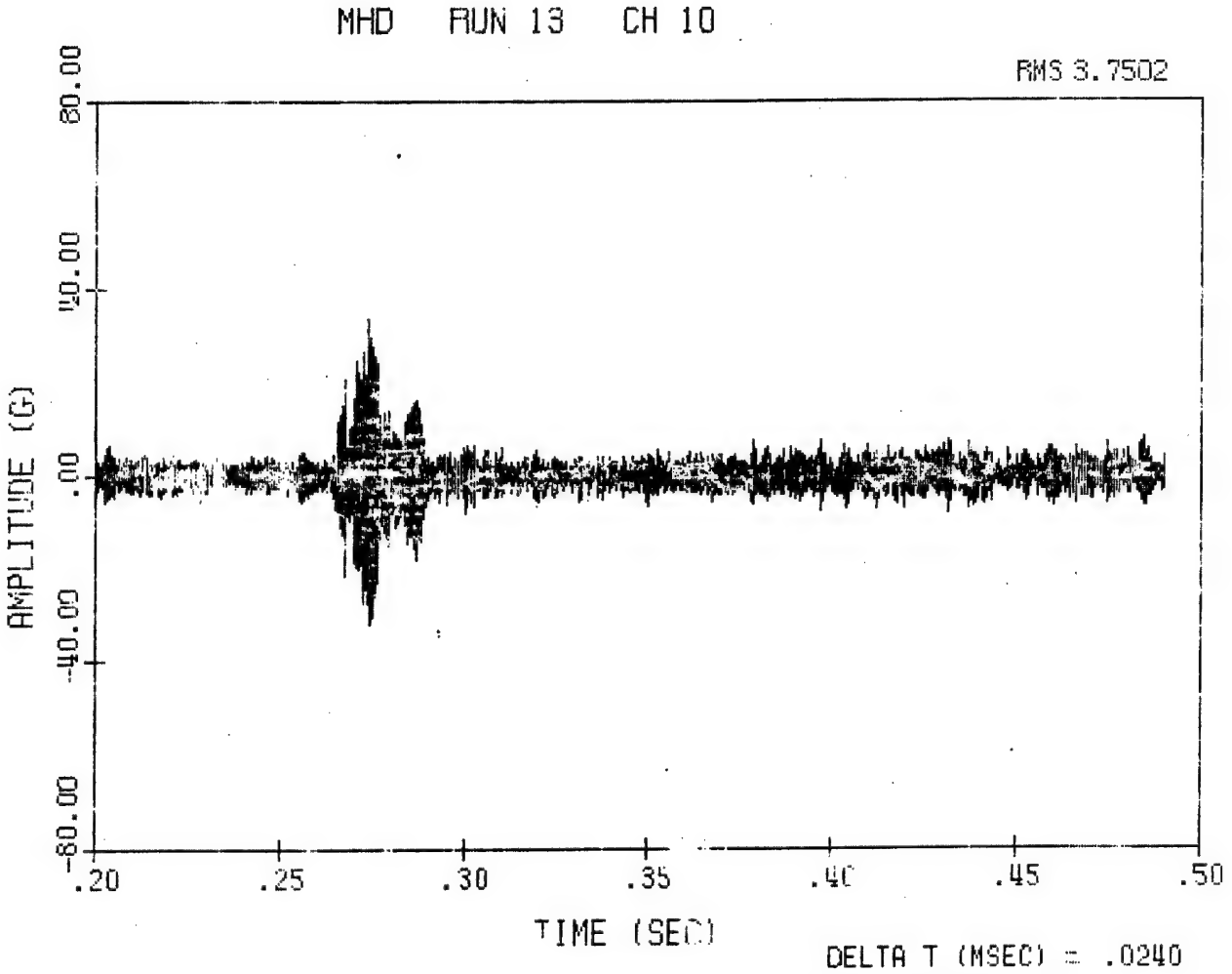


**Figure 12a.** Time History of Accelerometer 10 During Run LWC 13 Starting Transient.

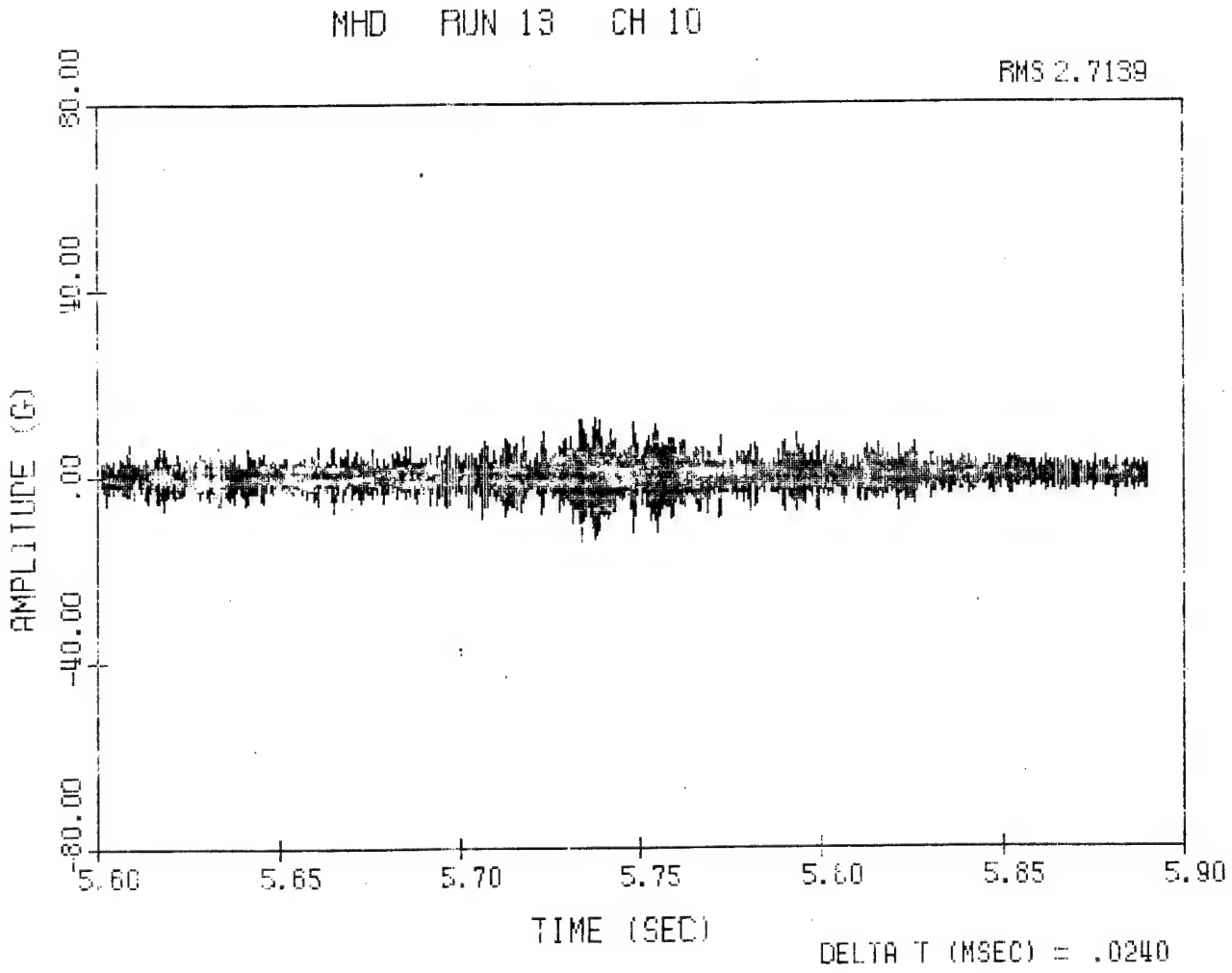


Figure 12b. Time History of Accelerometer 10 During Run LWC 13 Ending Transient.

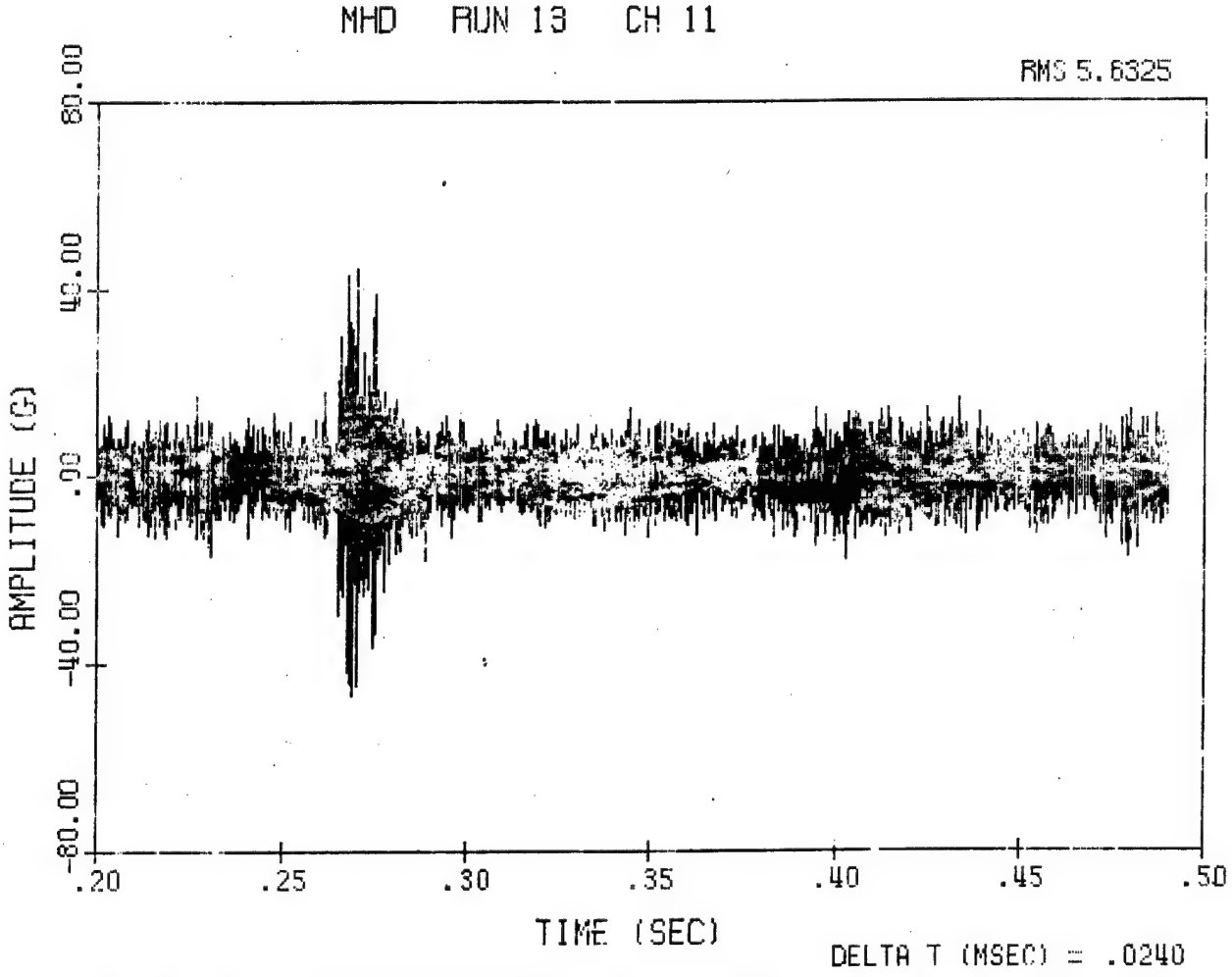


**Figure 13a. Time History of Accelerometer 11 During Run LWC 13 Starting Transient.**

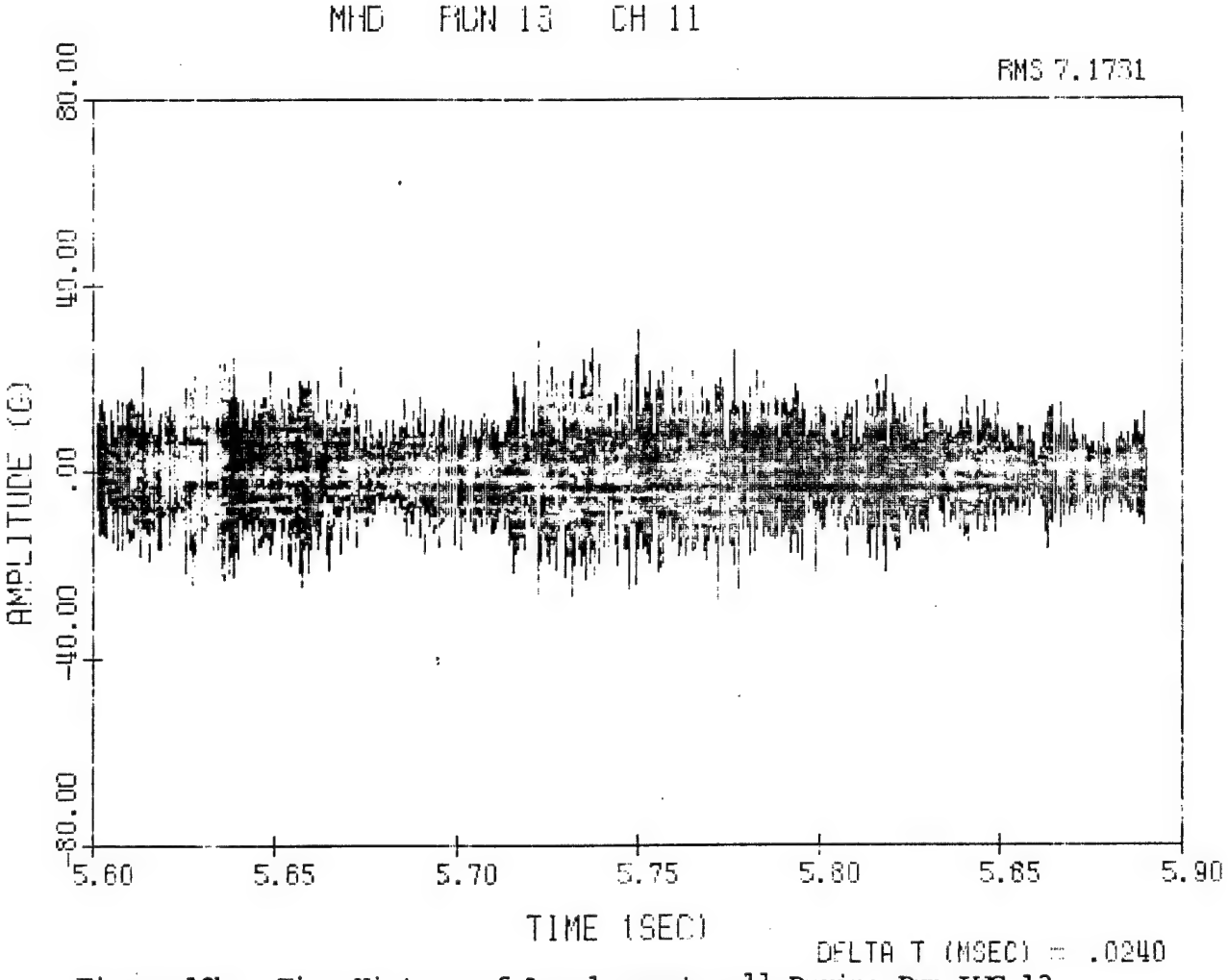


Figure 13b. Time History of Accelerometer 11 During Run LWC 13 Ending Transient.

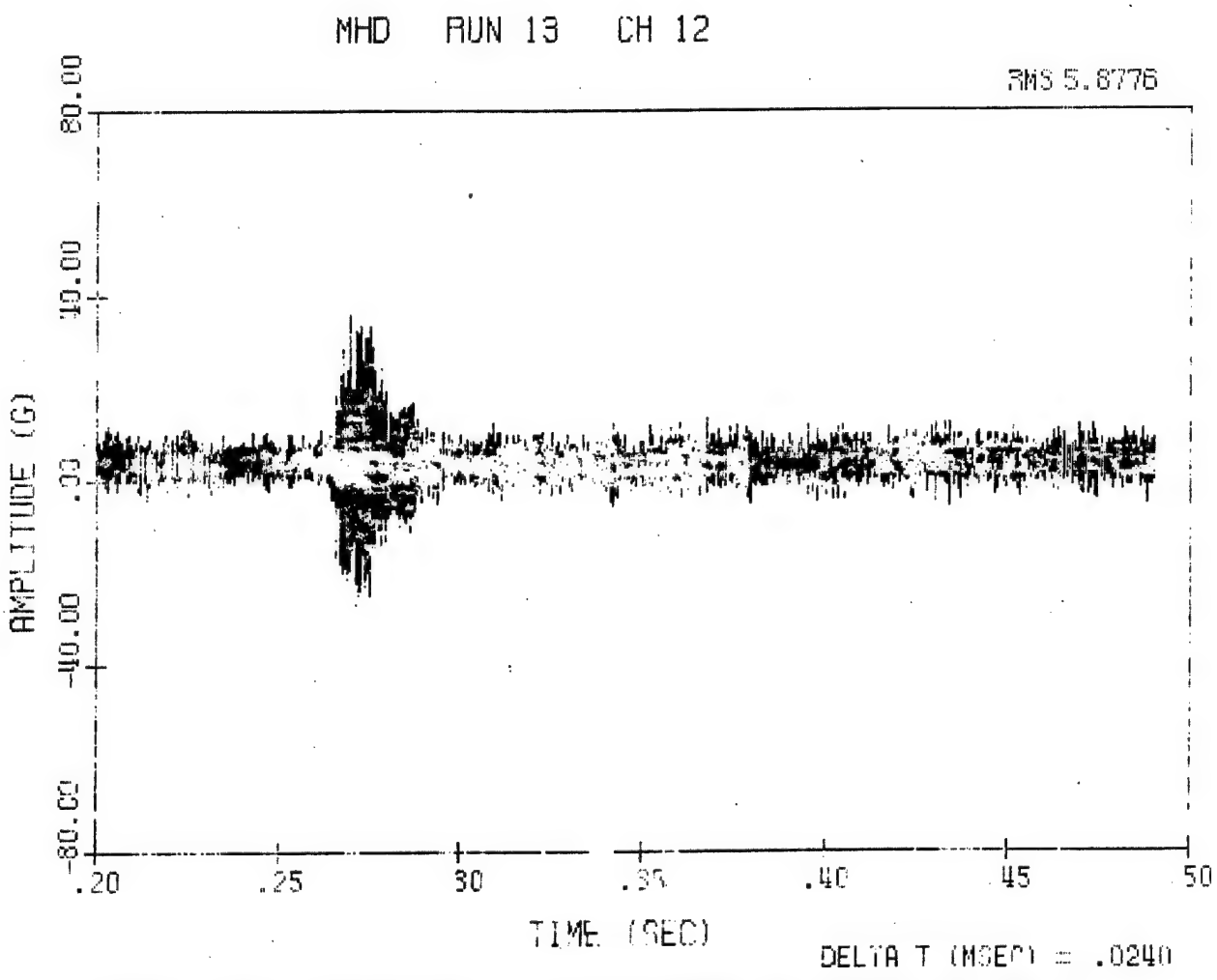


Figure 14a. Time History of Accelerometer 12 During Run LWC 13 Starting Transient.

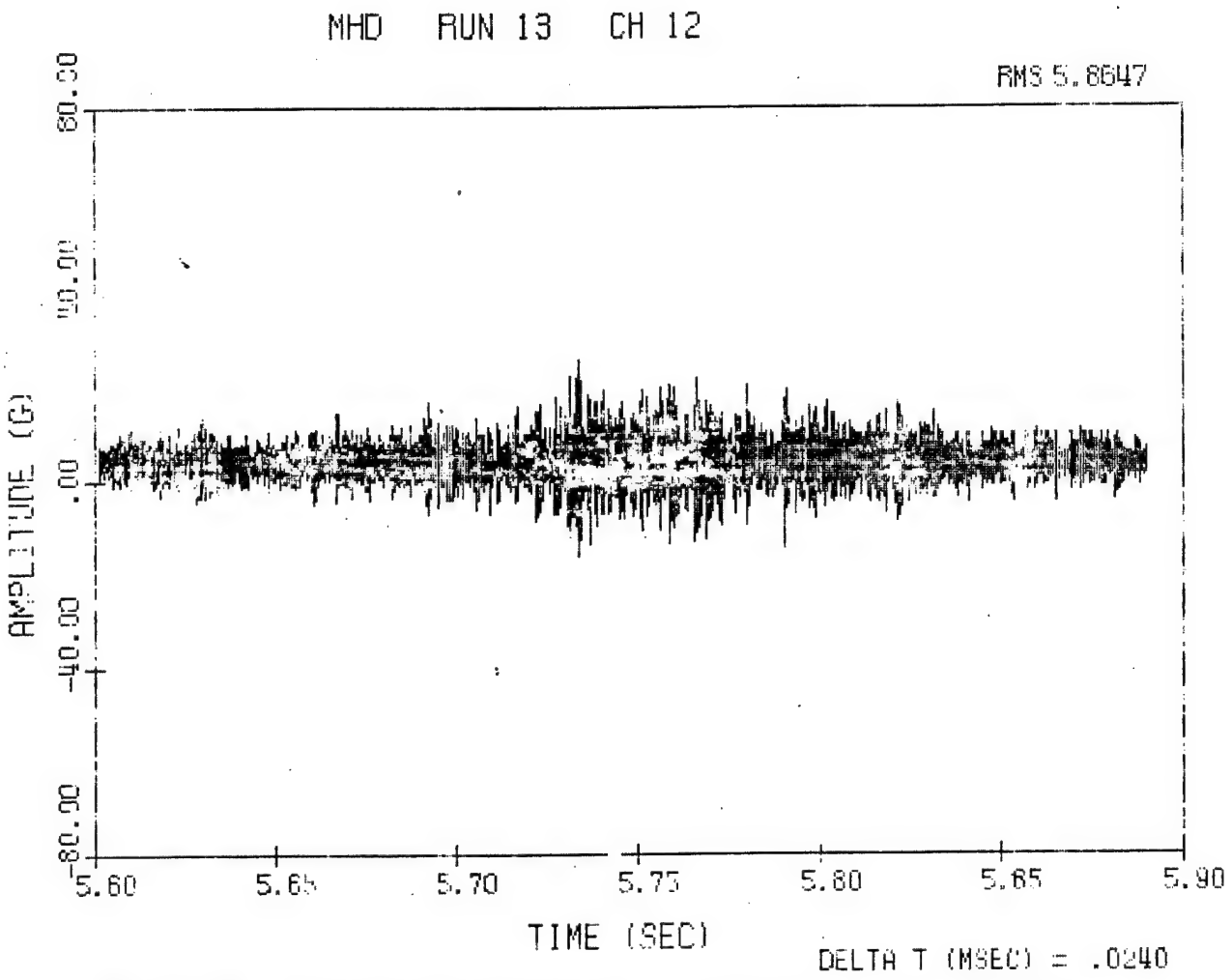


Figure 14b. Time History of Accelerometer 12 During Run LWC 13 Ending Transient.

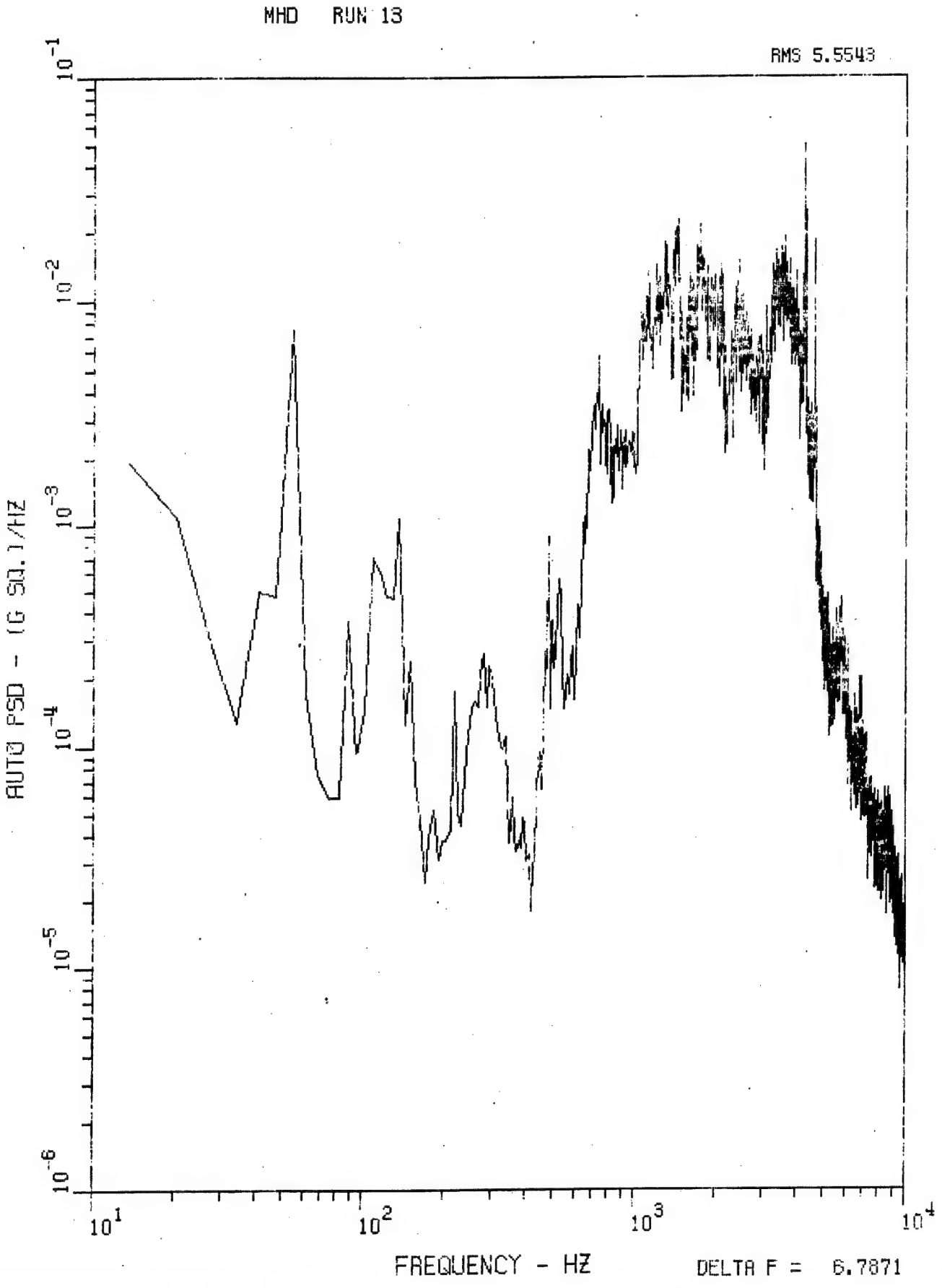


**Figure 15. Accelerometer 1 PSD, 0-10 kHz, Run LWC 13.**

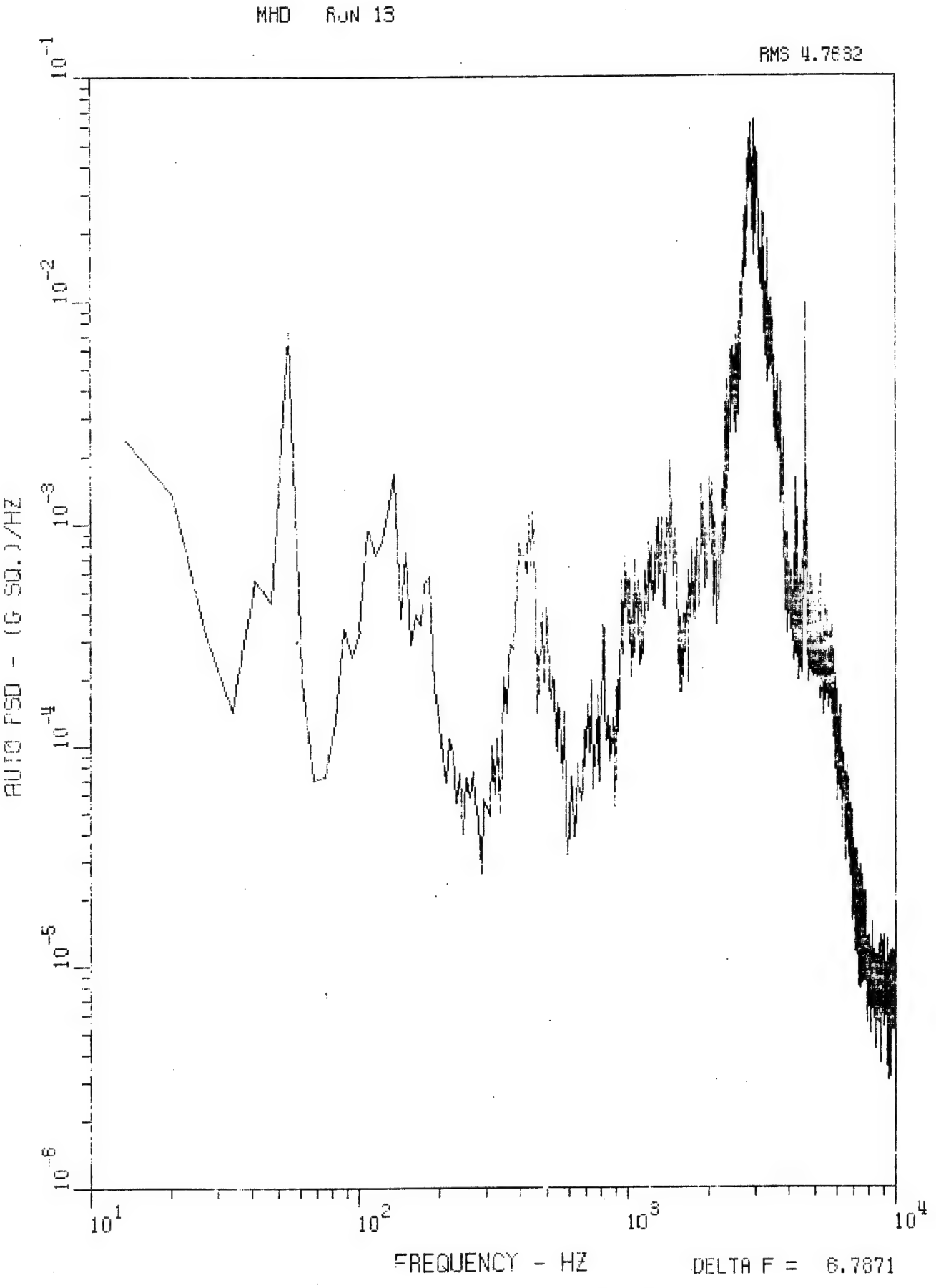


Figure 16. Accelerometer 2 PSD, 0-10 kHz, Run LWC 13.

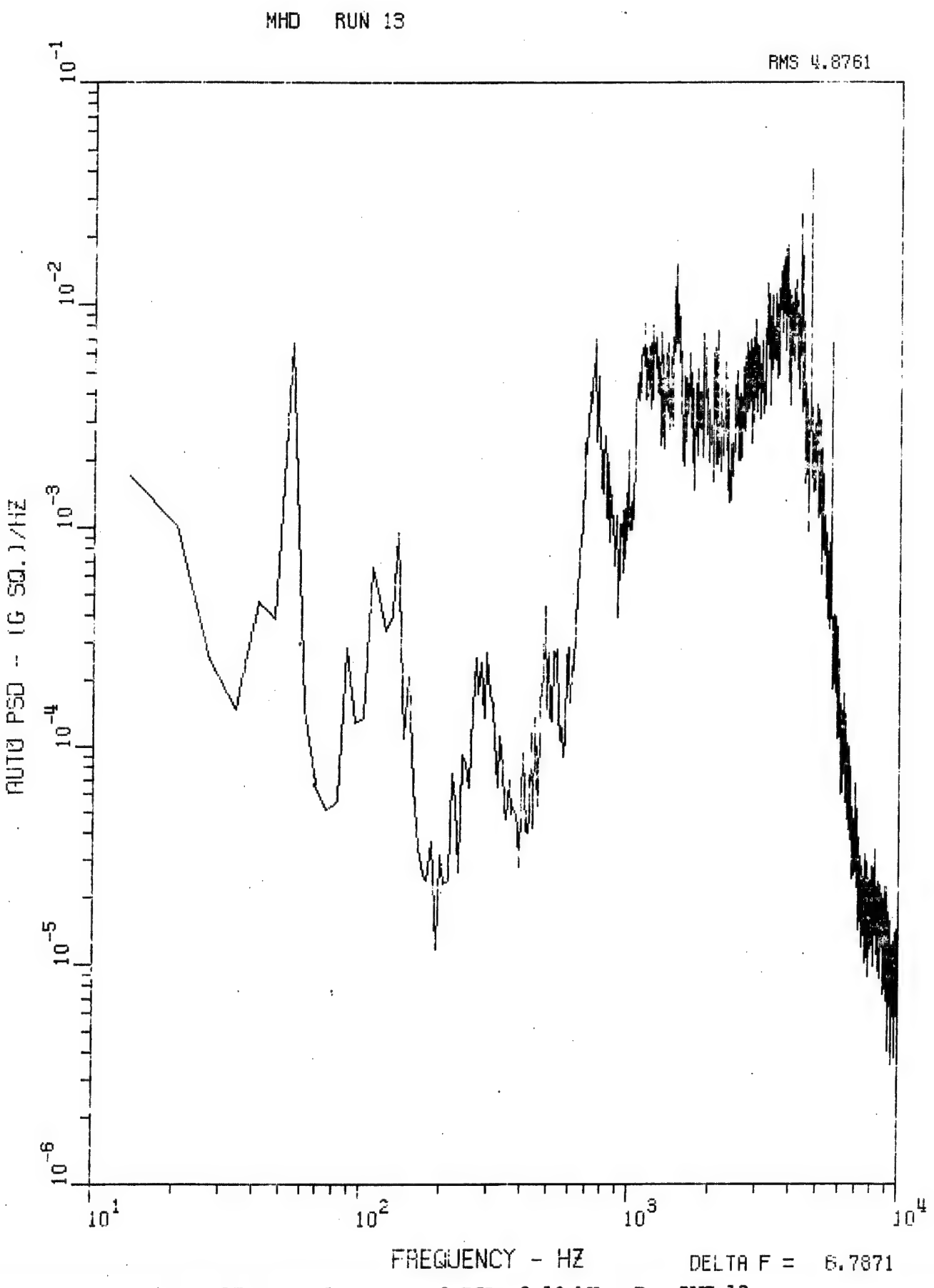


**Figure 17. Accelerometer 3 PSD, 0-10 kHz, Run LWC 13.**

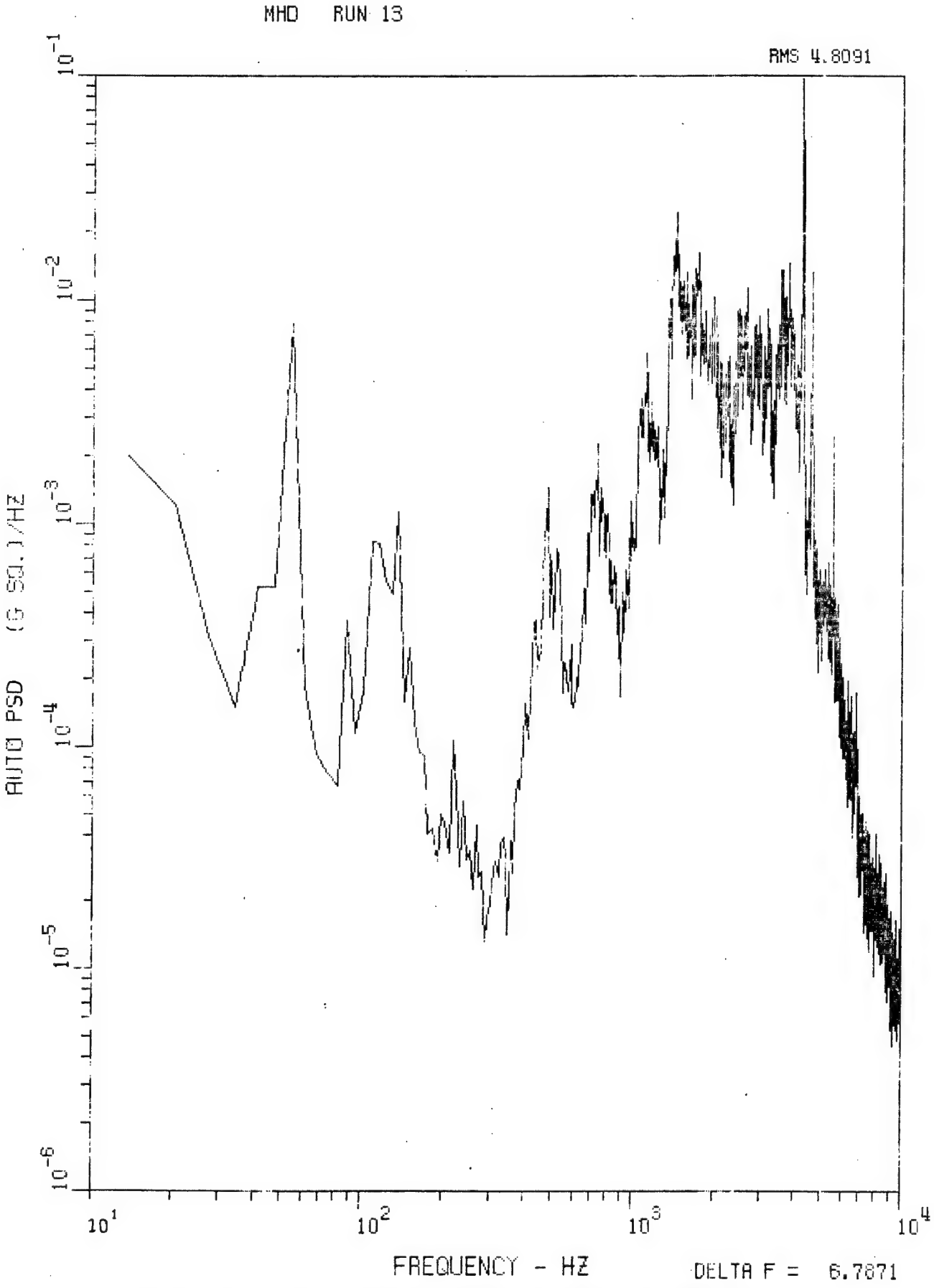


Figure 18. Accelerometer 5 PSD, 0-10 kHz, Run LWC 13.

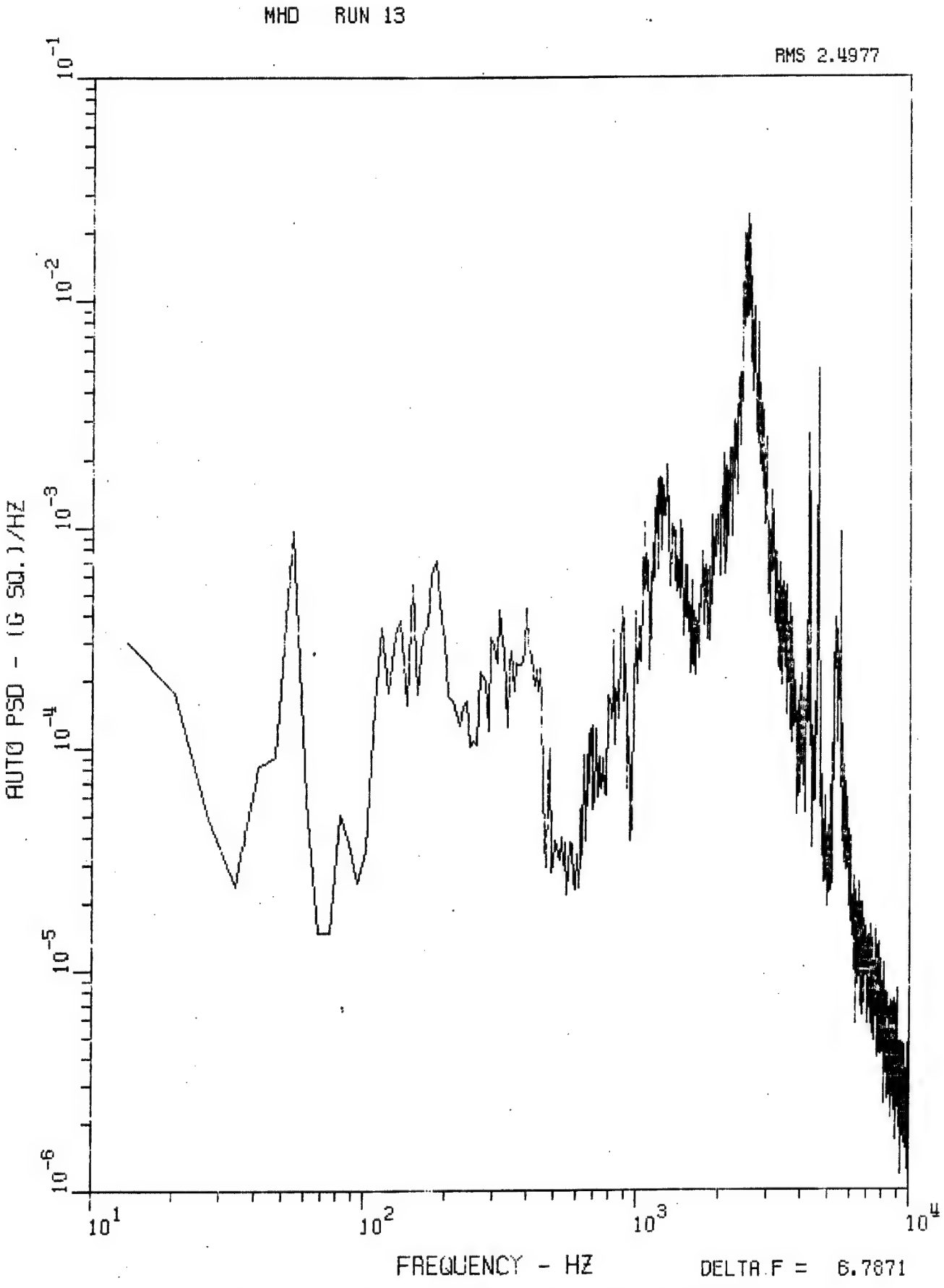


**Figure 19. Accelerometer 6 PSD, 0-10 kHz, Run LWC 13.**

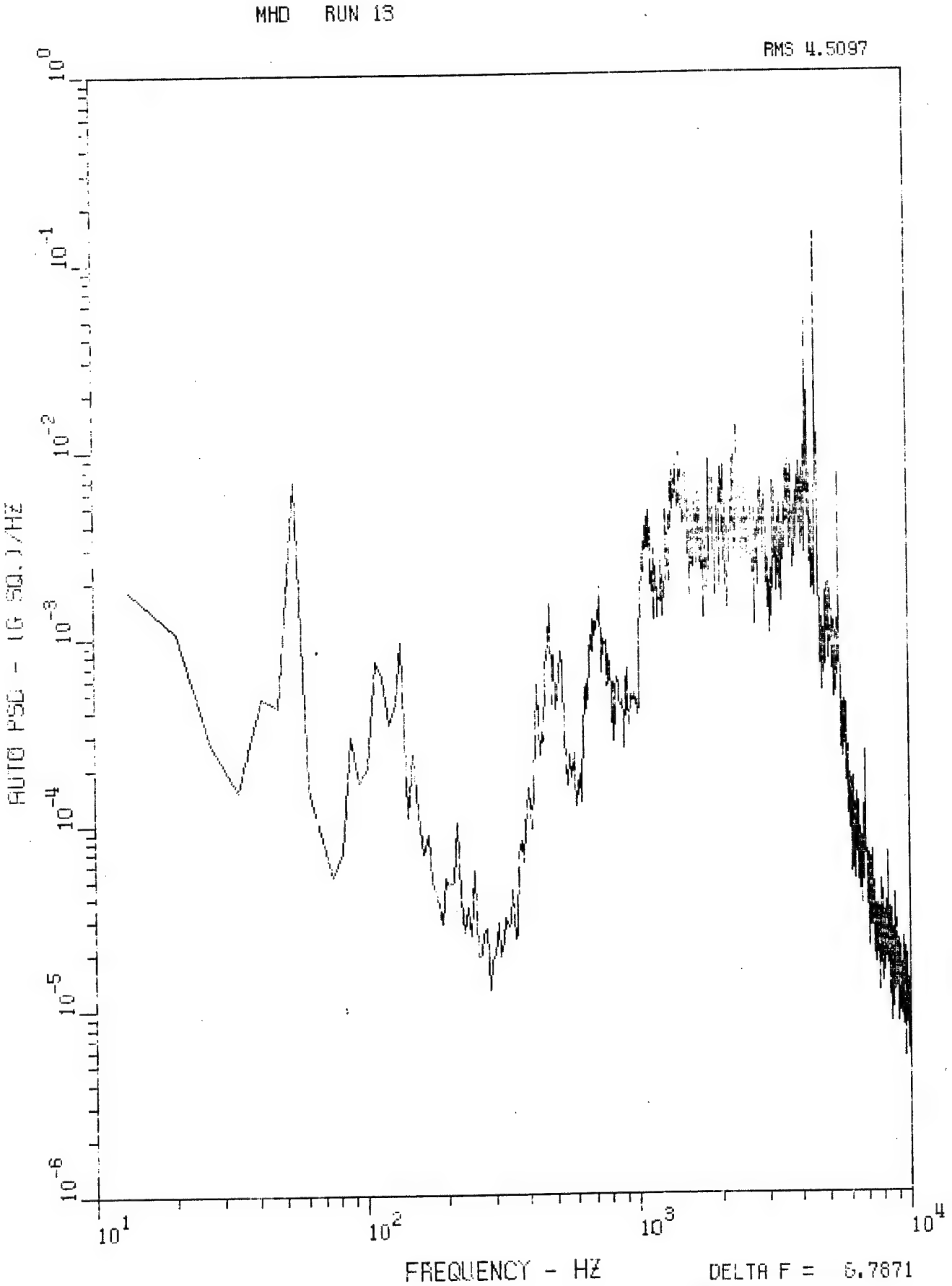


Figure 20. Accelerometer 7 PSD, 0-10 kHz, Run LWC 13.

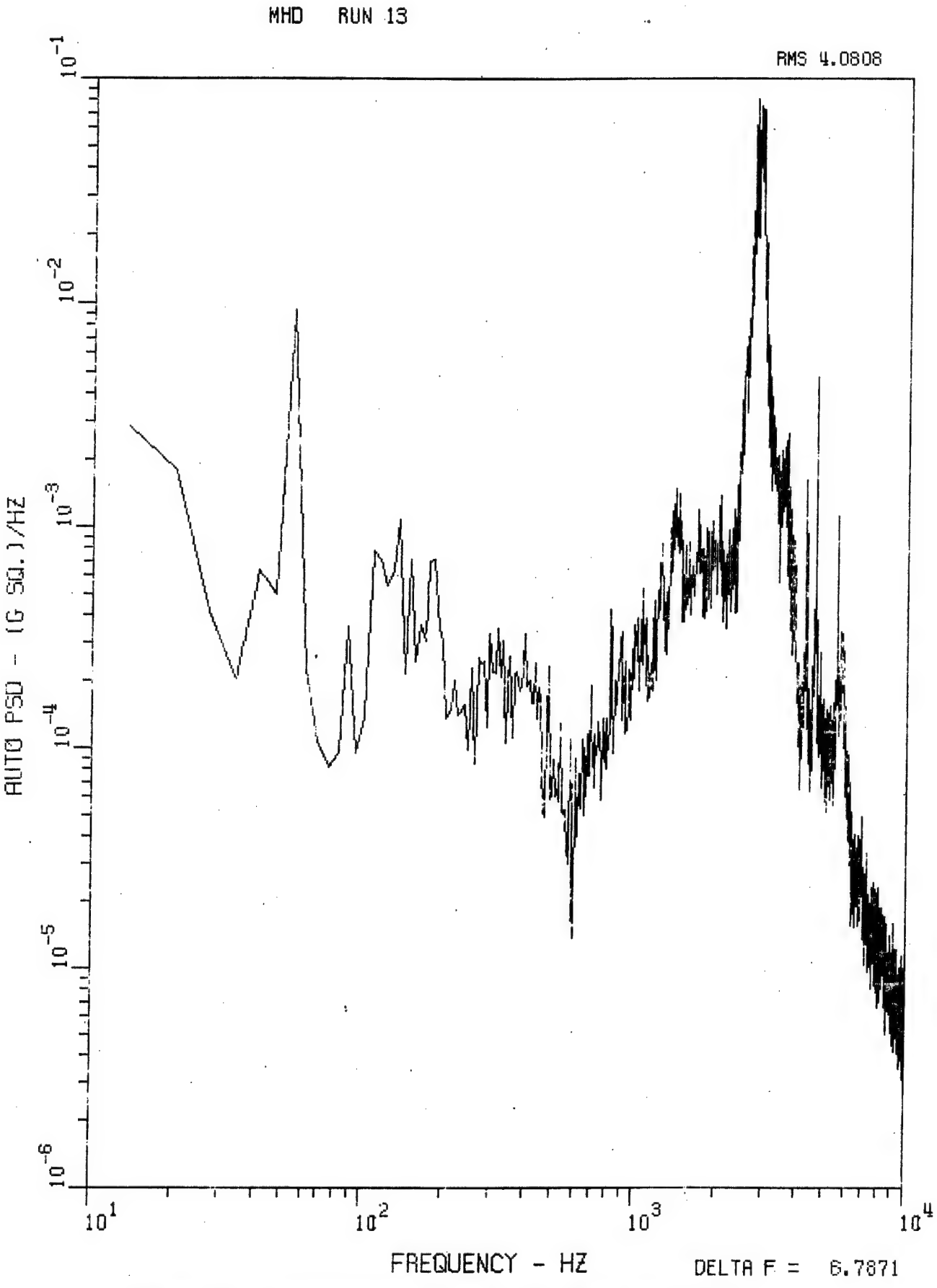


Figure 21. Accelerometer 8 PSD, 0-10 kHz, Run LWC 13.

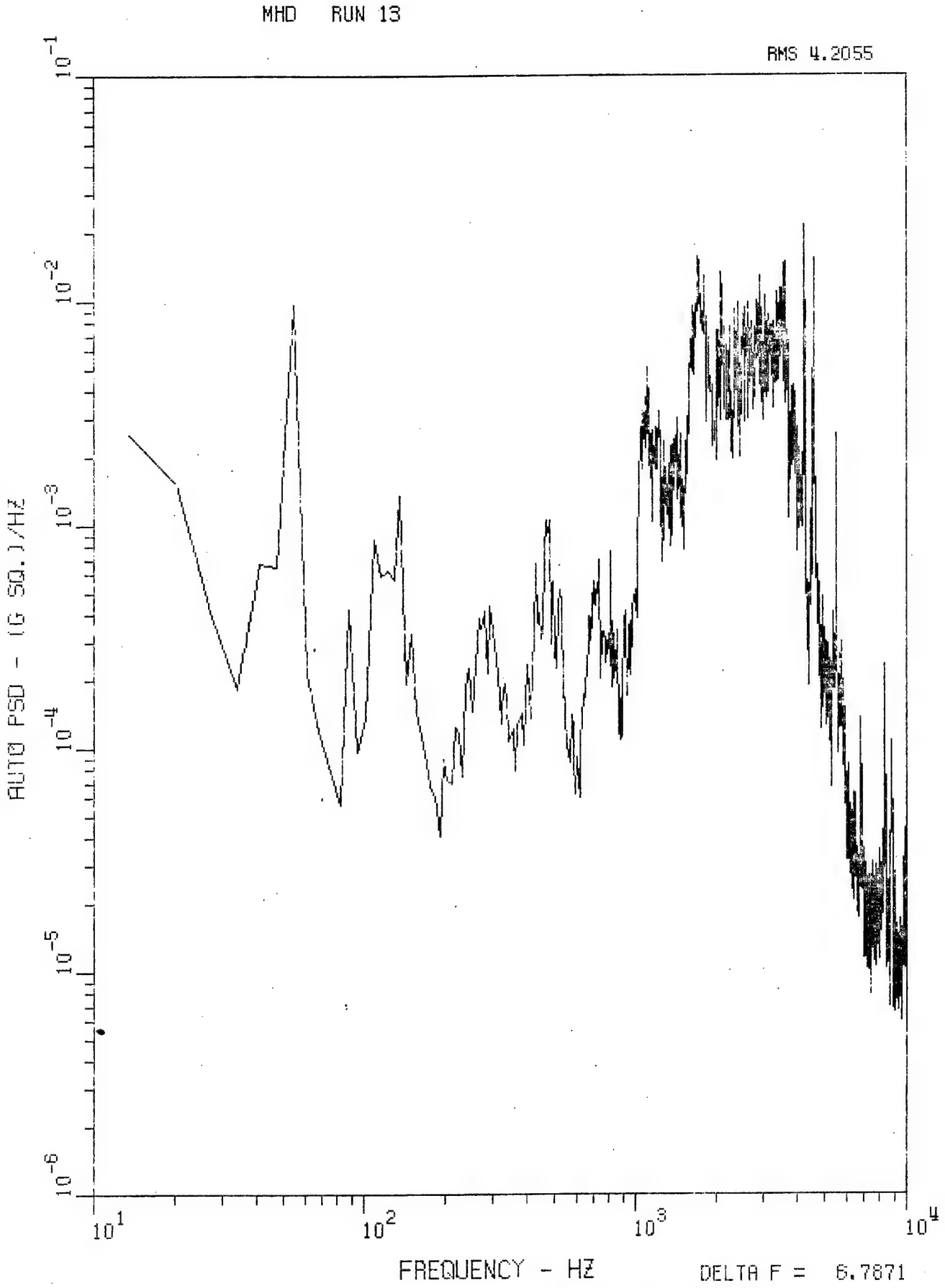


Figure 22. Accelerometer 9 PSD, 0-10 kHz, Run LWC 13.

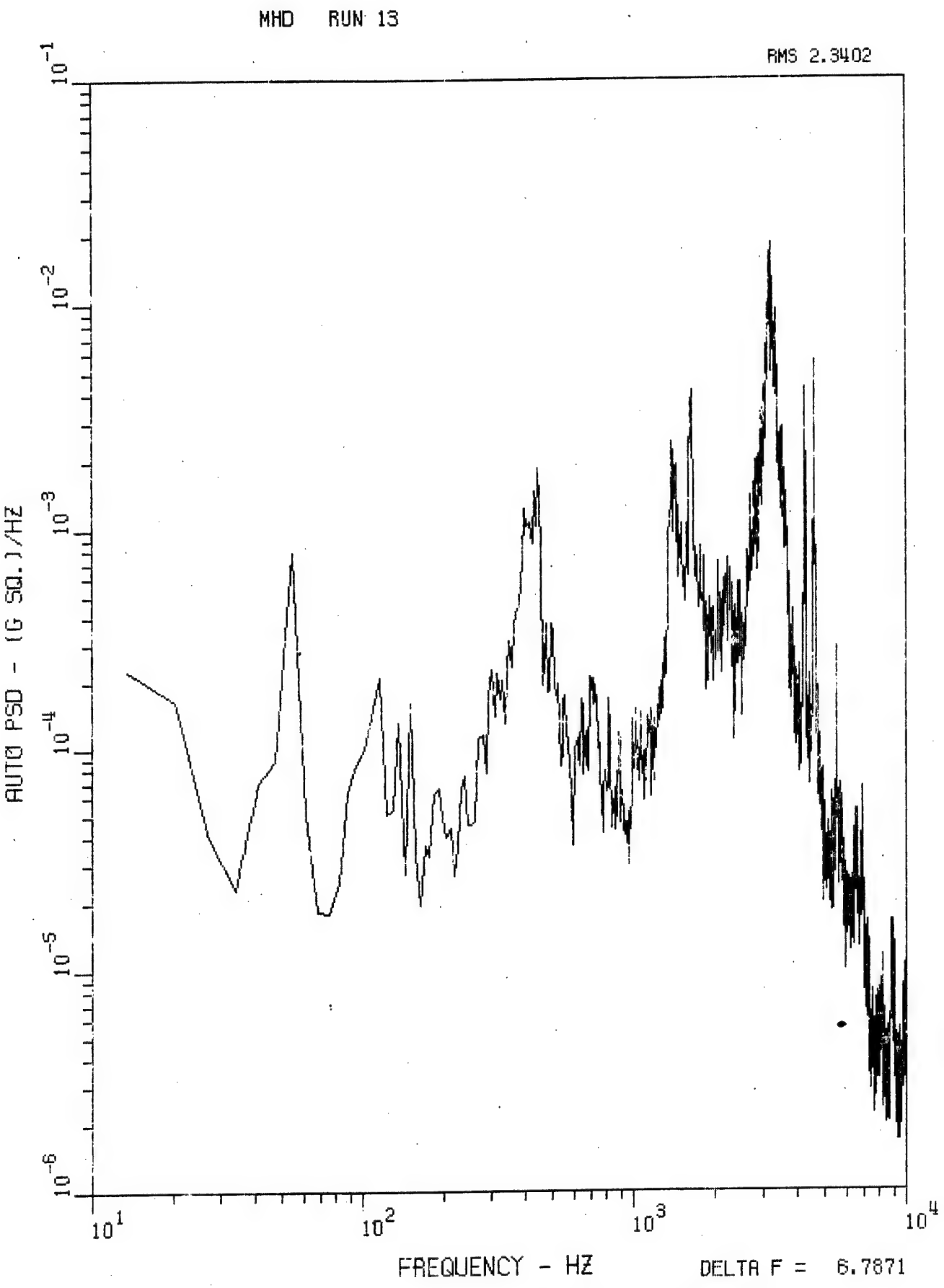


Figure 23. Accelerometer 10 PSD, 0-10 kHz, Run LWC 13.

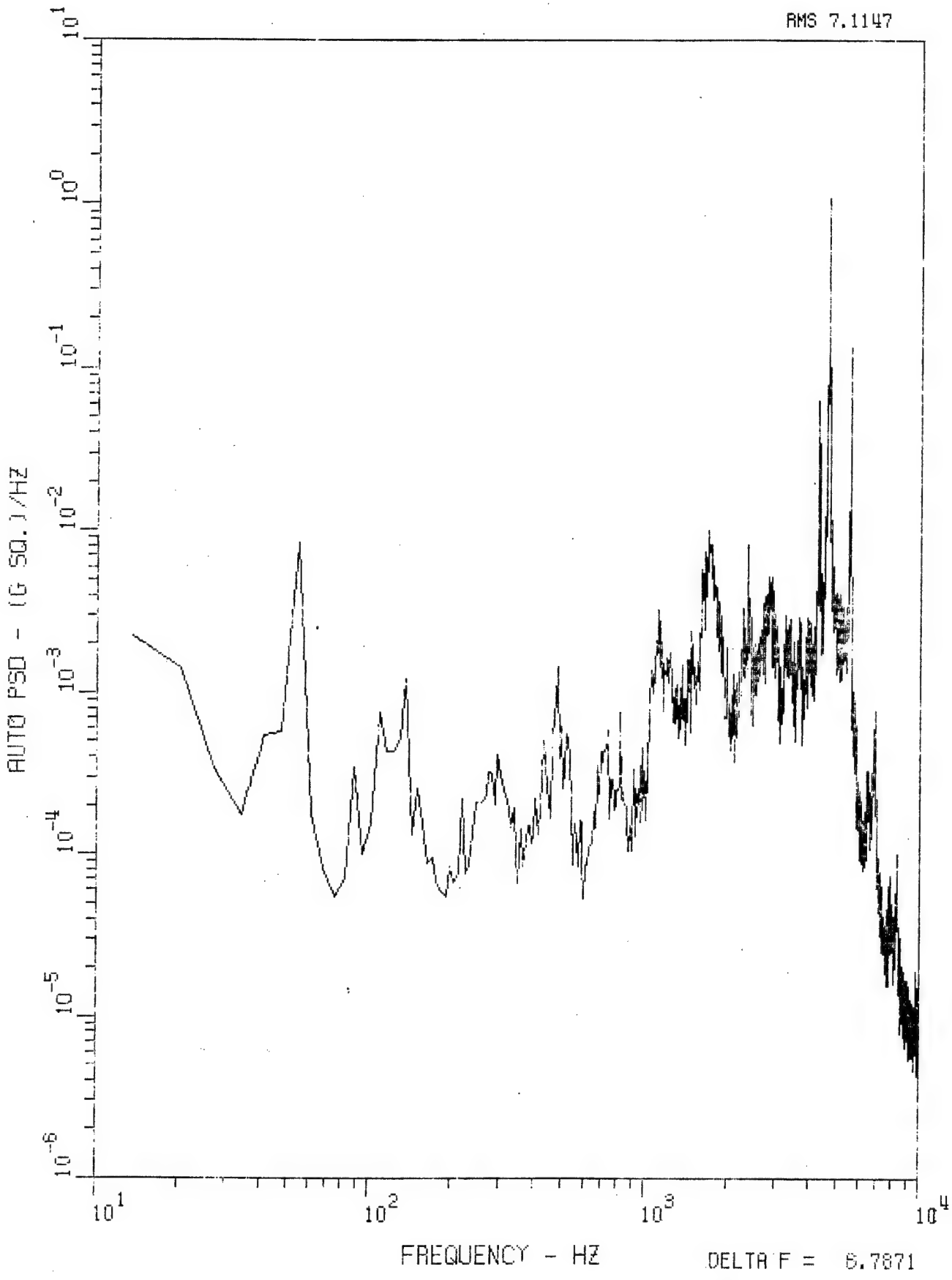


Figure 24. Accelerometer 11 PSD, 0-10 kHz, Run LWC 13.

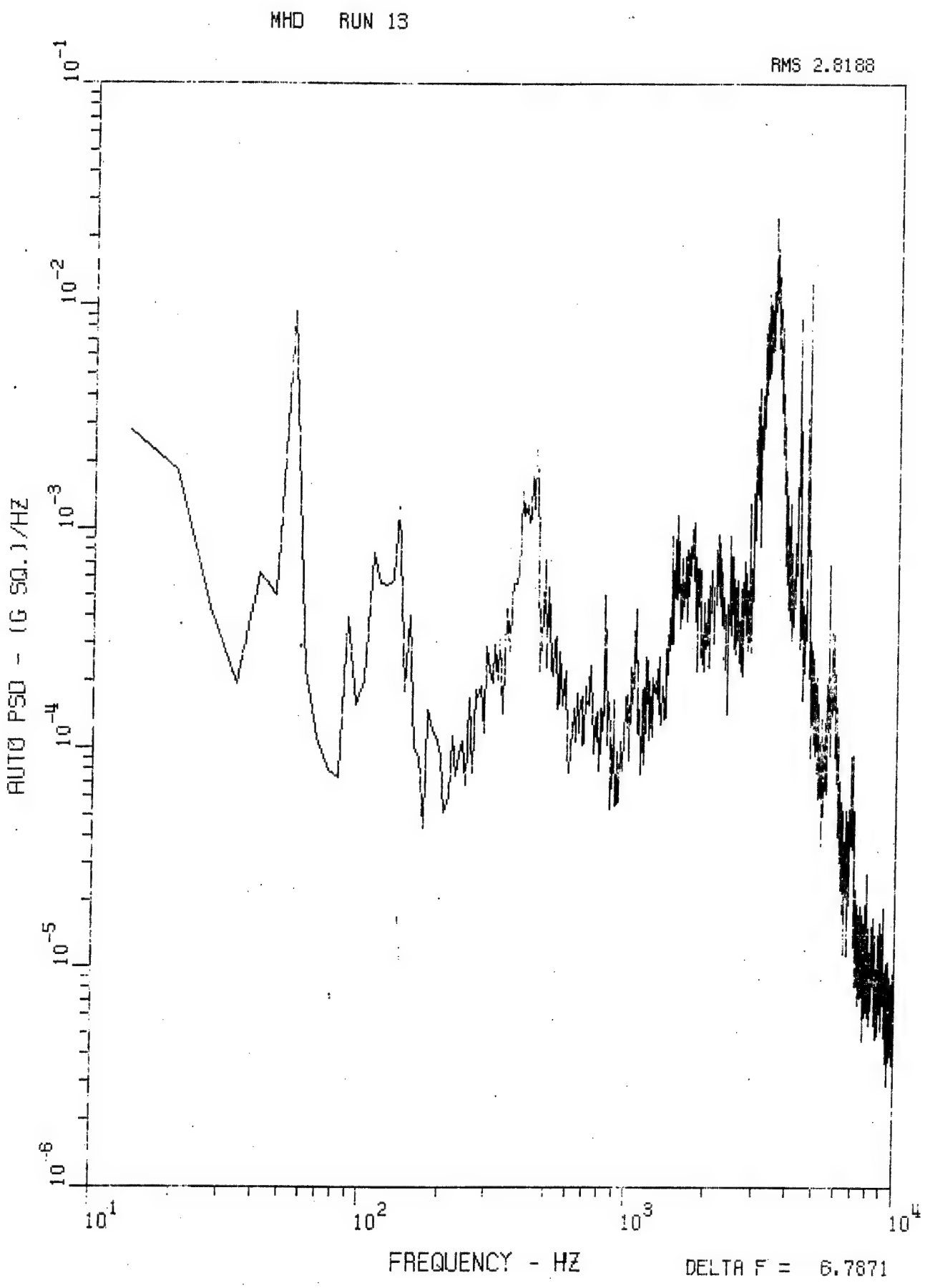


**Figure 25. Accelerometer 12 PSD, 0-10 kHz, Run LWC 13.**

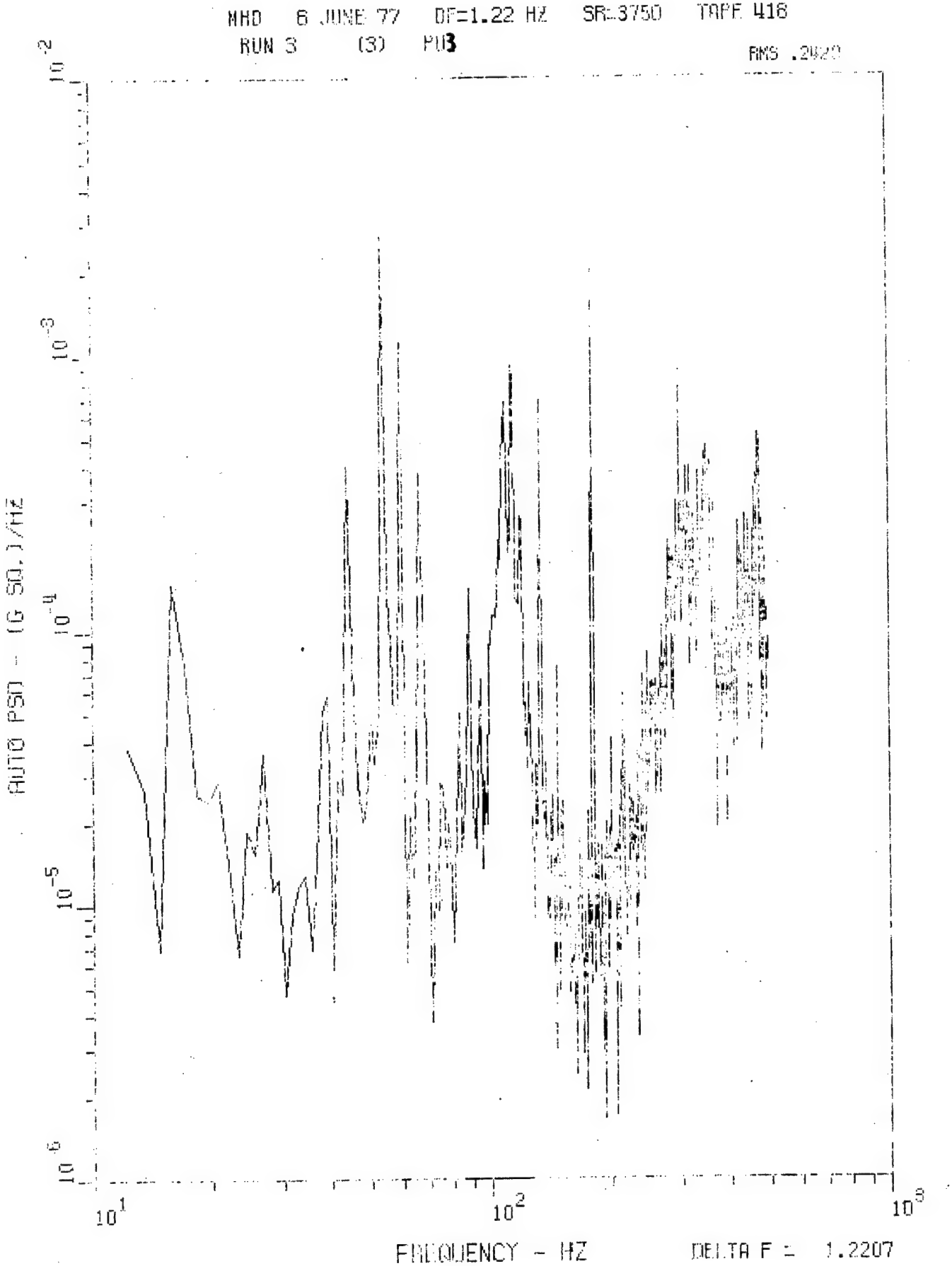


Figure 26. Accelerometer 3 PSD, 0-500 Hz, Run LWC 3.

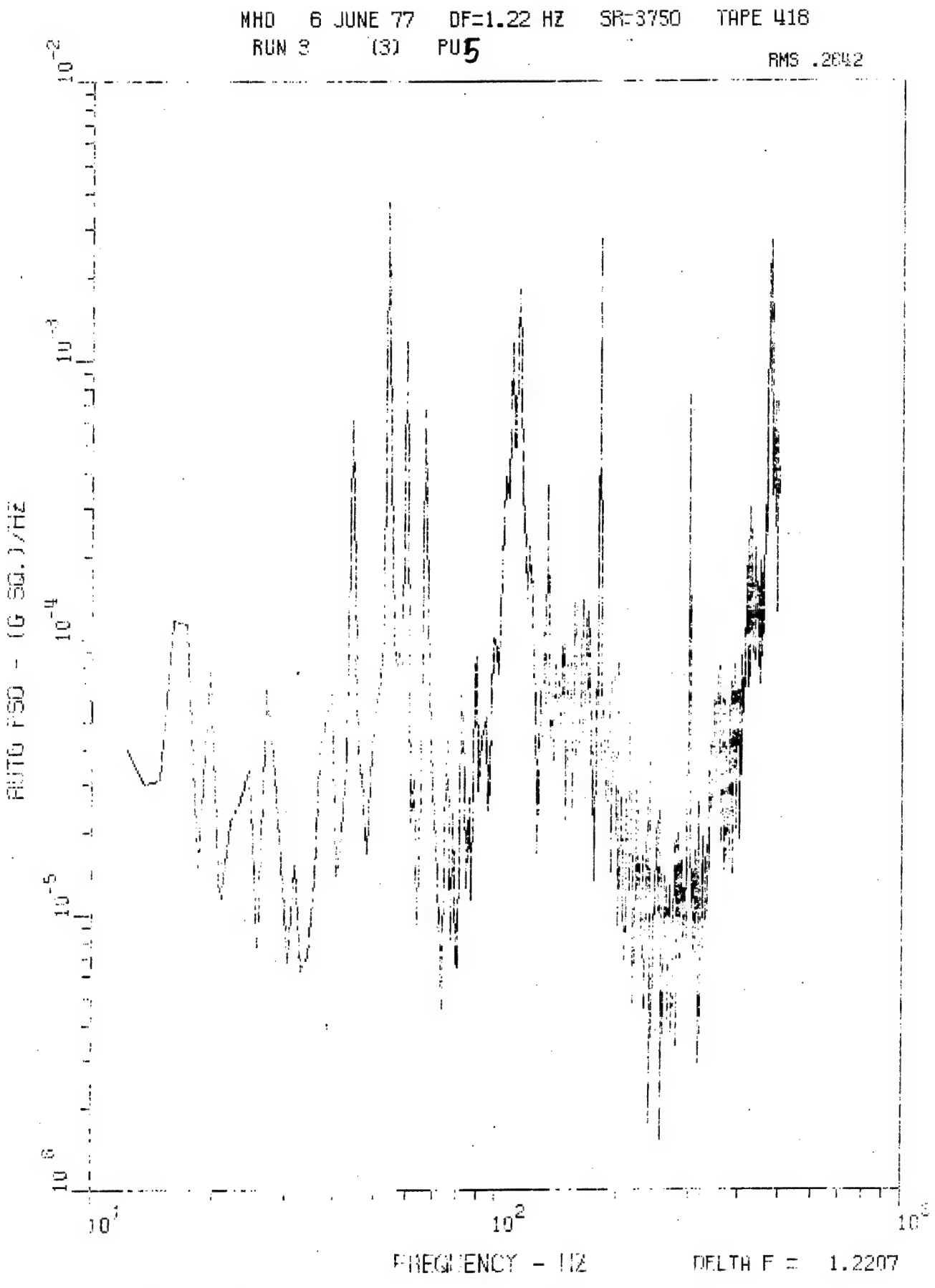


Figure 27. Accelerometer 5 PSD, 0-500 Hz, Run LWC 3.

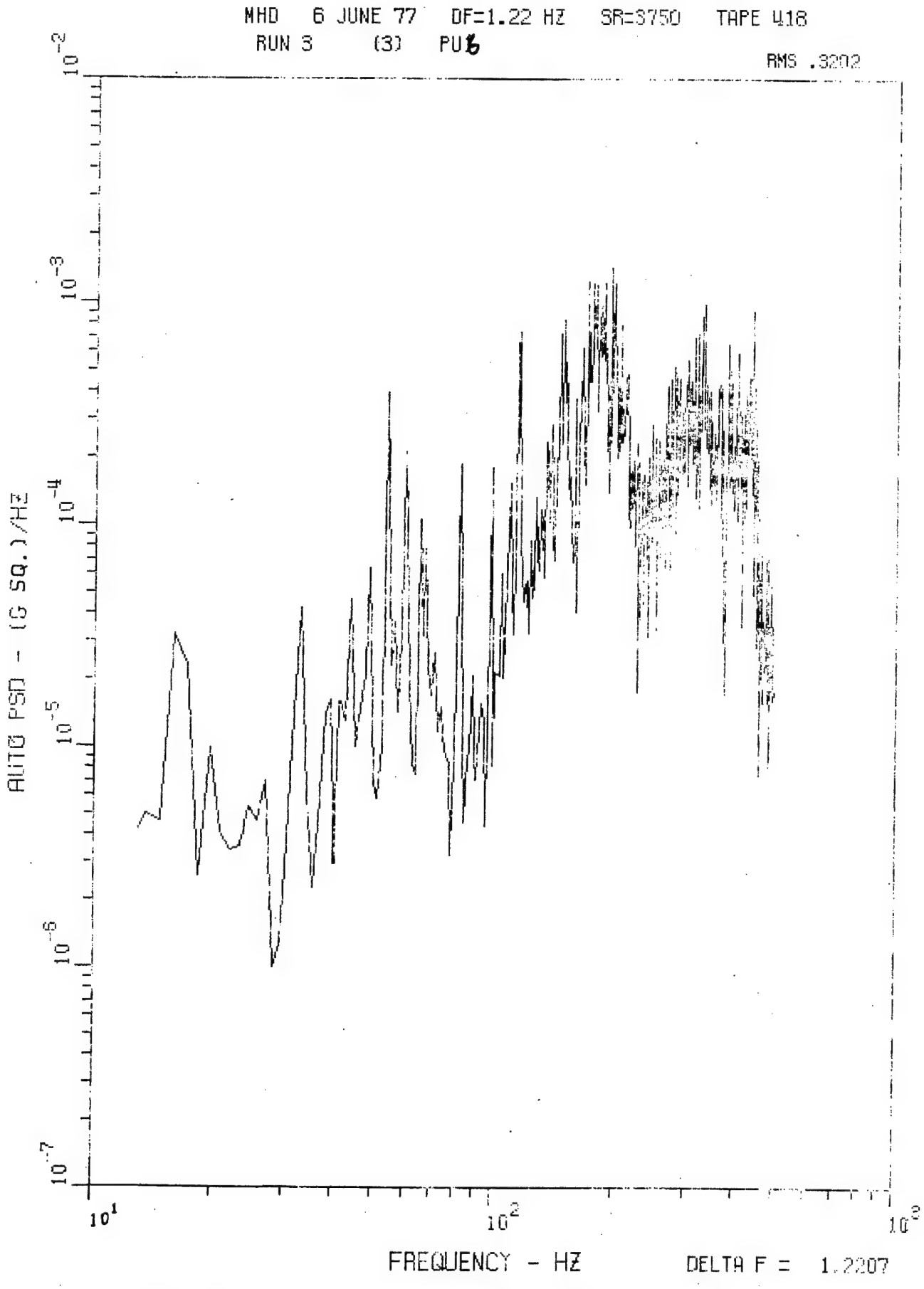


Figure 28. Accelerometer 6 PSD, 0-500 Hz, Run LWC 3.

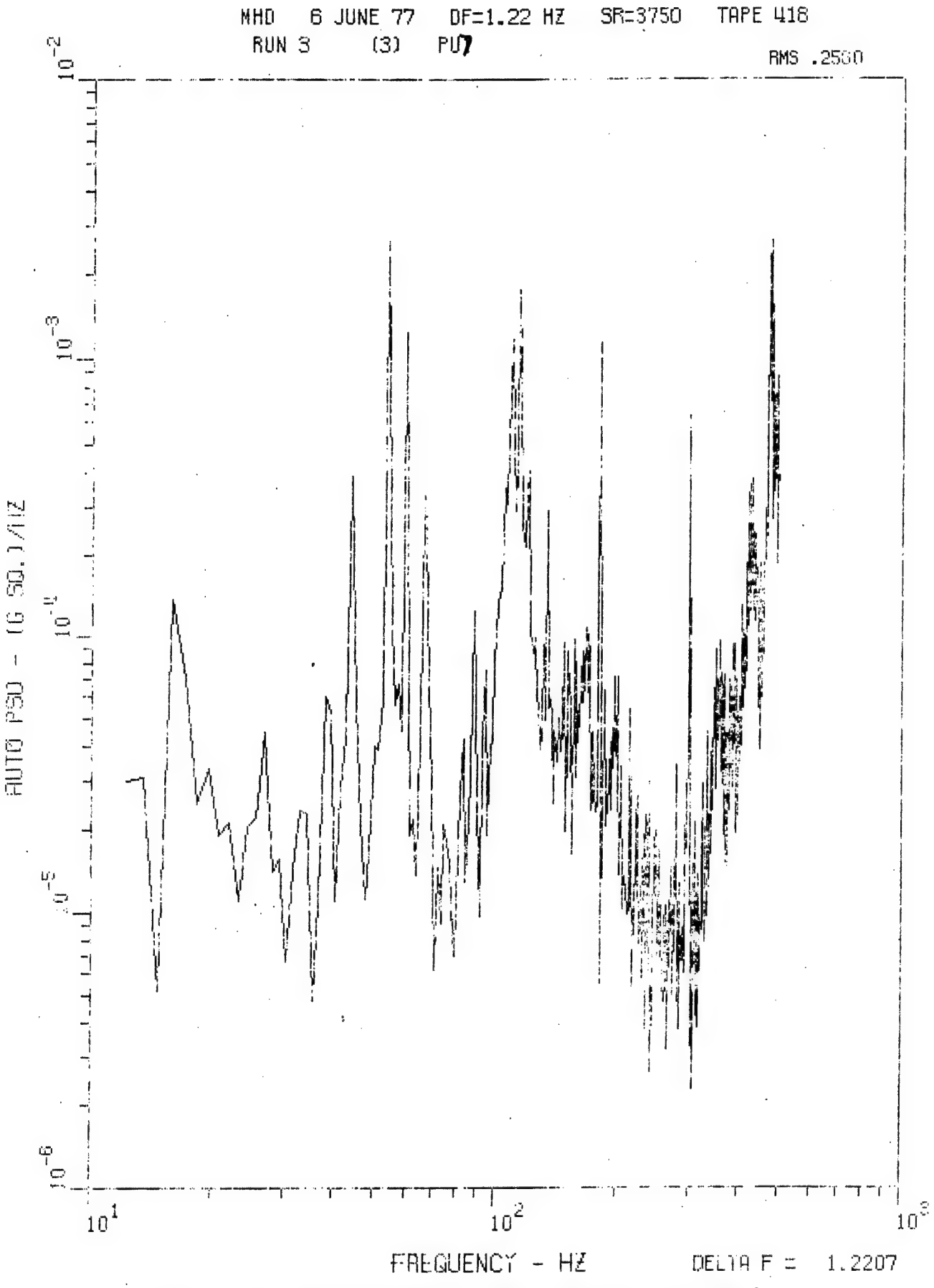


**Figure 29. Accelerometer 7 PSD, 0-500 Hz, Run LWC 3.**

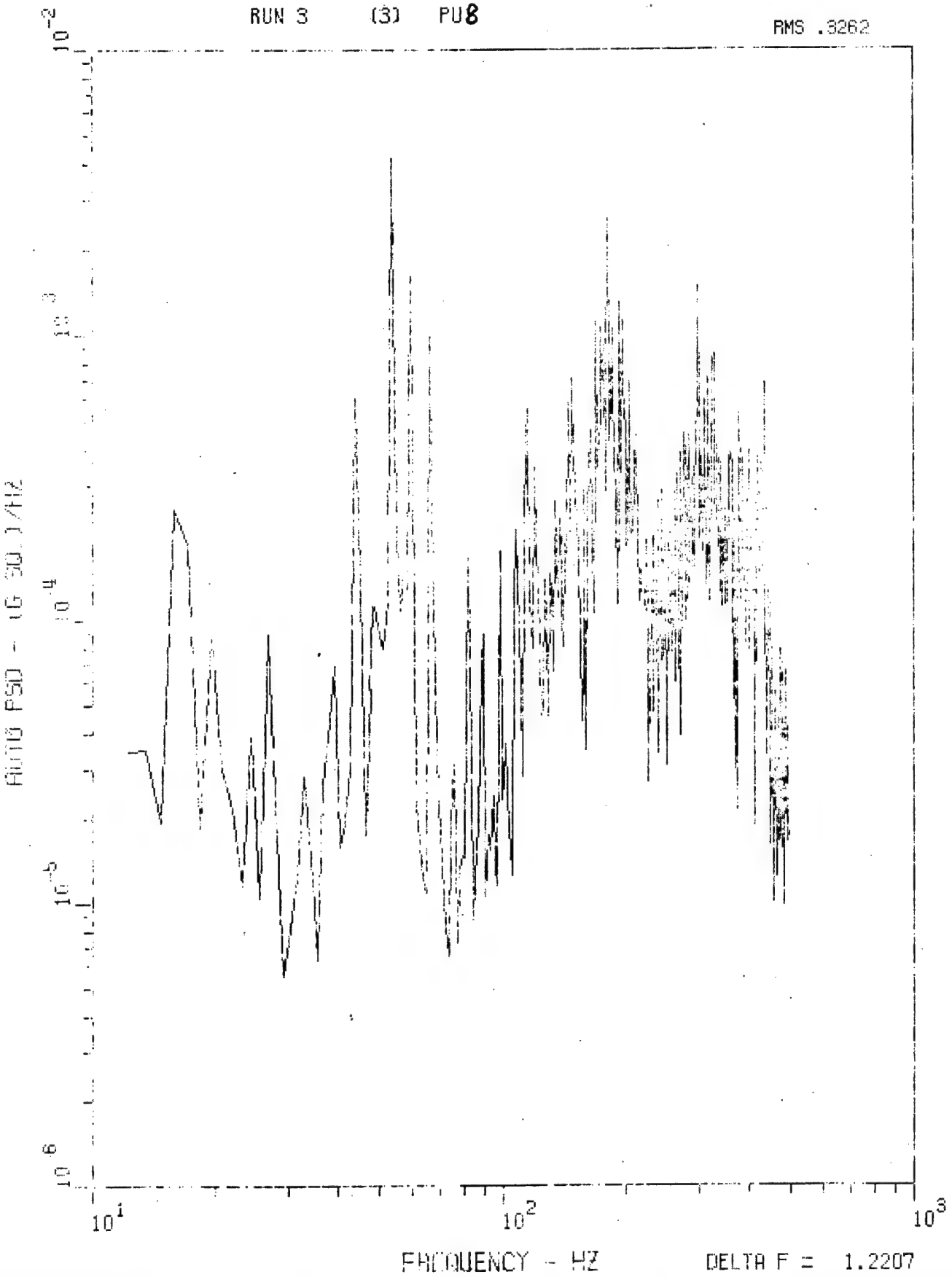


**Figure 30. Accelerometer 8 PSD, 0-500 Hz, Run LWC 3.**

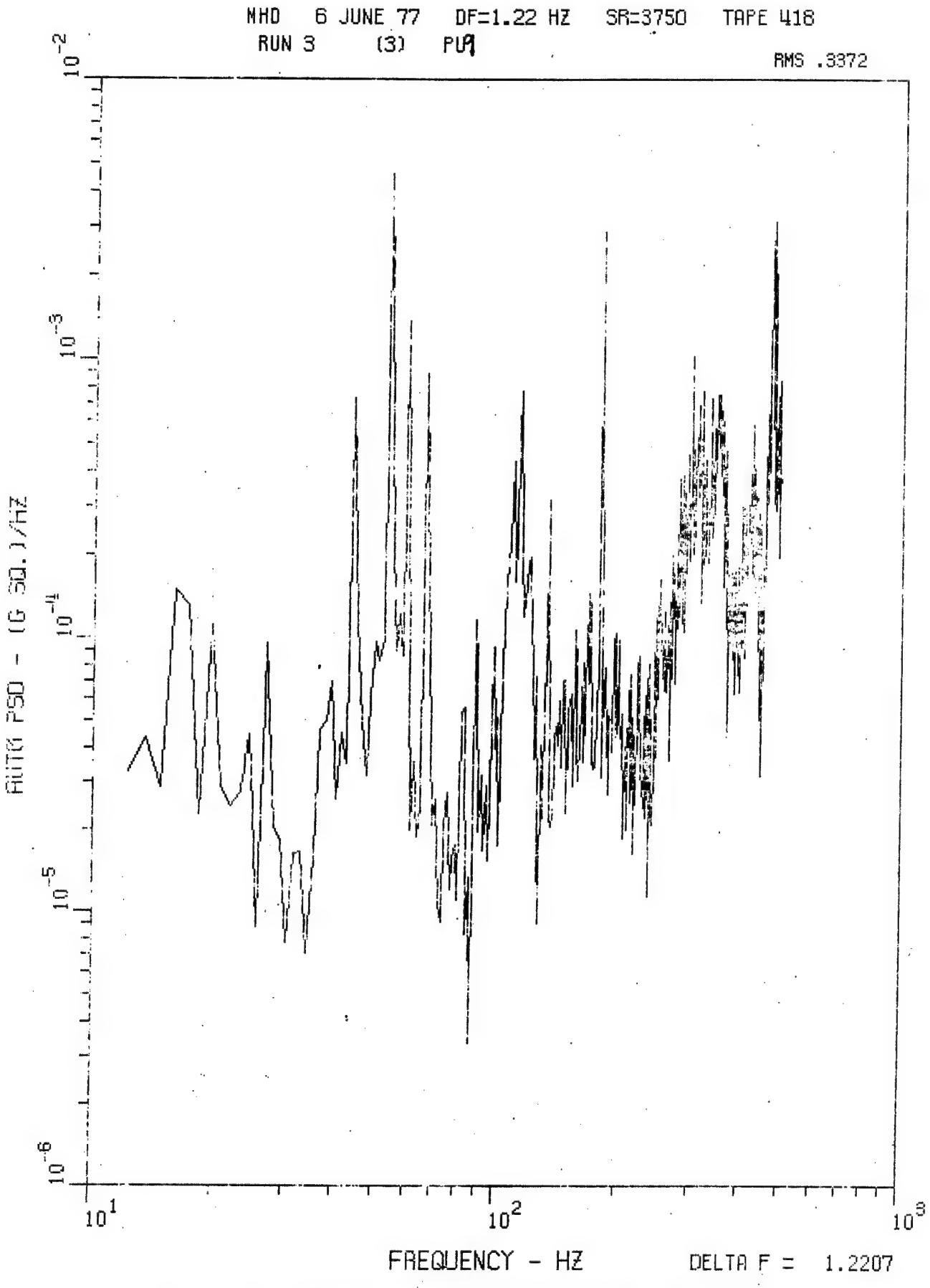


**Figure 31. Accelerometer 9 PSD, 0-500 Hz, Run LWC 3.**

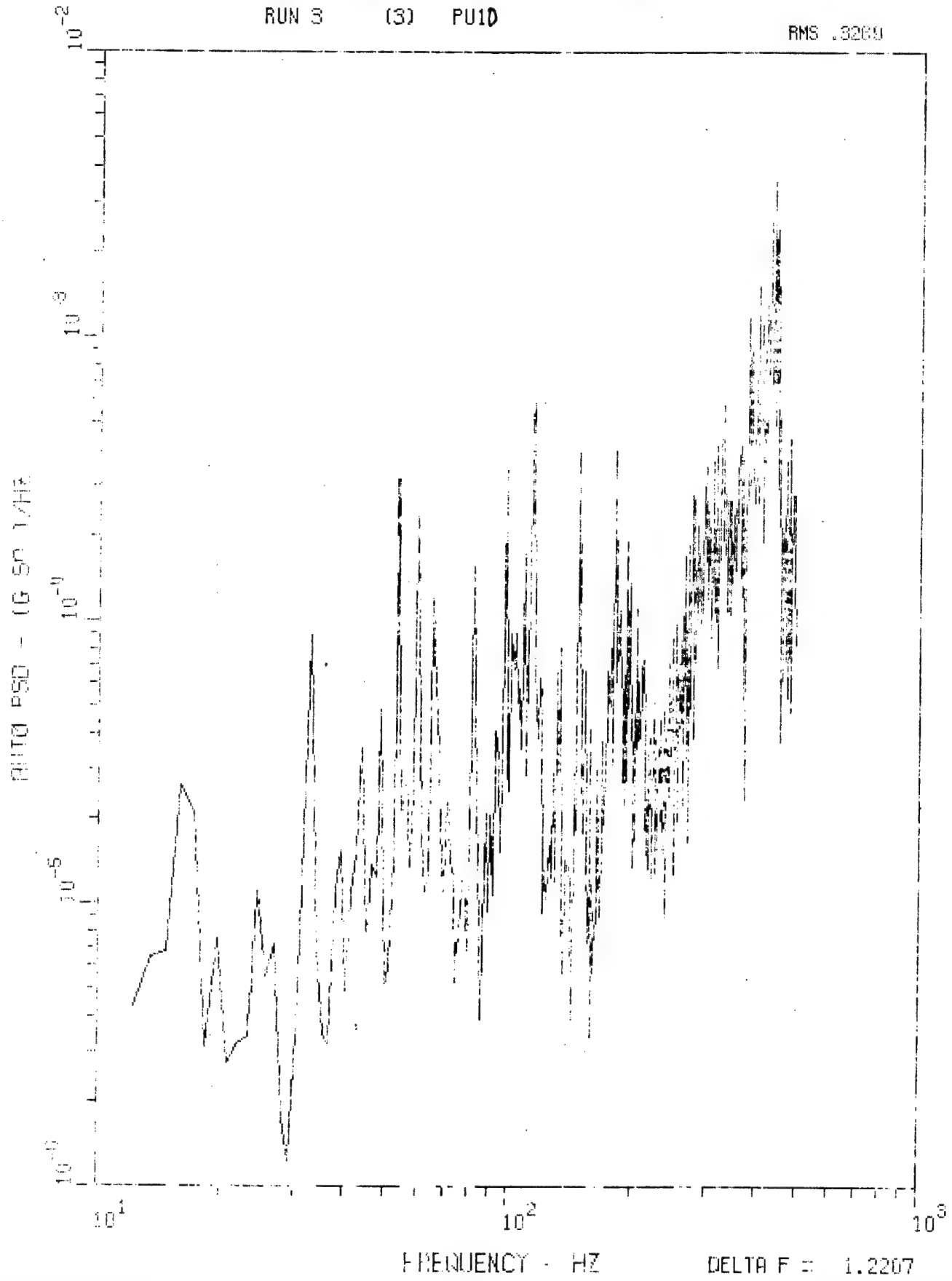


Figure 32. Accelerometer 10 PSD, 0-500 Hz, Run LWC 3.

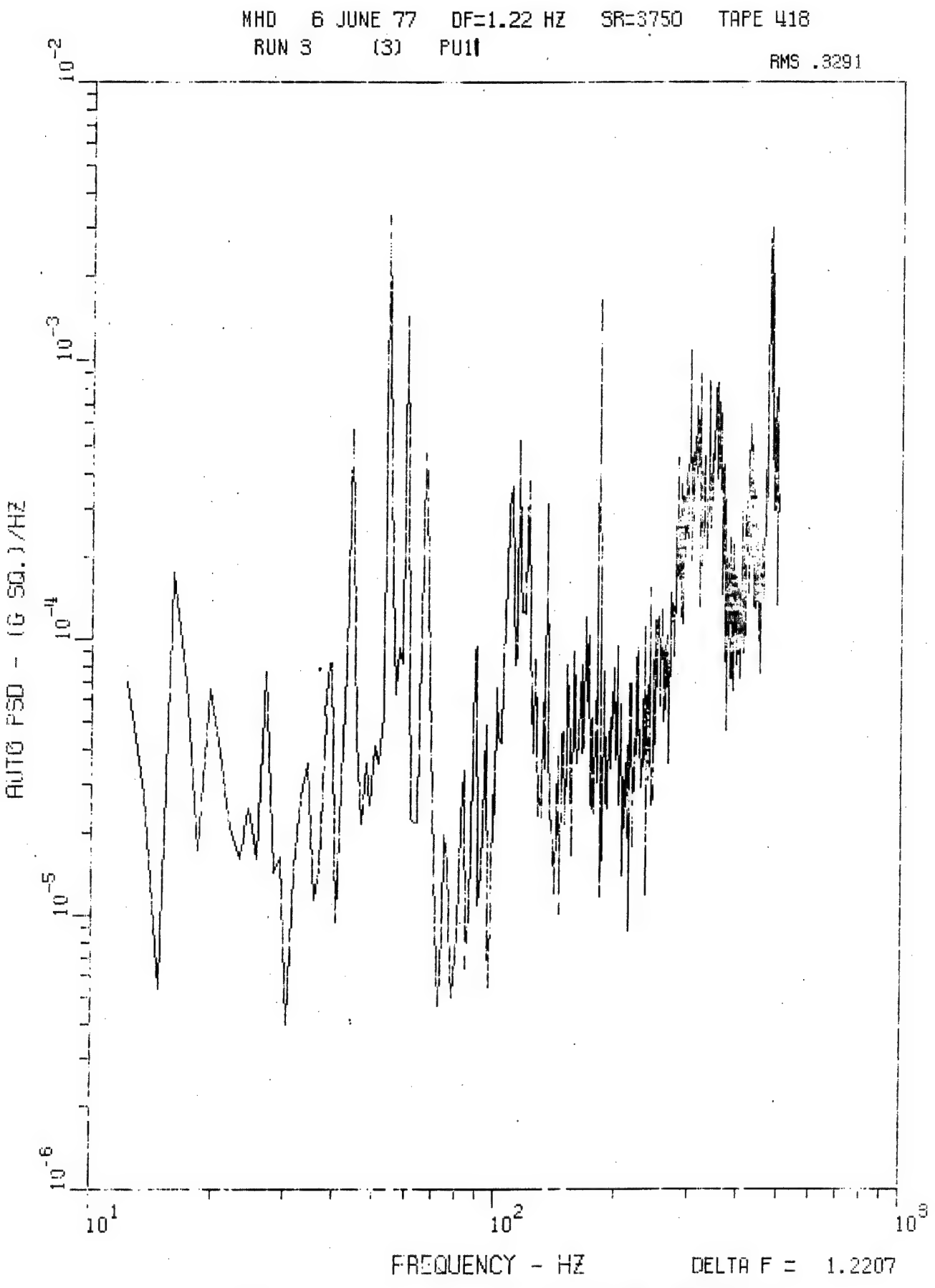


Figure 33. Accelerometer 11 PSD, 0-500 Hz, Run LWC 3.

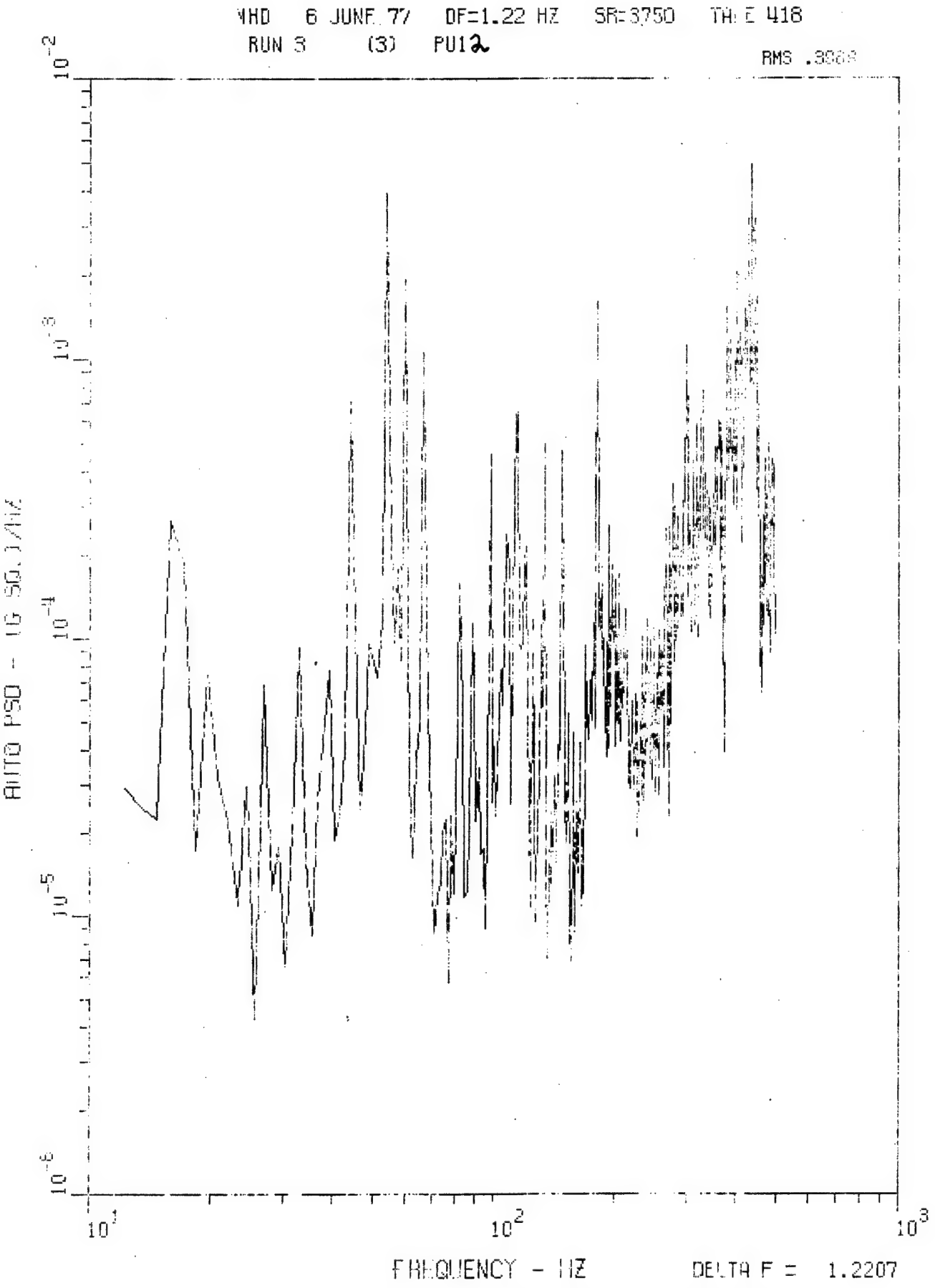


Figure 34. Accelerometer 12 PSD, 0-500 Hz, Run LWC 3.

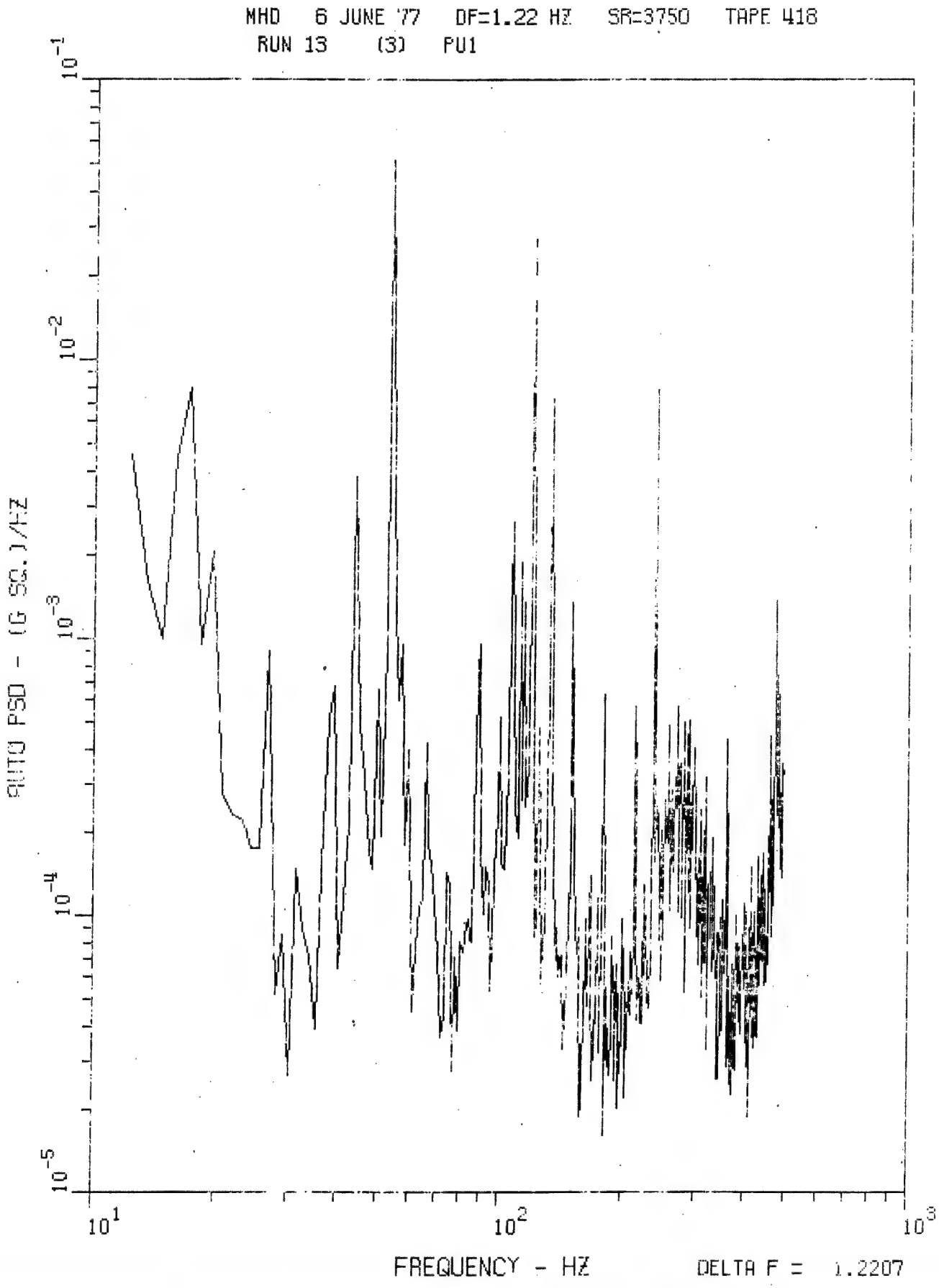


Figure 35. Accelerometer 1 PSD, 0-500 Hz, Run LWC 13.

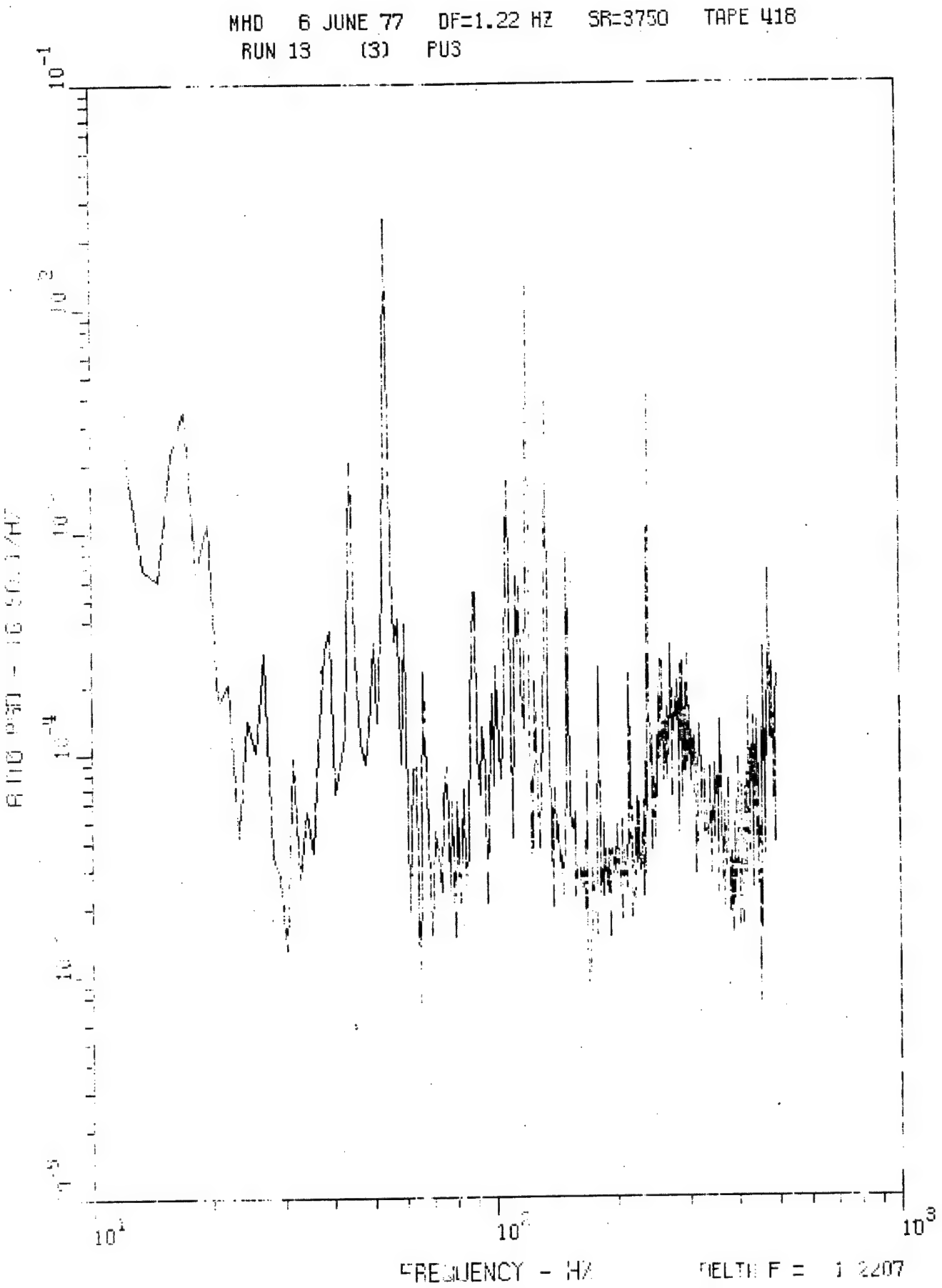


Figure 36. Accelerometer 3 PSD, 0-500 Hz, Run LWC 13.

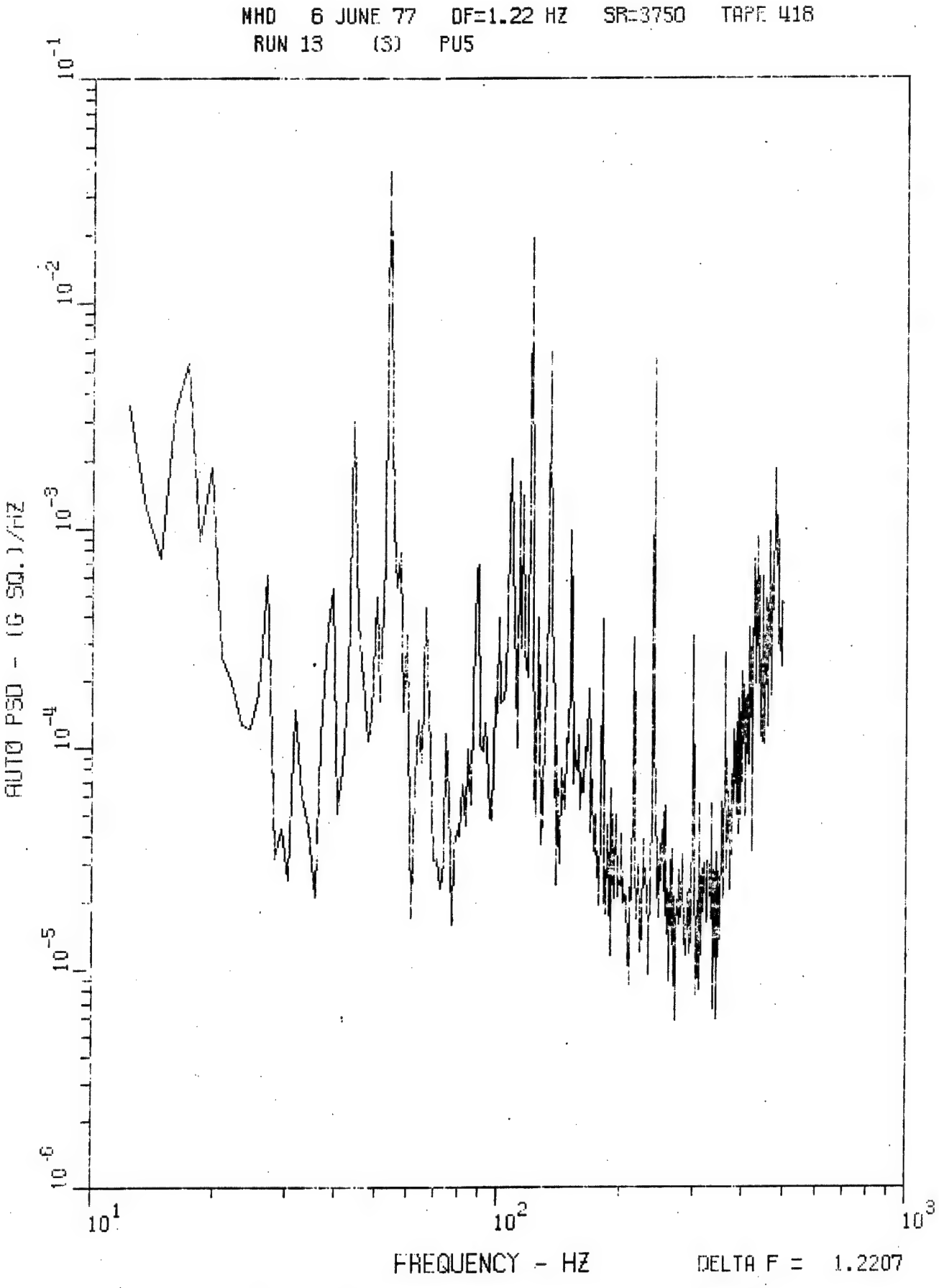


Figure 37. Accelerometer 5 PSD, 0-500 Hz, Run LWC 13.

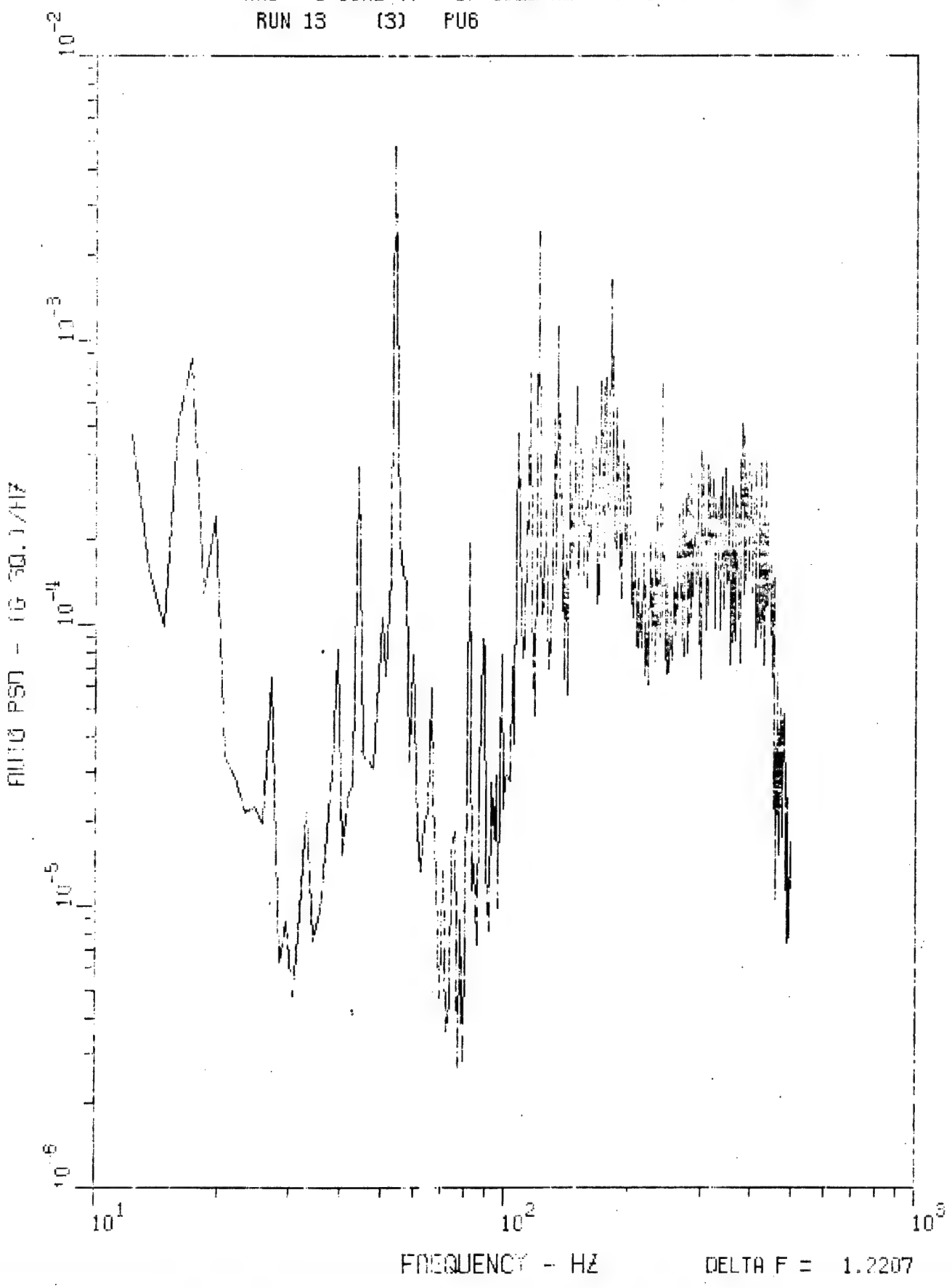


Figure 38. Accelerometer 6 PSD, 0-500 Hz, Run LWC 13.

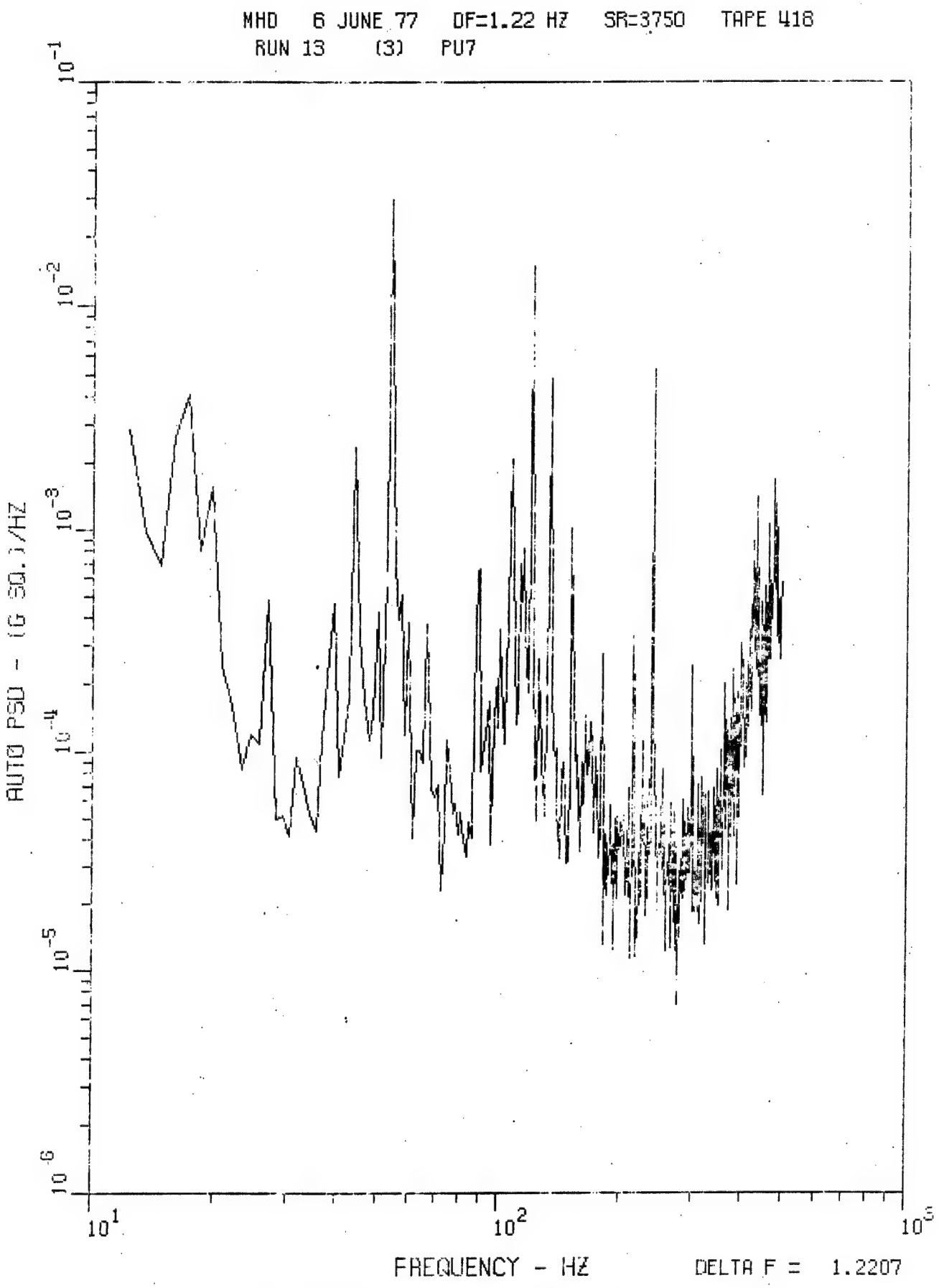


**Figure 39. Accelerometer 7 PSD, 0-500 Hz, Run LWC 13.**

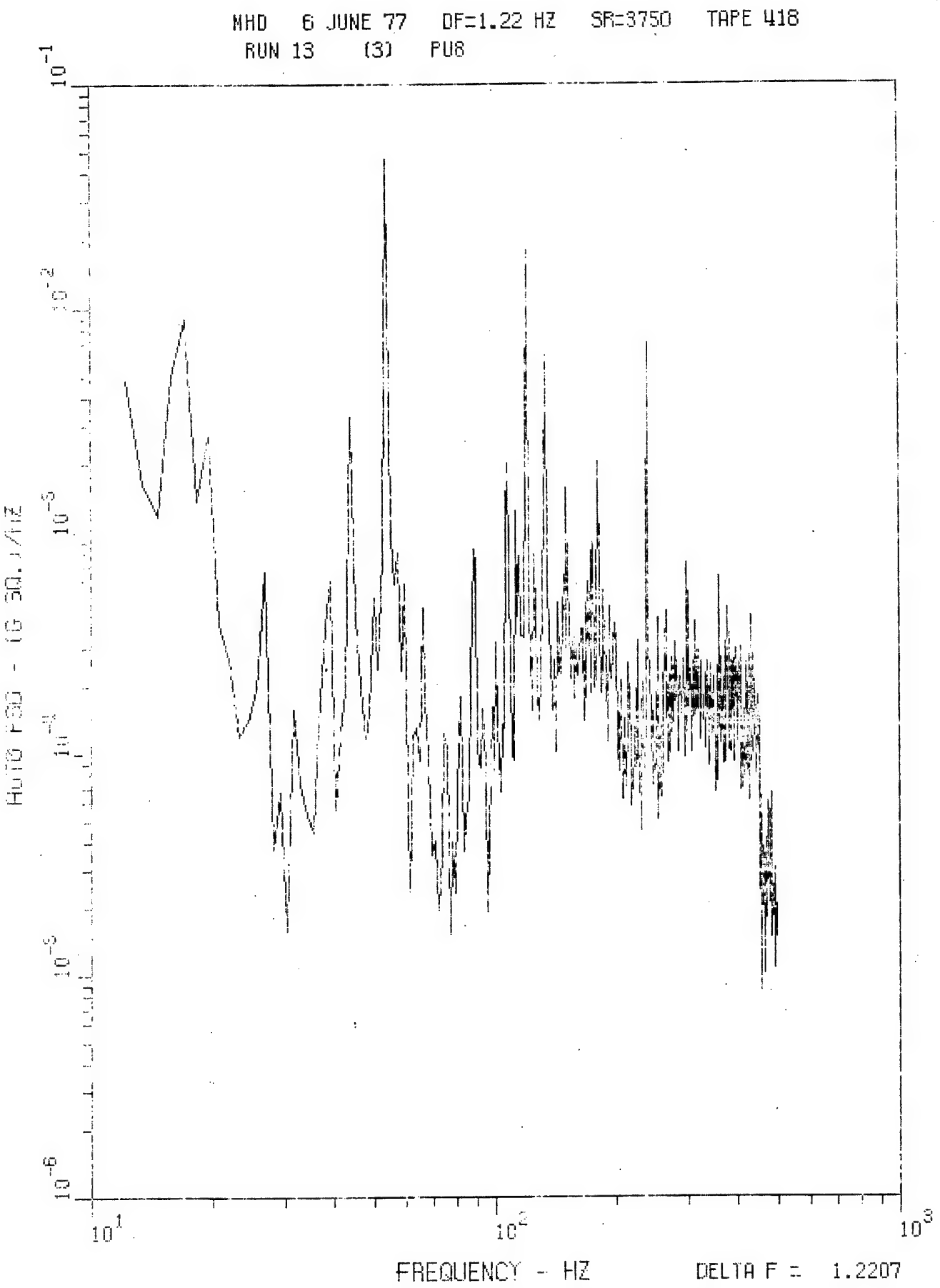


Figure 40. Accelerometer 8 PSD, 0-500 Hz, Run LWC 13.

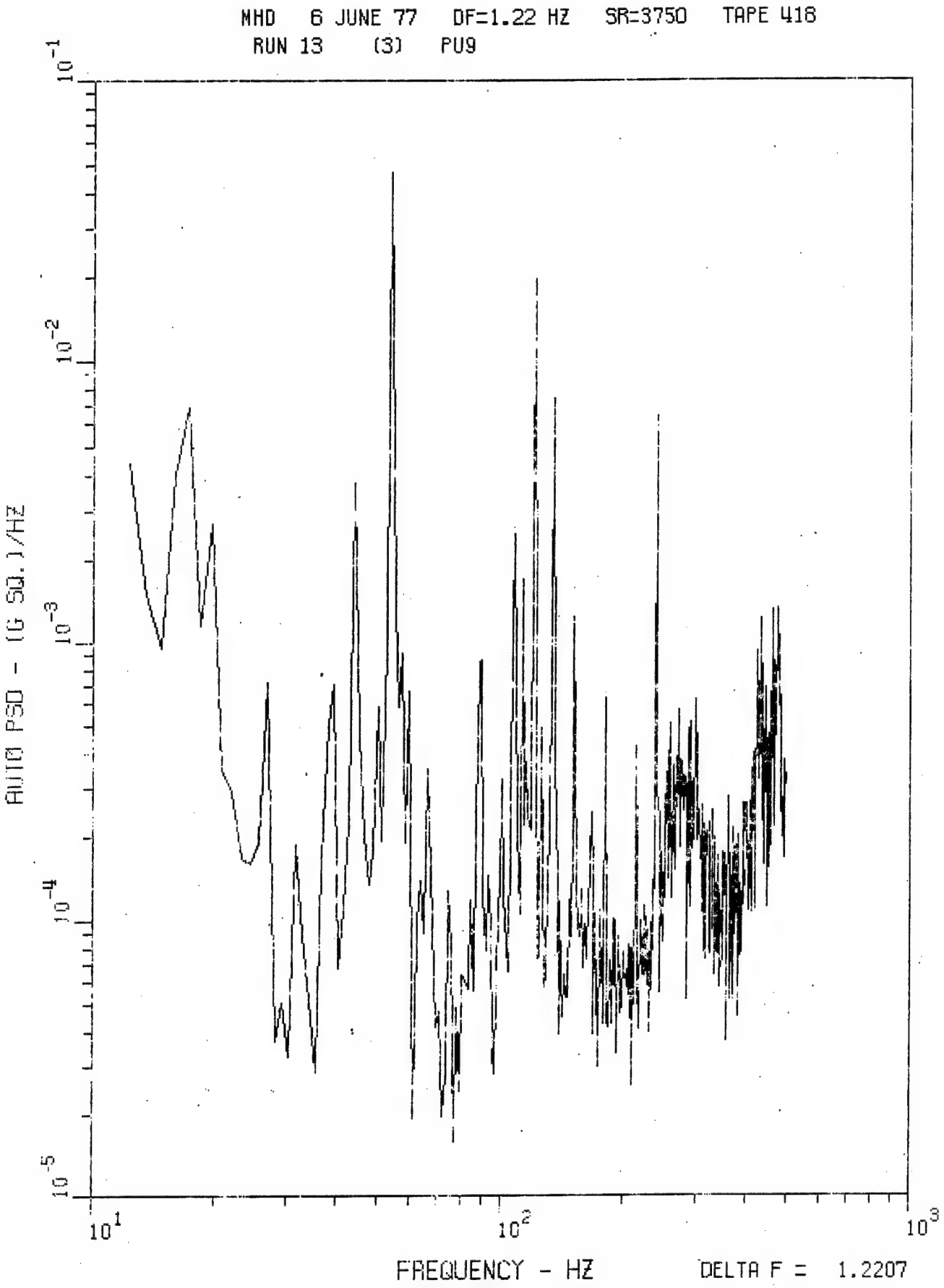


**Figure 41. Accelerometer 9 PSD, 0-500 Hz, Run LWC 13.**

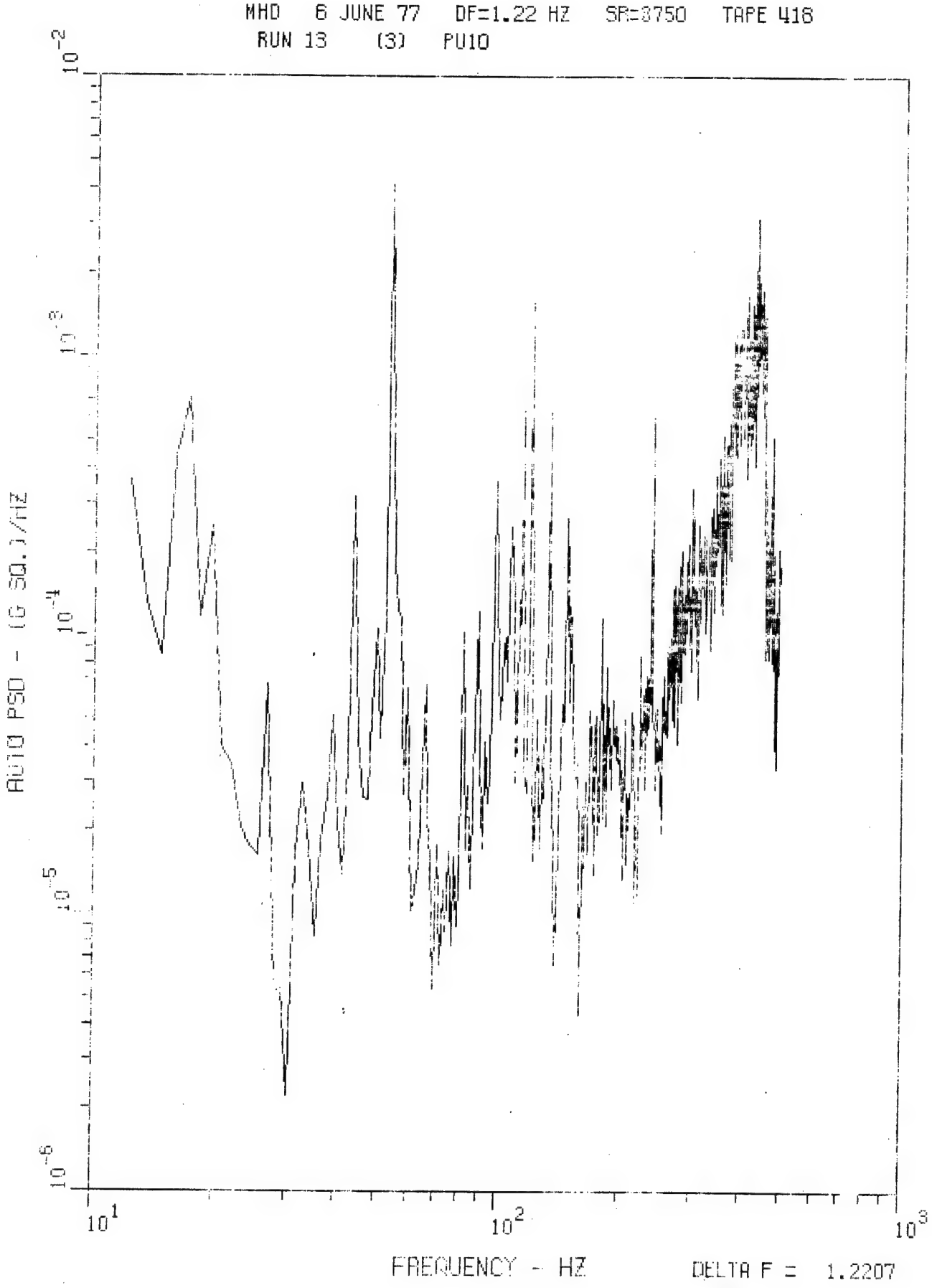


Figure 42. Accelerometer 10 PSD, 0-500 Hz, Run LWC 13.

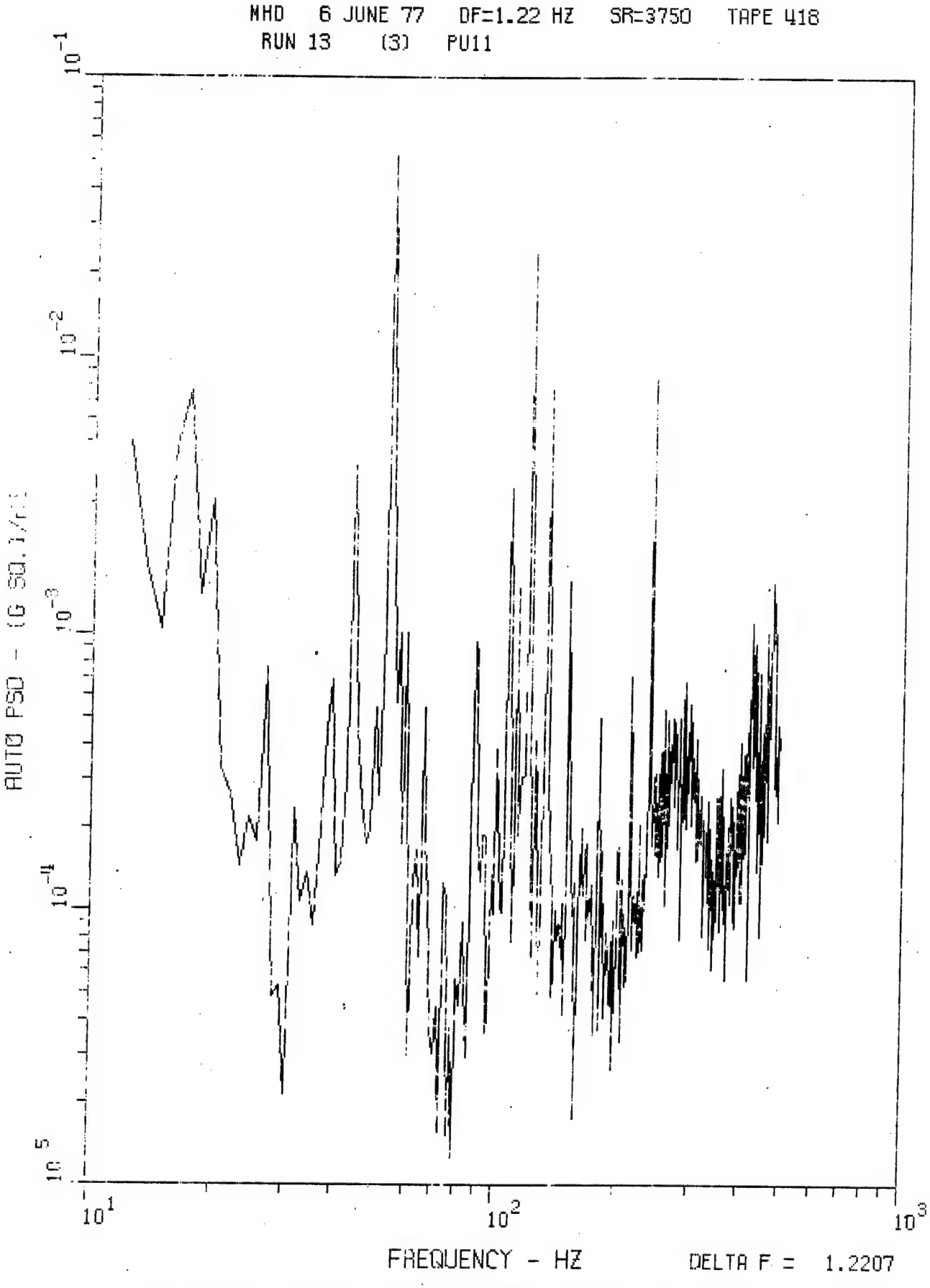


Figure 43. Accelerometer 11 PSD, 0-500 Hz, Run LWC 13.

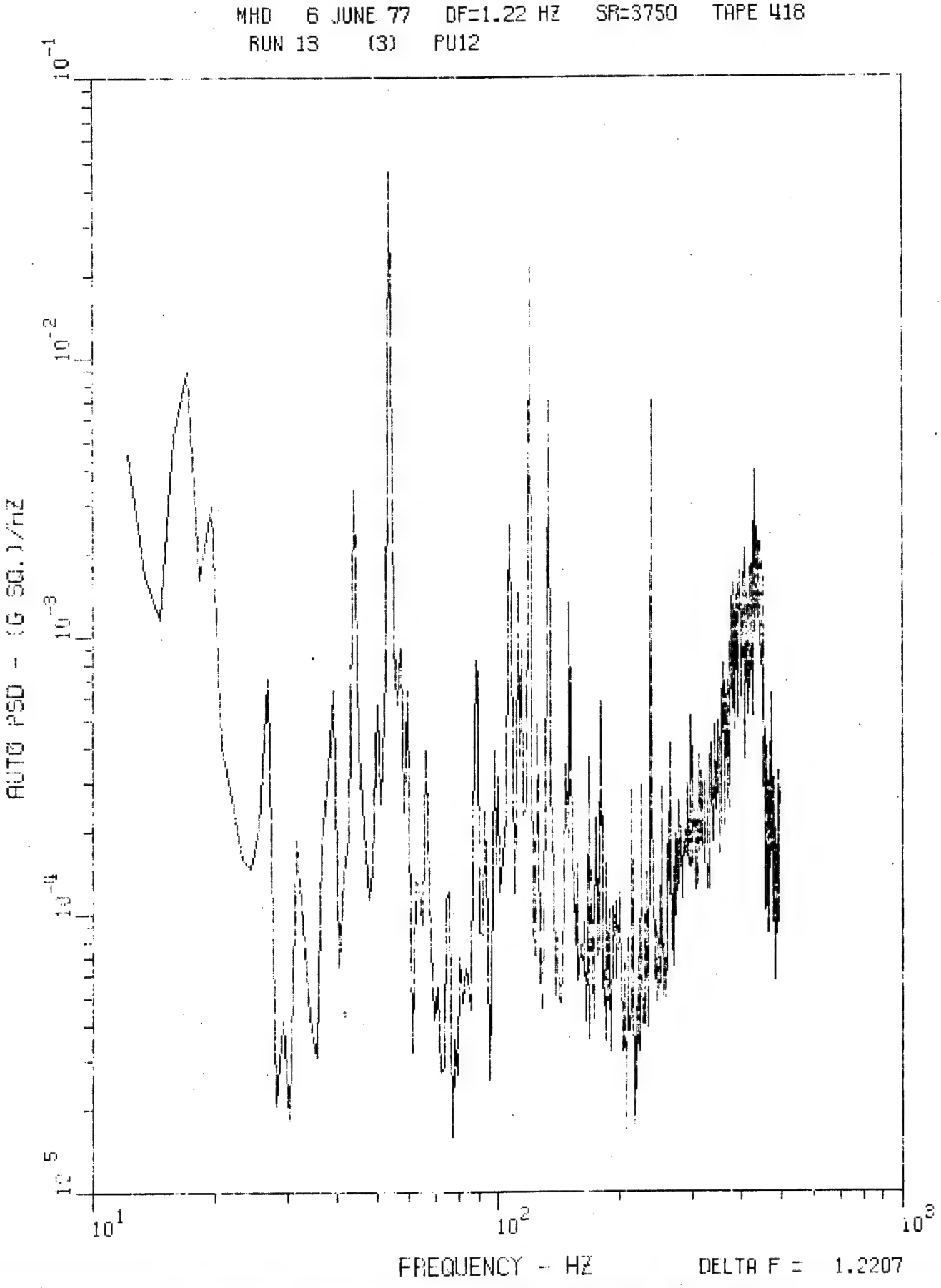


**Figure 44.** Accelerometer 12 PSD, 0-500 Hz, Run LWC 13.

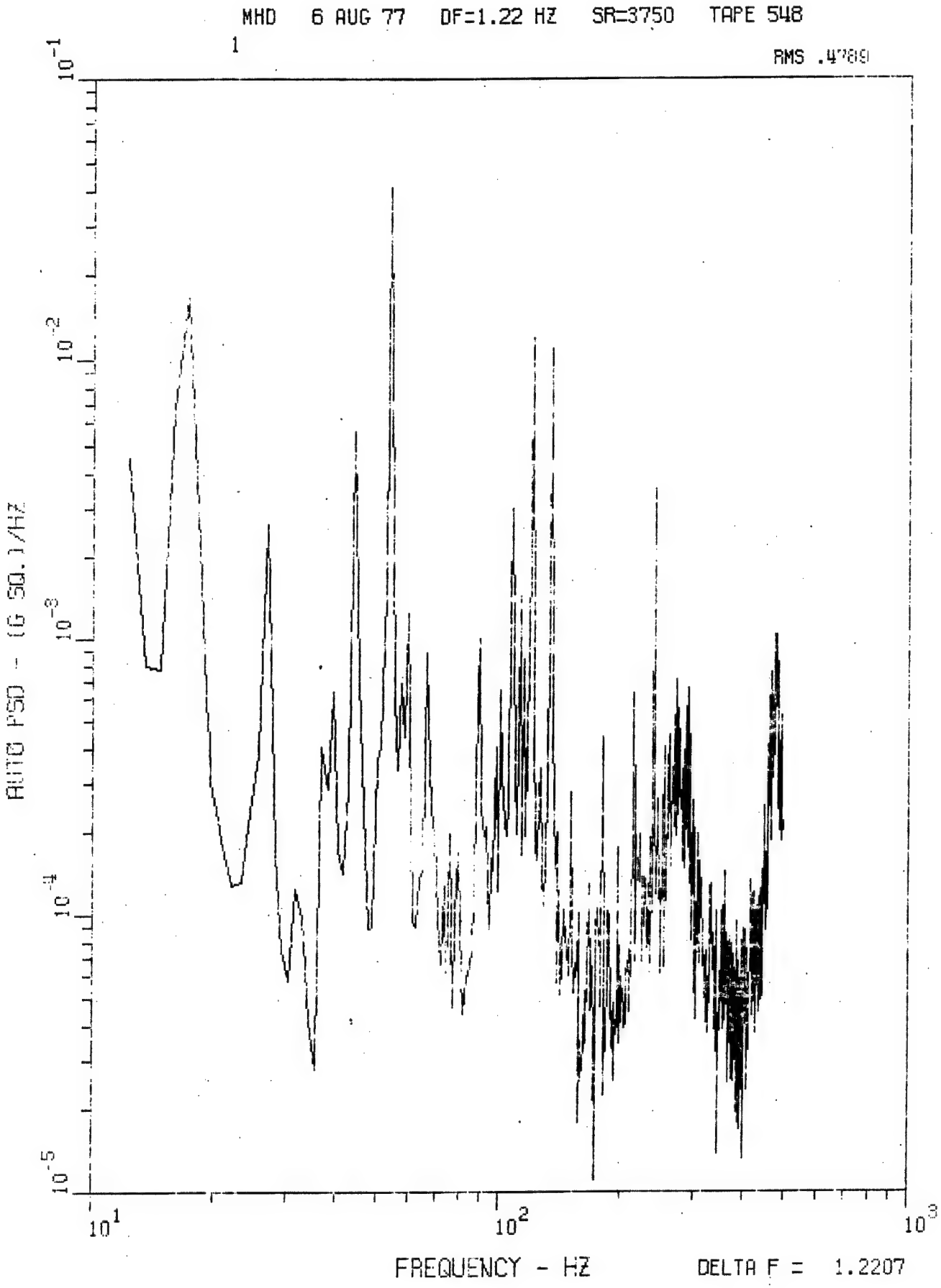


Figure 45. Accelerometer 1 PSD, 0-500 Hz, Run LWC 23.

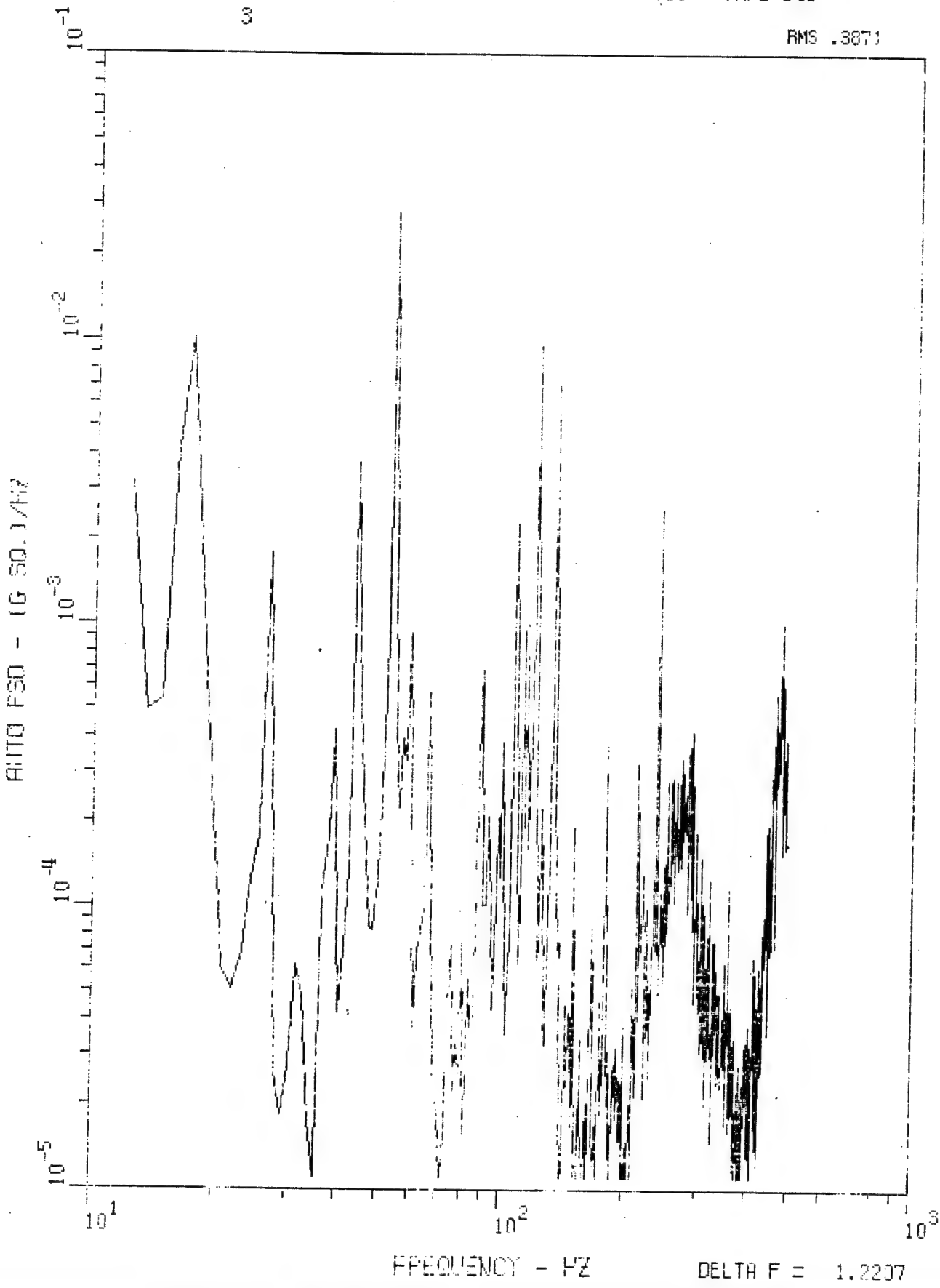


Figure 46. Accelerometer 3 PSD, 0-500 Hz, Run LWC 23.

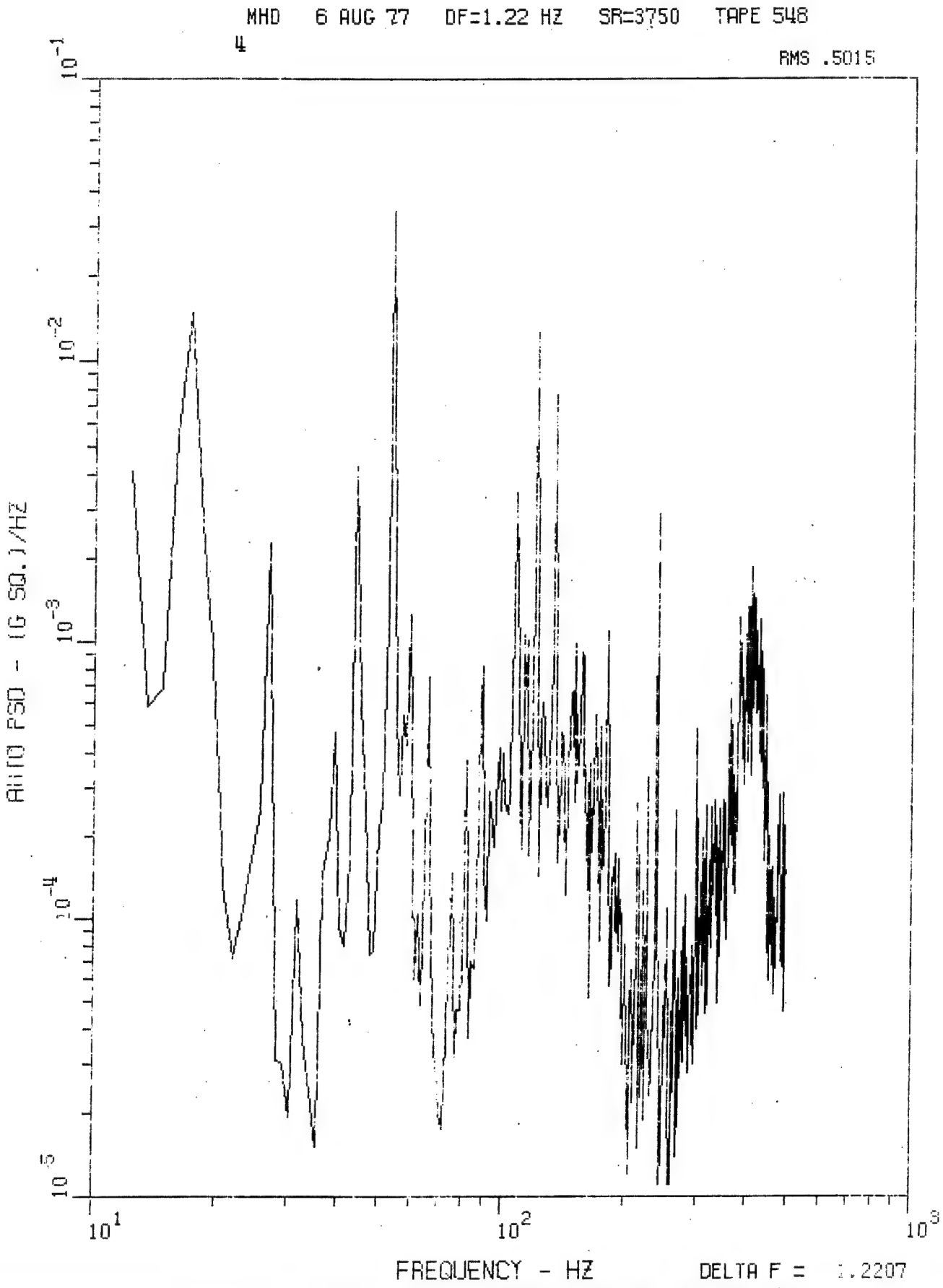


**Figure 47. Accelerometer 4 PSD, 0-500 Hz, Run LWC 23.**

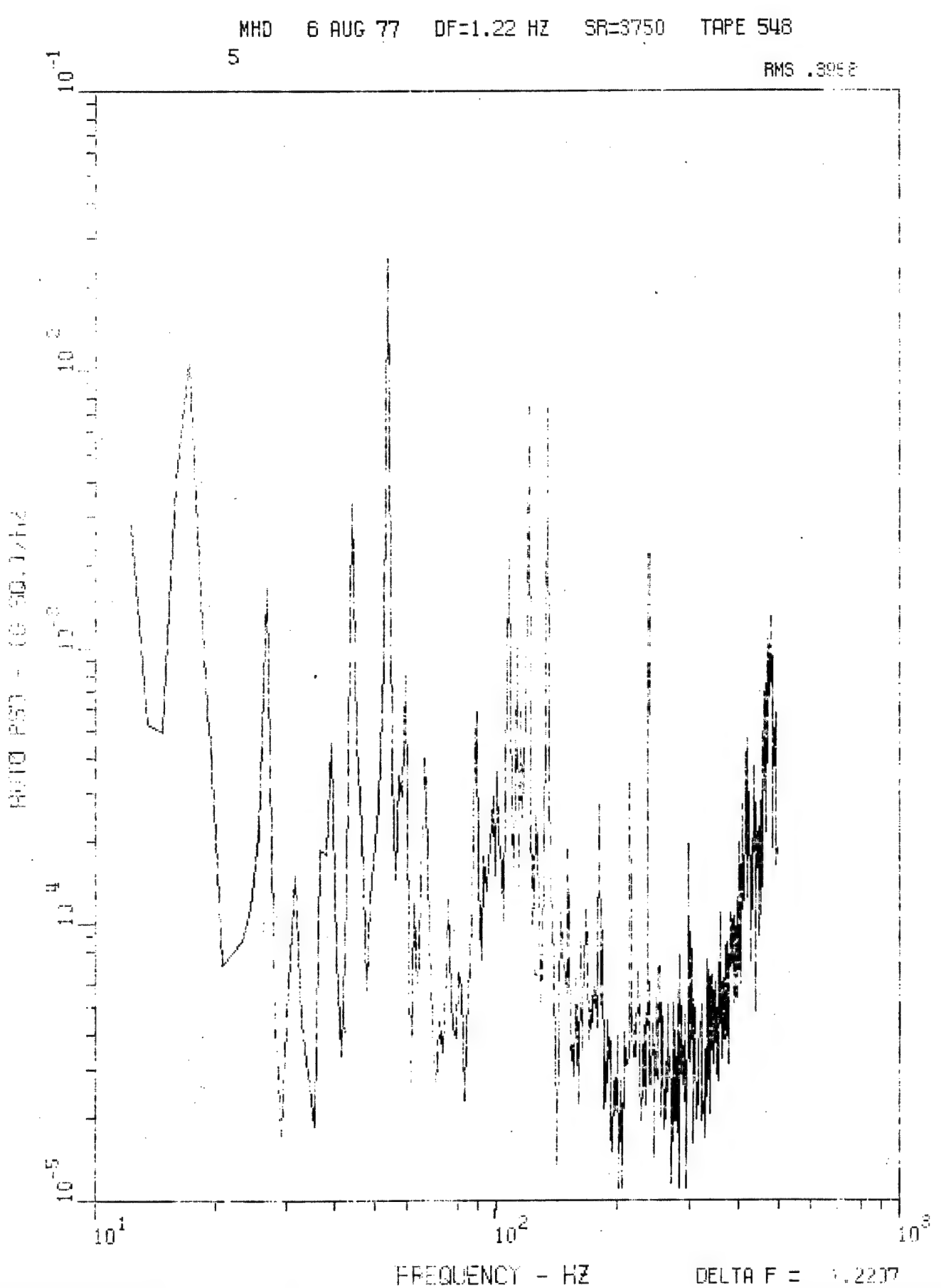


Figure 48. Accelerometer 5 PSD, 0-500 Hz, Run LWC 23.

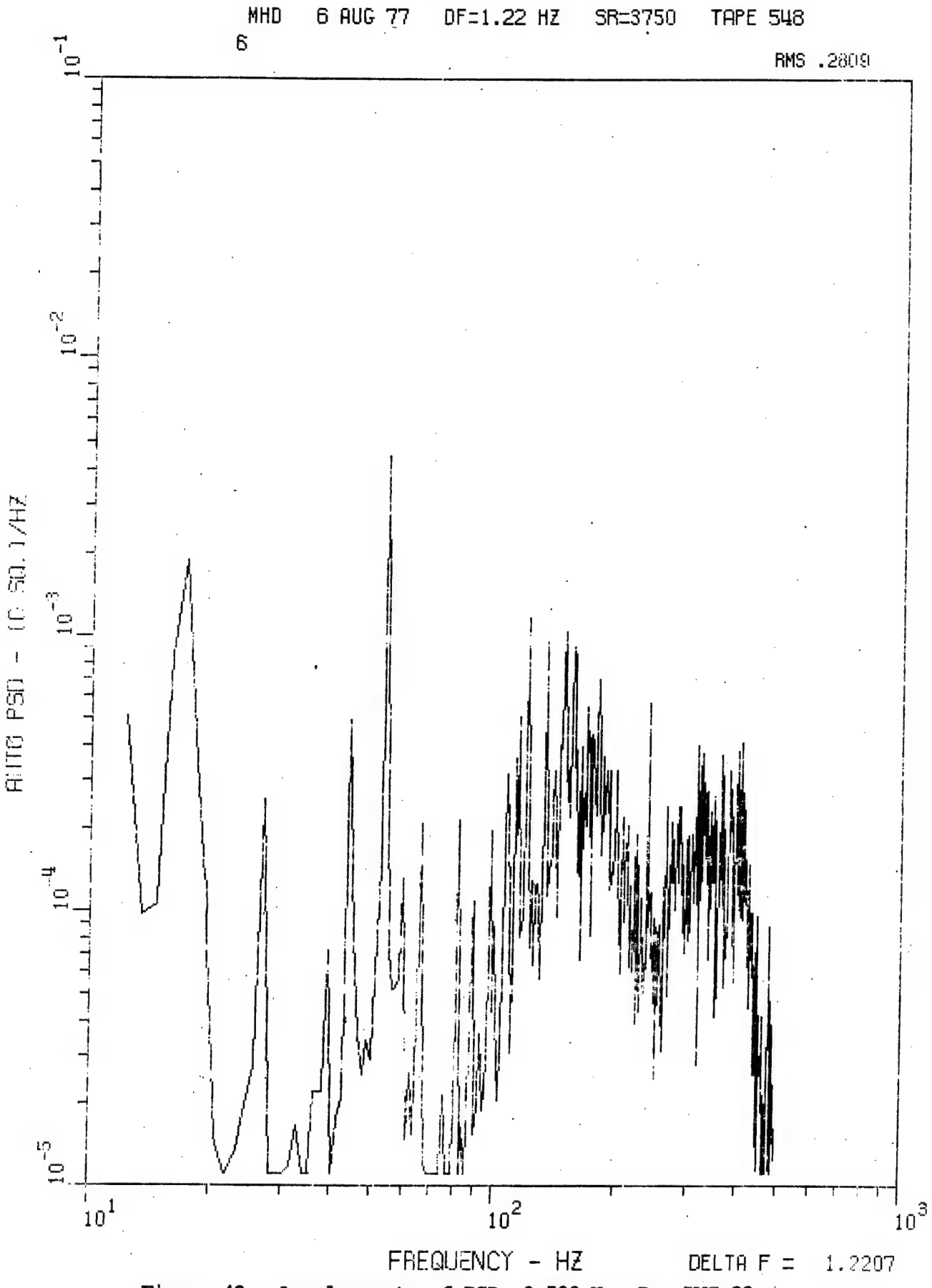


**Figure 49. Accelerometer 6 PSD, 0-500 Hz, Run LWC 23.**

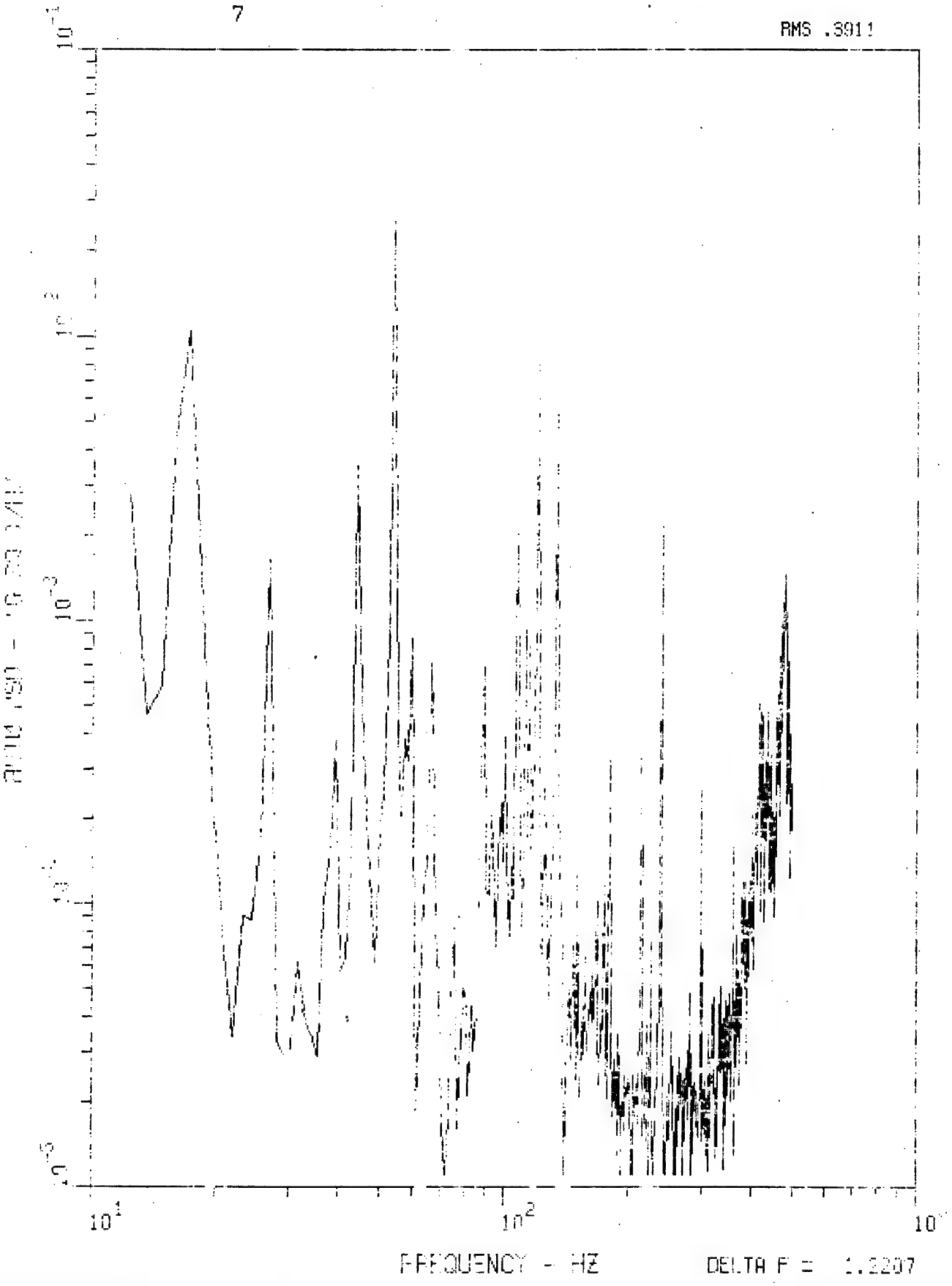


Figure 50. Accelerometer 7 PSD, 0-500 Hz, Run LWC 23.

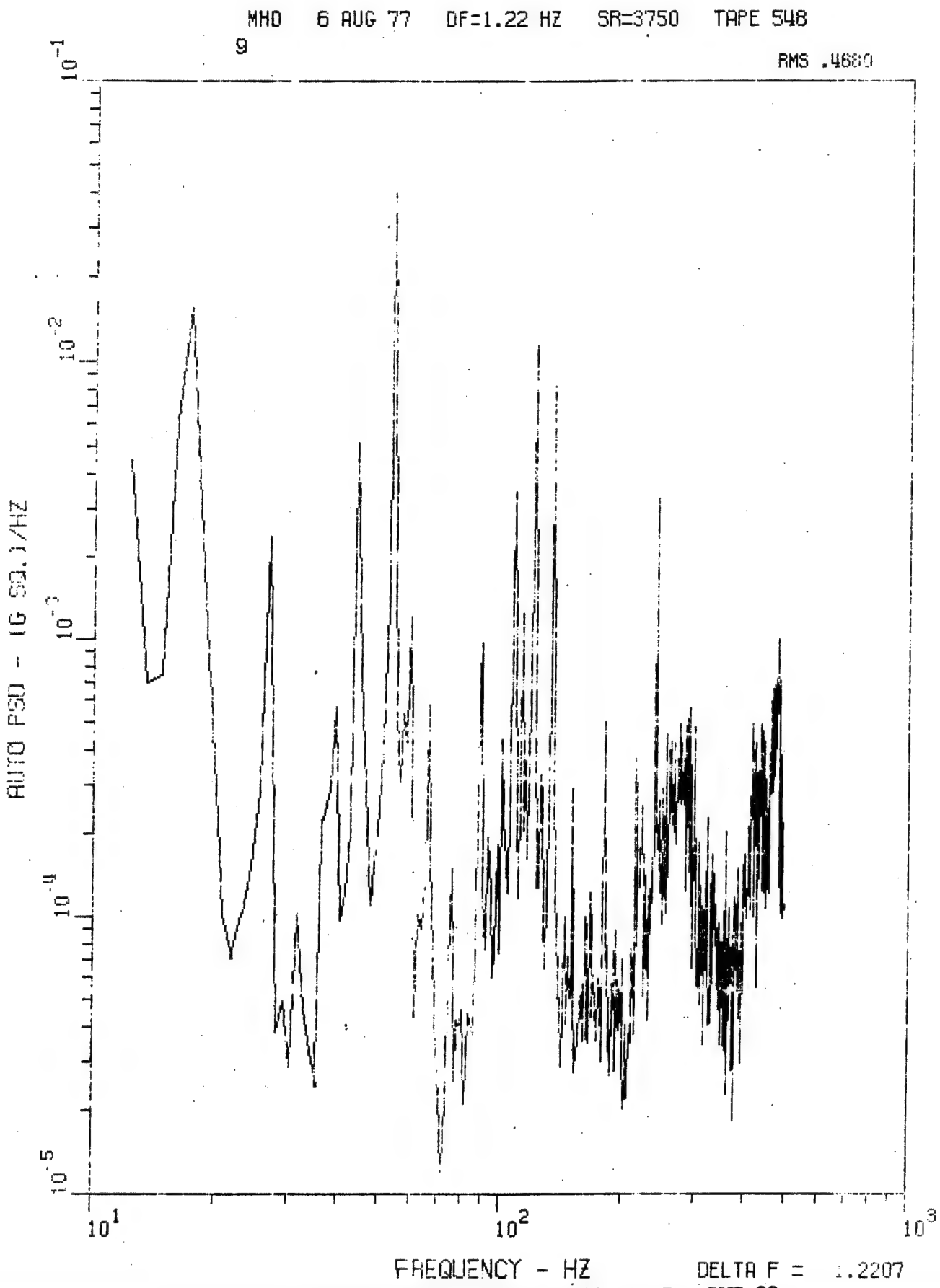


**Figure 51. Accelerometer 9 PSD, 0-500 Hz, Run LWC 23.**

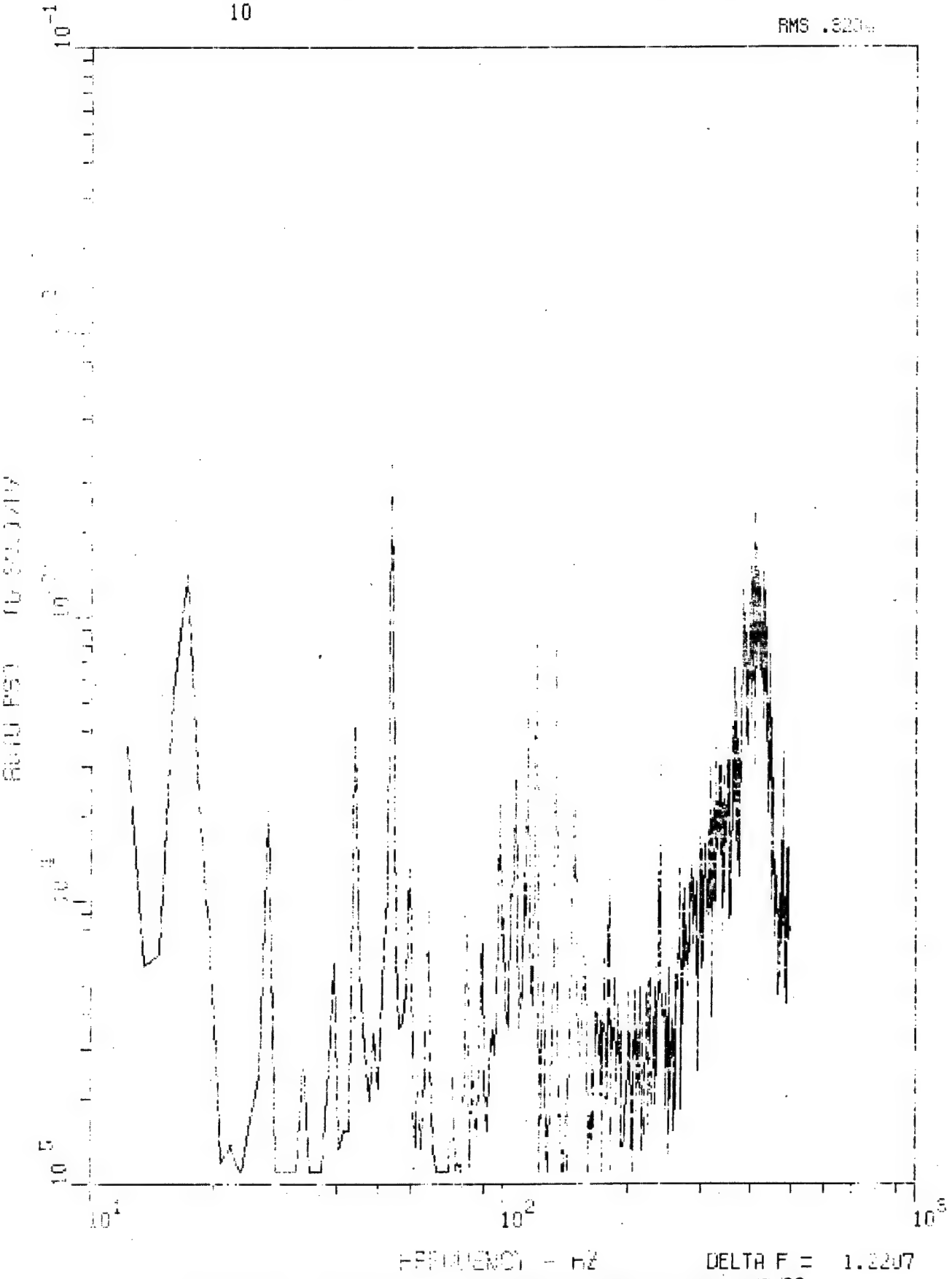


Figure 52. Accelerometer 10 PSD, 0-500 Hz, Run LWC 23.

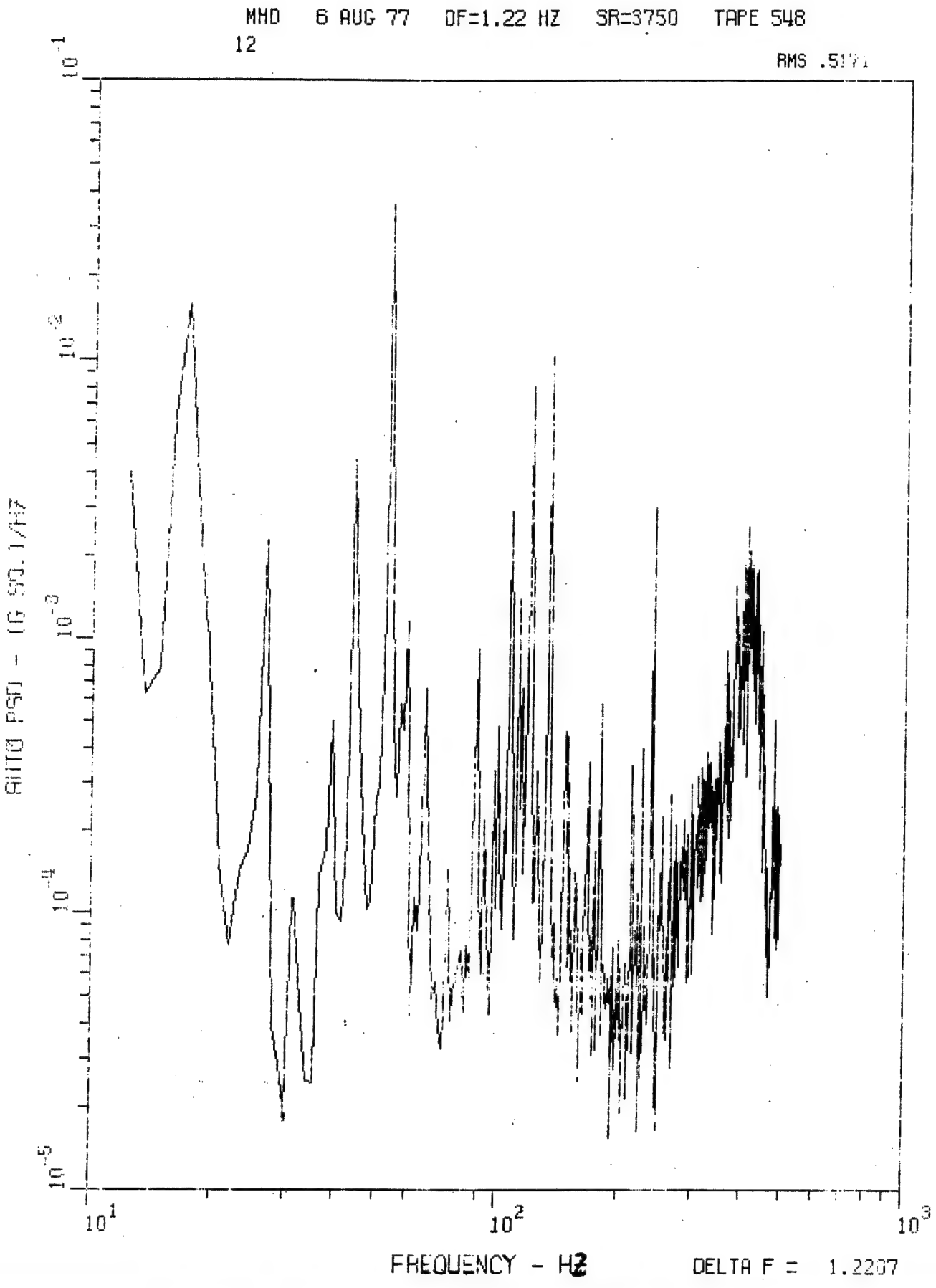


**Figure 53. Accelerometer 12 PSD, 0-500 Hz, Run LWC 23.**

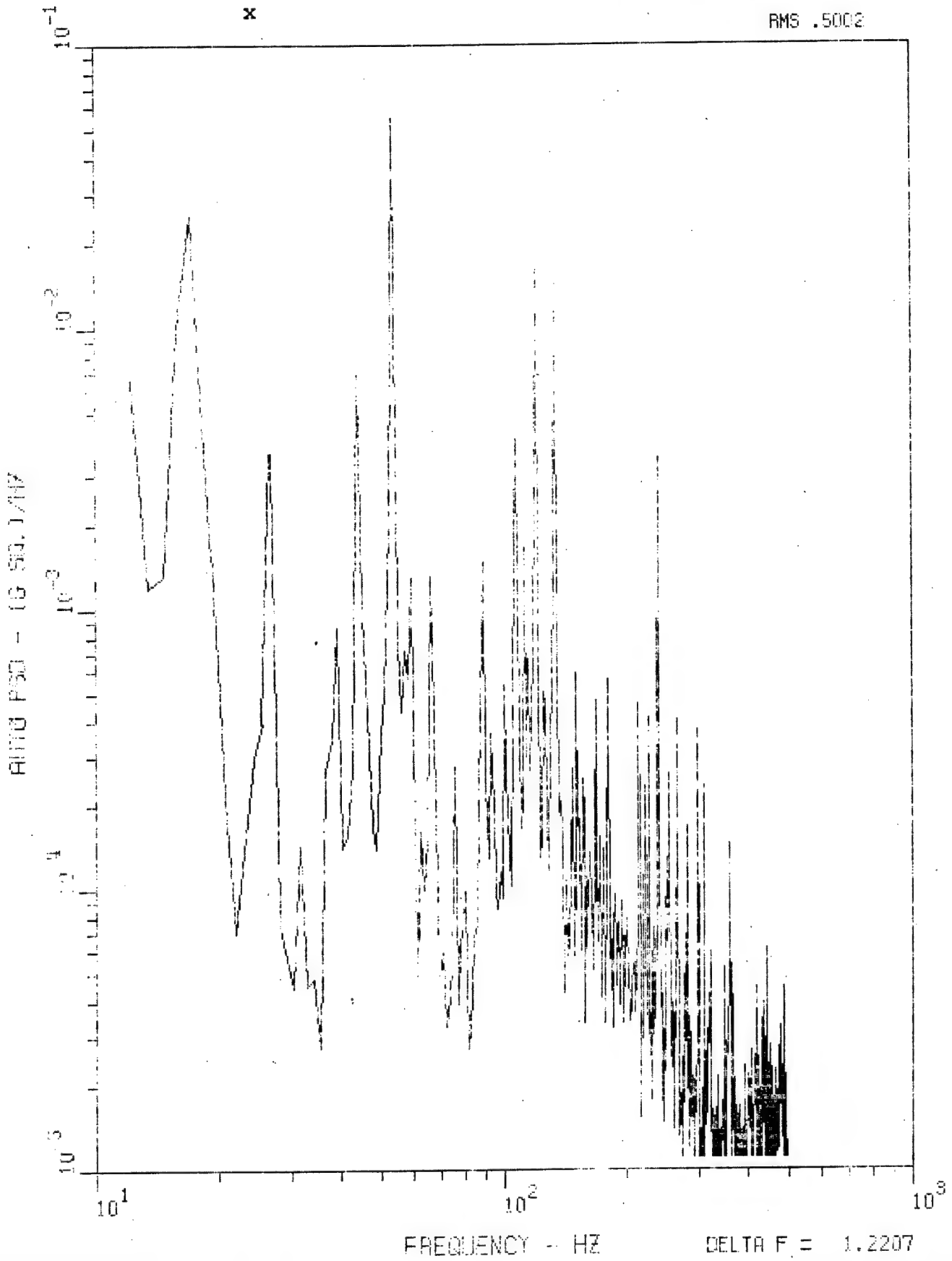


Figure 54. Accelerometer x PSD, 0-500 Hz, Run LWC 23.

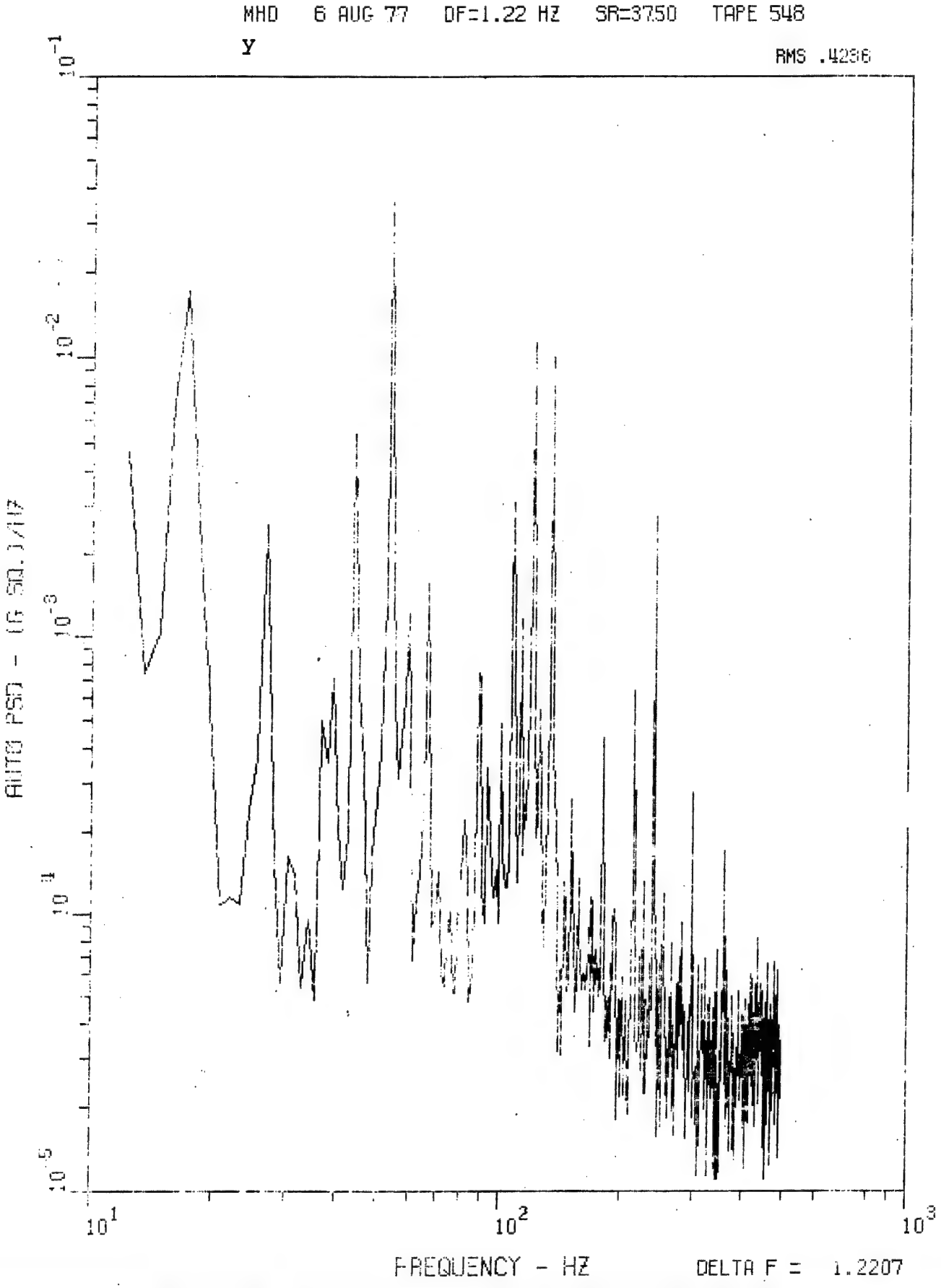


Figure 55. Accelerometer y PSD, 0-500 Hz, Run LWC 23.

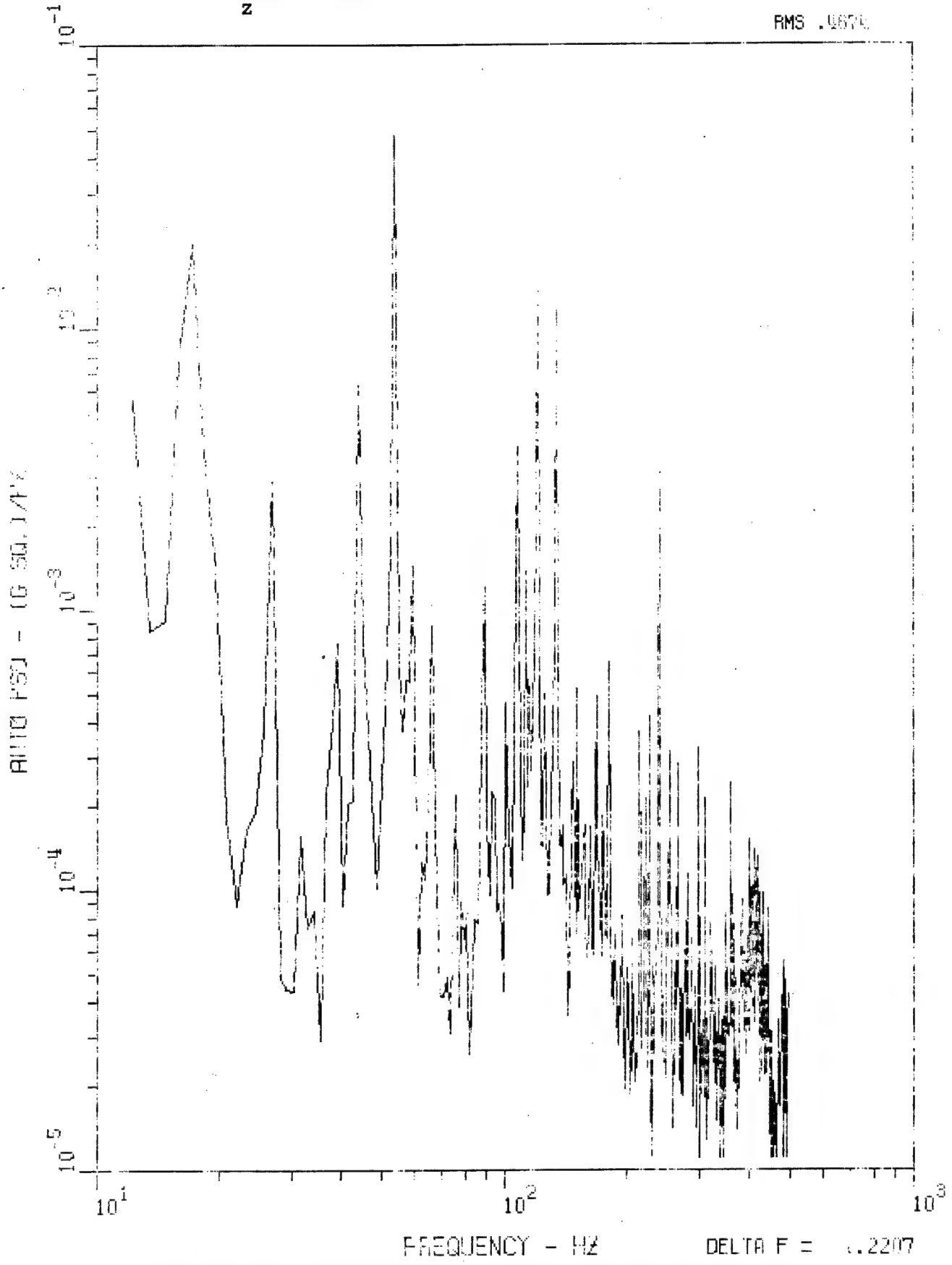


Figure 56. Accelerometer z PSD, 0-500 Hz, Run LWC 23.

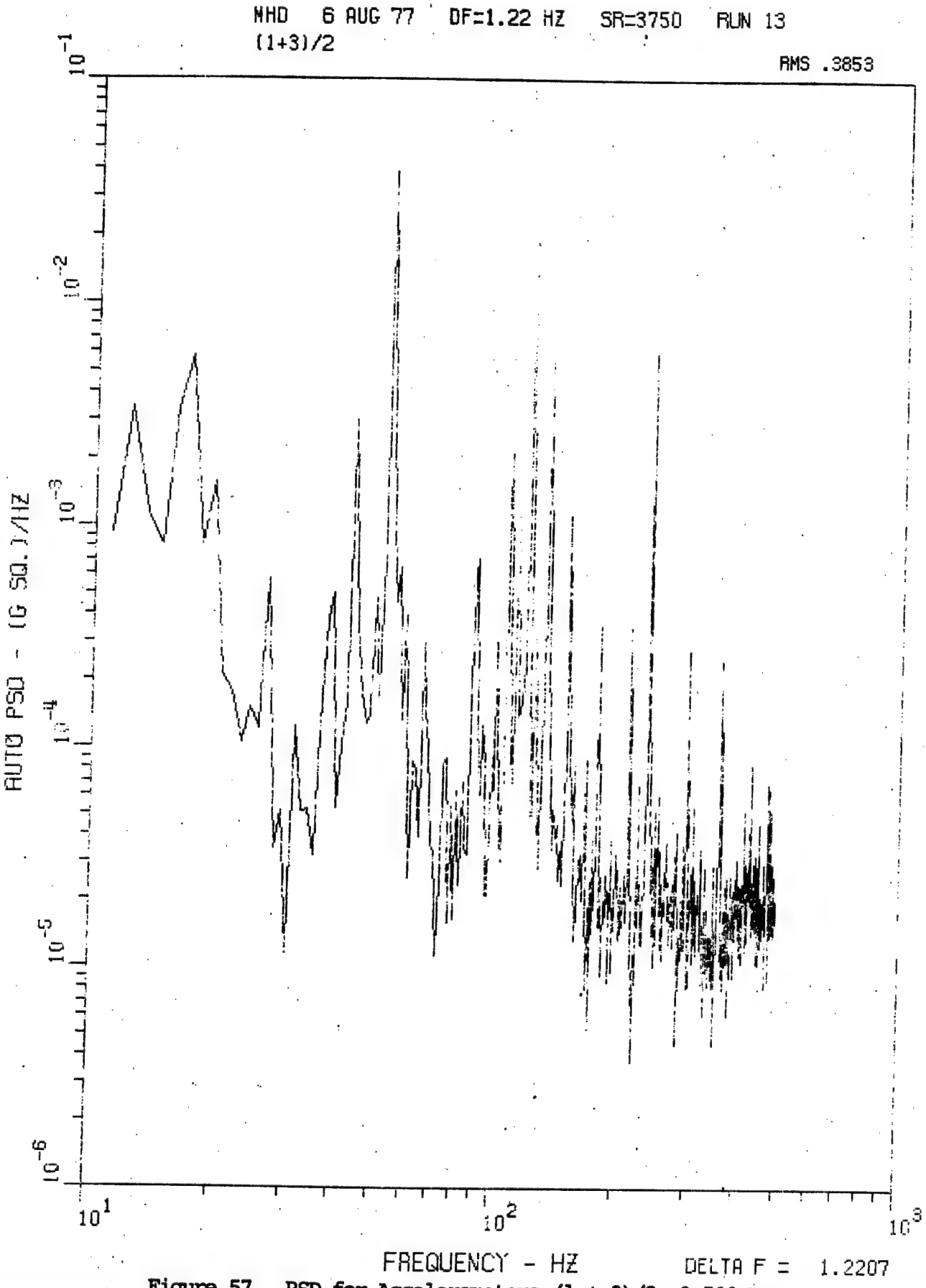


**Figure 57.** PSD for Accelerometers (1 + 3)/2, 0-500 Hz, Run LWC 13.

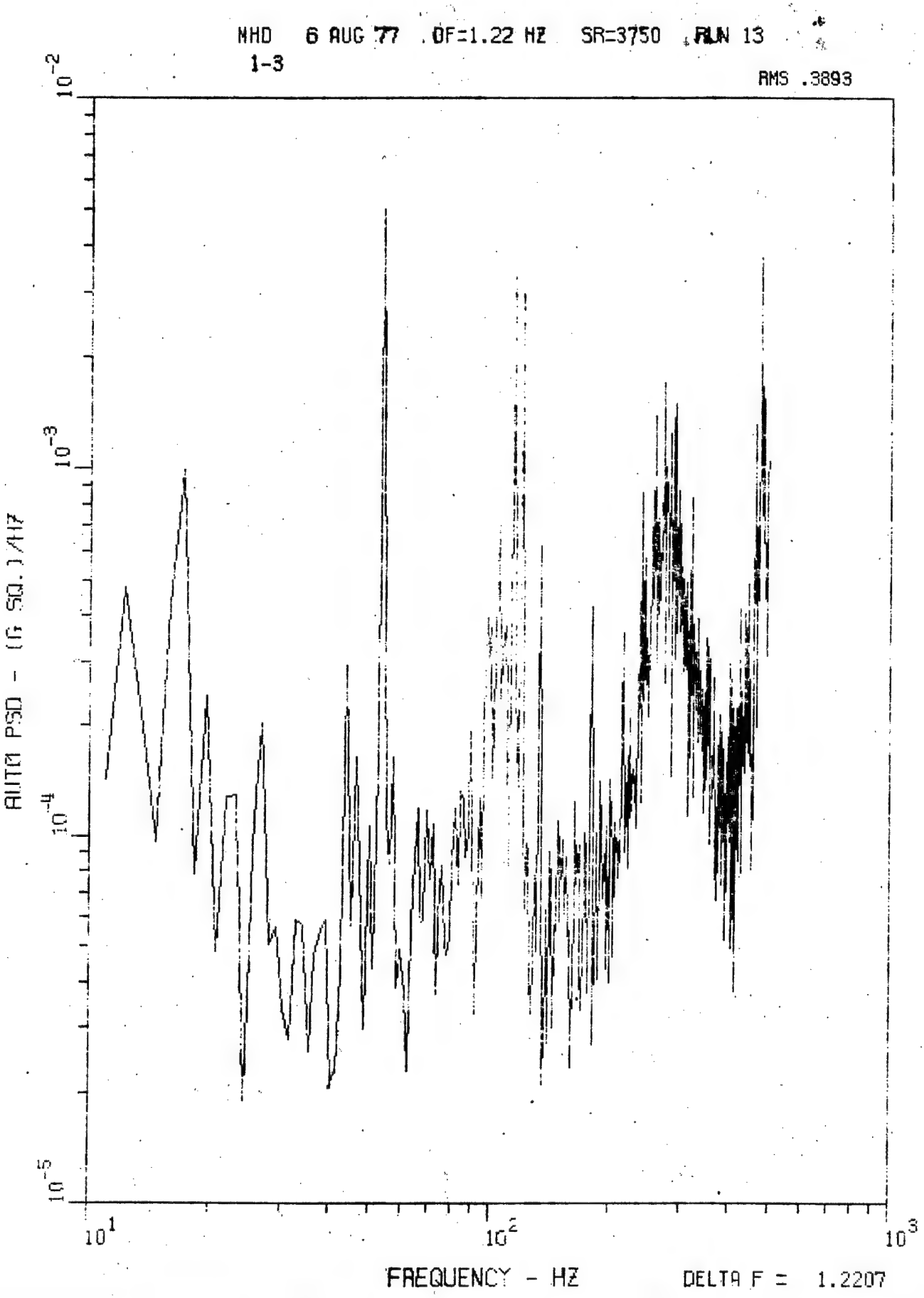


**Figure 58. PSD for Accelerometers 1-3, 0-500 Hz, Run LWC 13.**

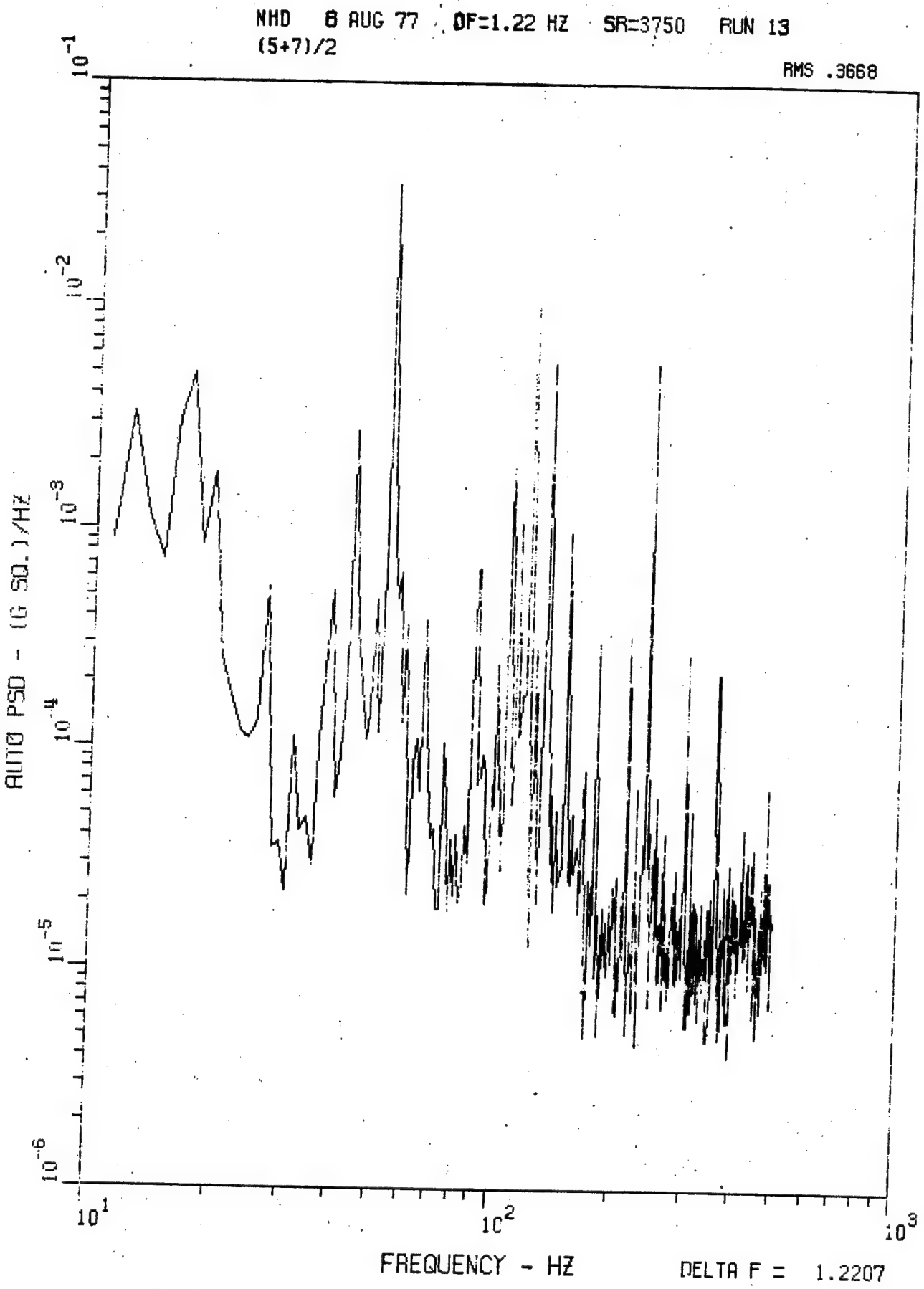


Figure 59. PSD for Accelerometers (5 + 7)/2, 0-500 Hz, Run LWC 13.

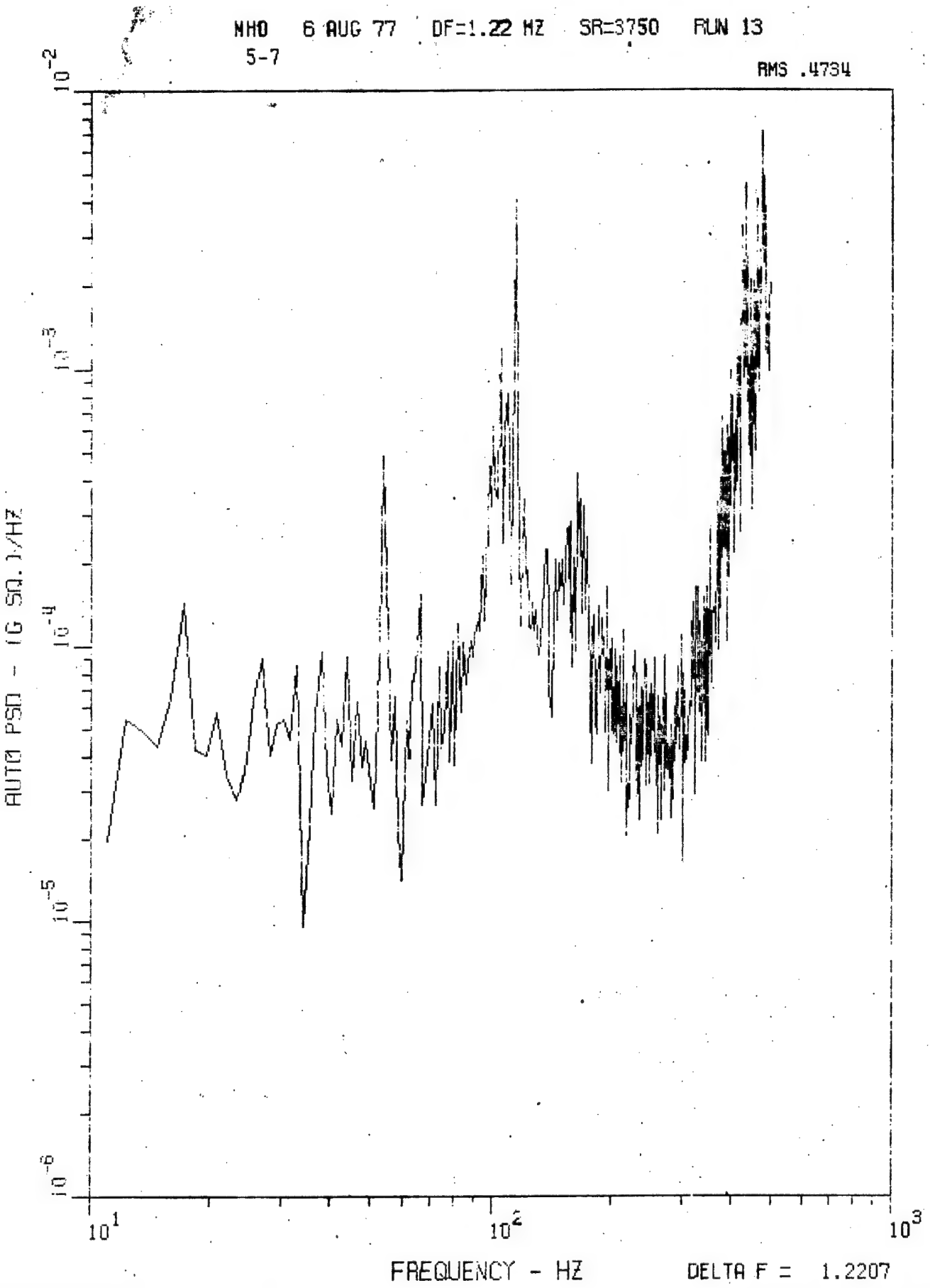


**Figure 60. PSD for Accelerometers 5-7, 0-500 Hz, Run LWC 13.**

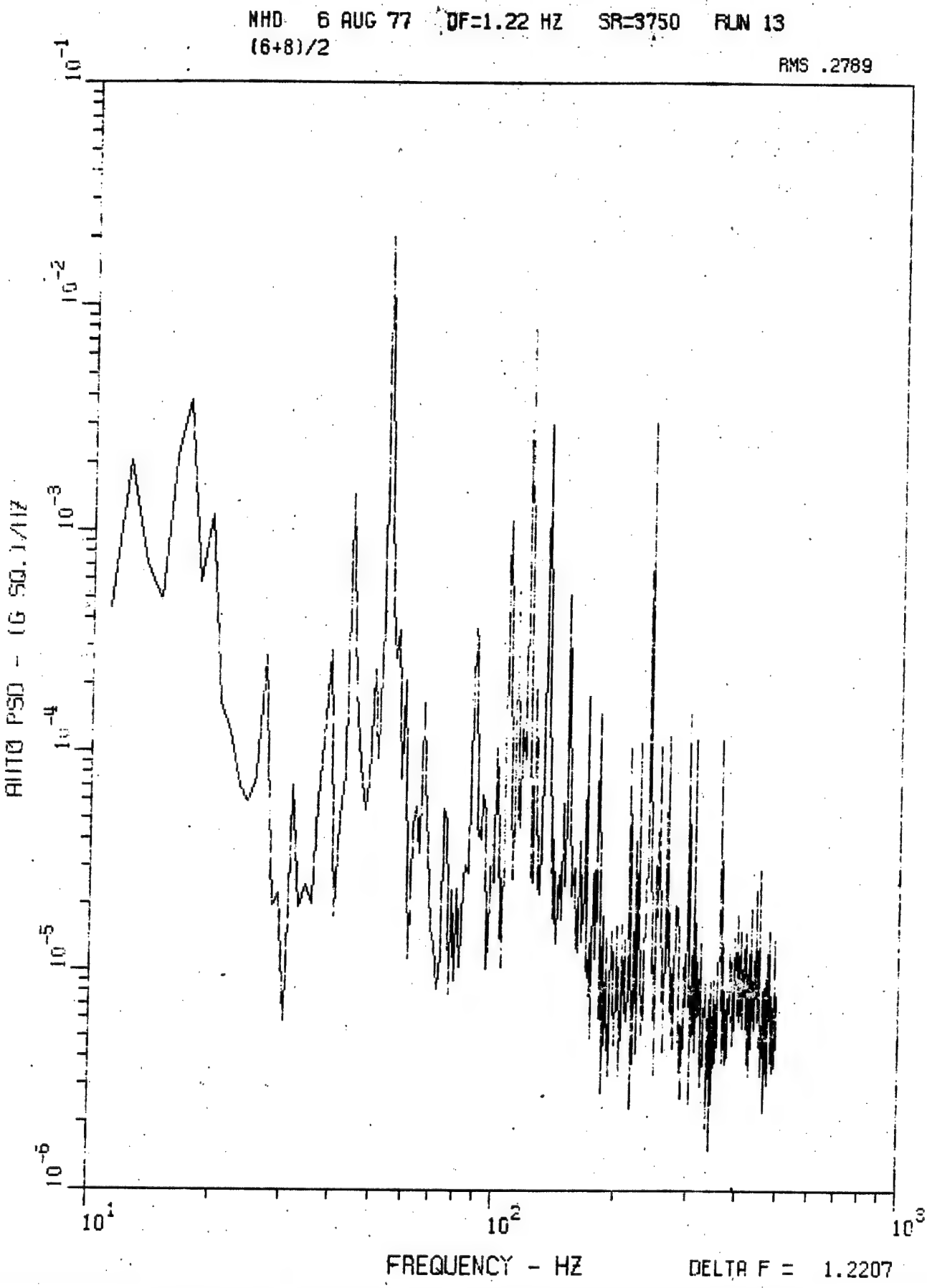


**Figure 61. PSD for Accelerometers (6 + 8)/2, 0-500 Hz, Run LWC 13.**

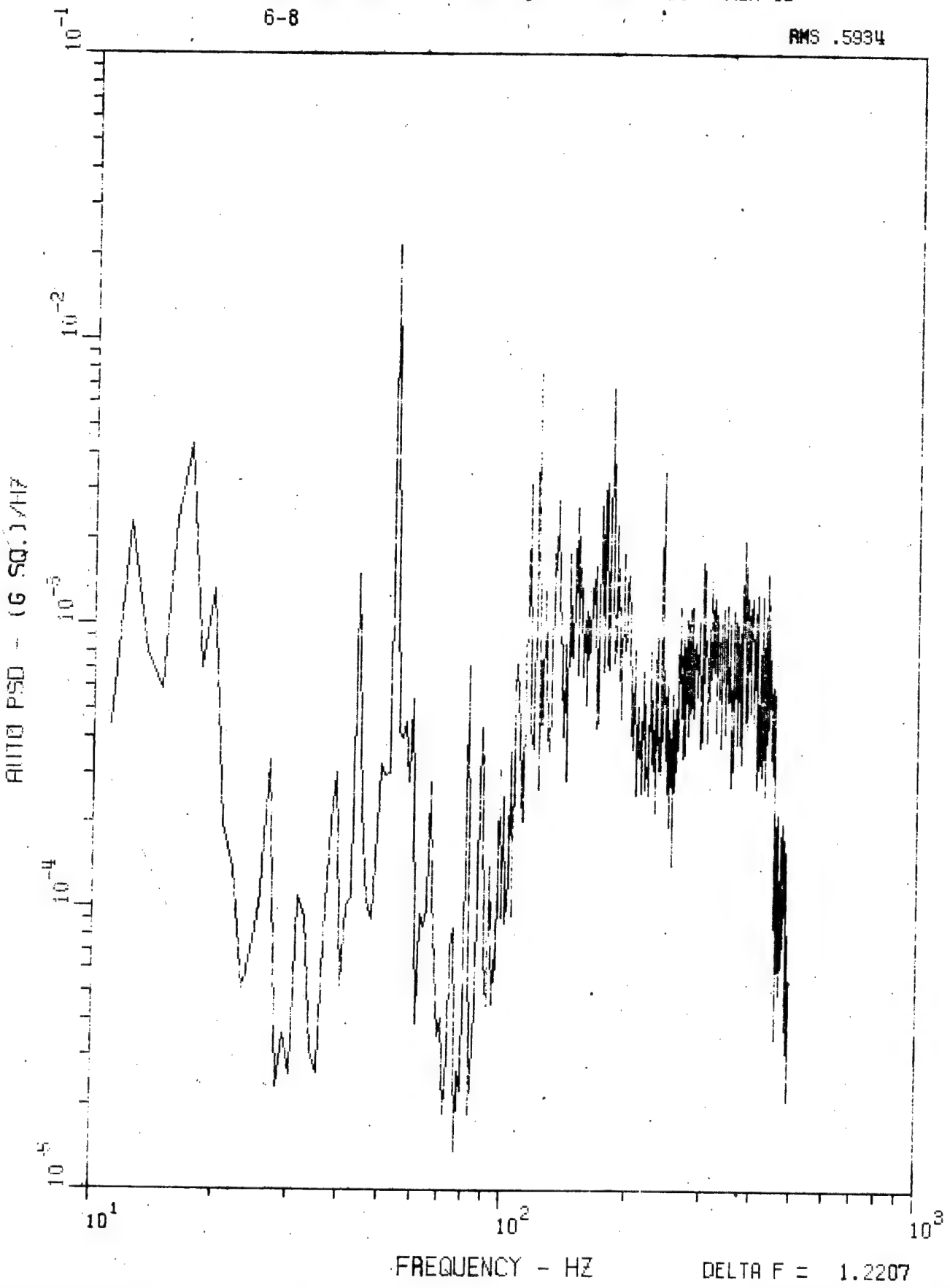


Figure 62. PSD for Accelerometers 6-8, 0-500 Hz, Run LWC 13.

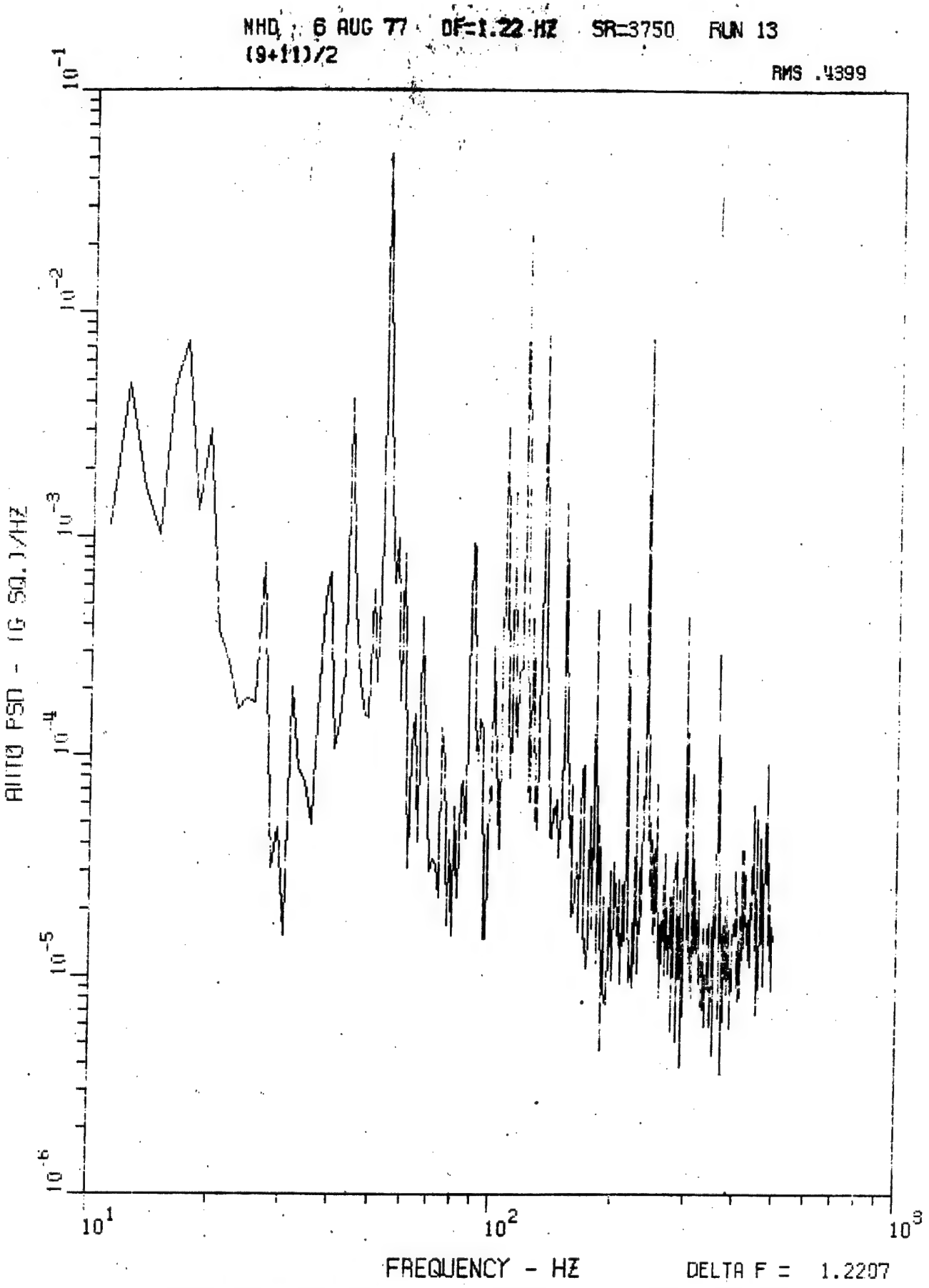


Figure 63. PSD for Accelerometers (9 + 11)/2, 0-500 Hz, Run LWC 13.

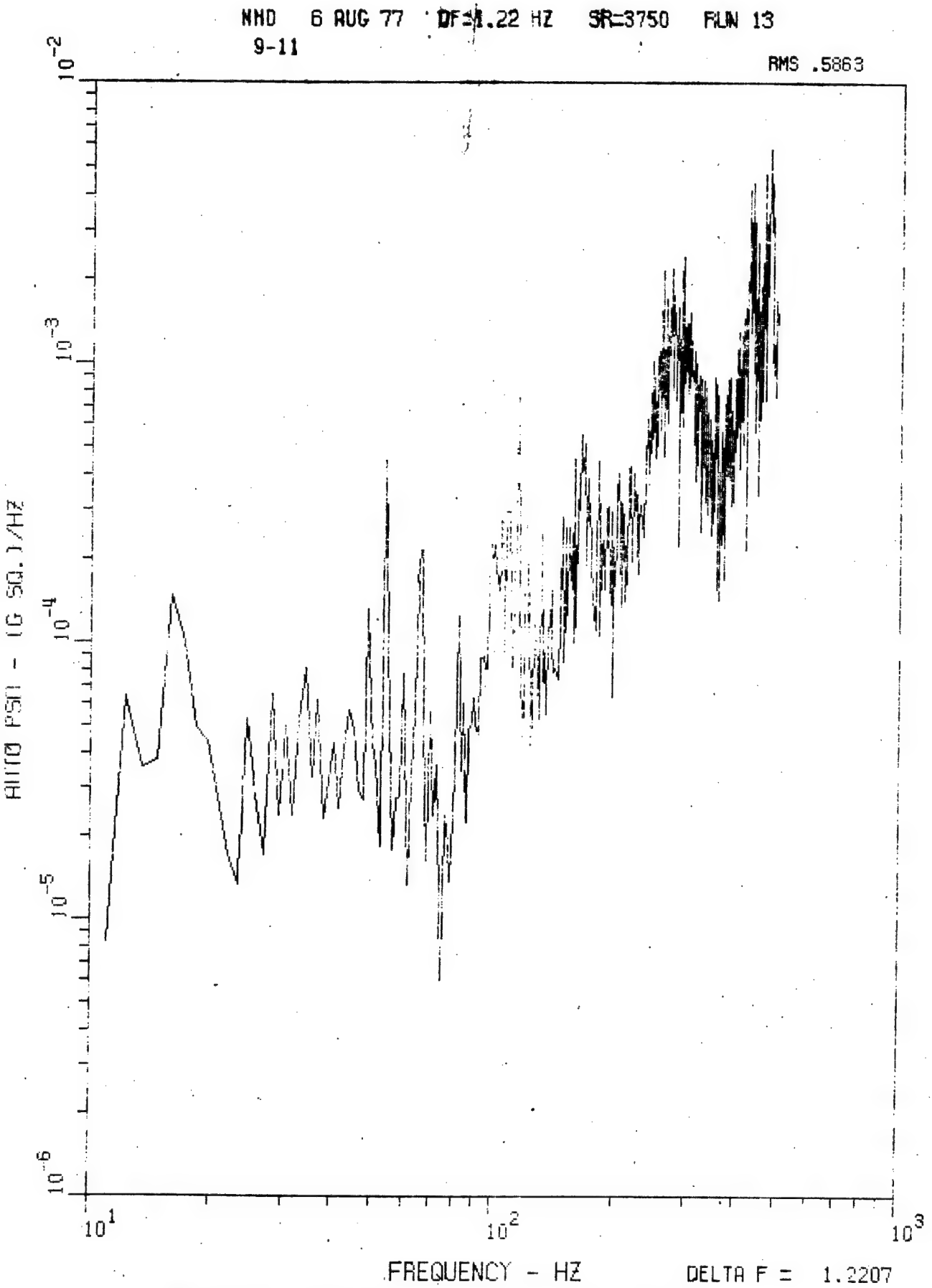


**Figure 64.** PSD for Accelerometers 9-11, 0-500 Hz, Run LWC 13.

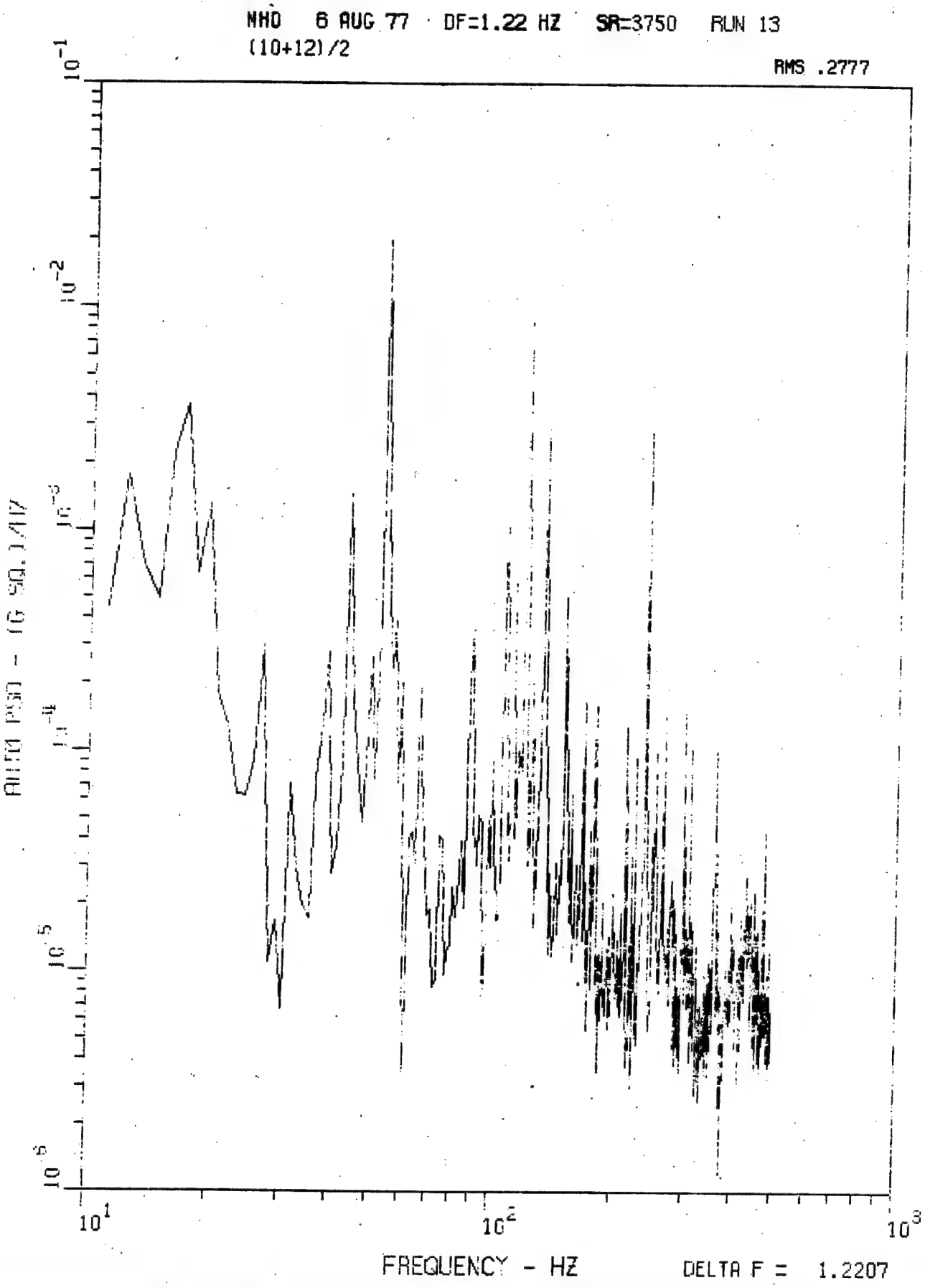


**Figure 65. PSD for Accelerometers (10 + 12)/2, 0–500 Hz, Run LWC 13.**

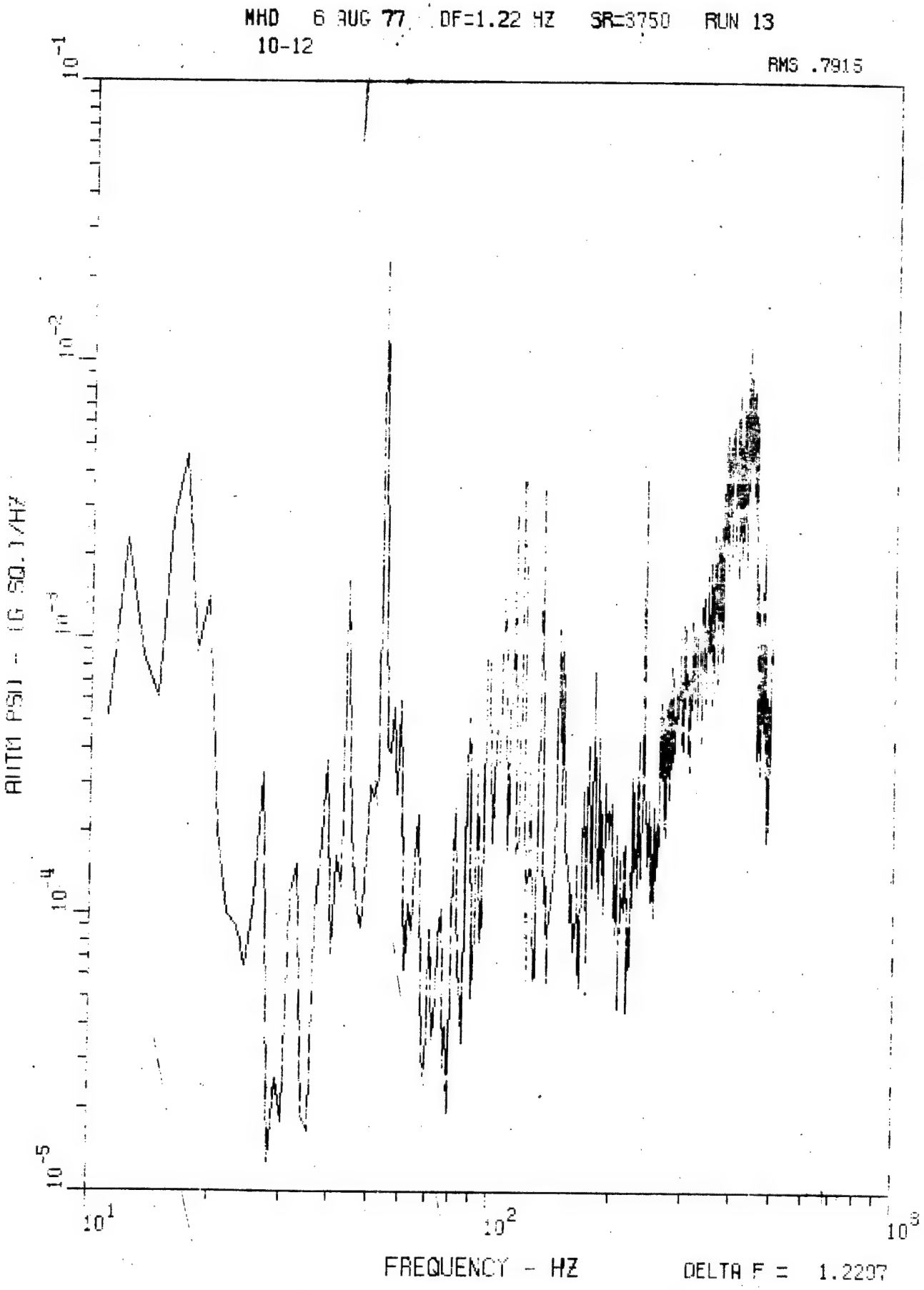


**Figure 66. PSD for Accelerometers 10-12, 0-500 Hz, Run LWC 13.**

a. Pinned-pinned beam

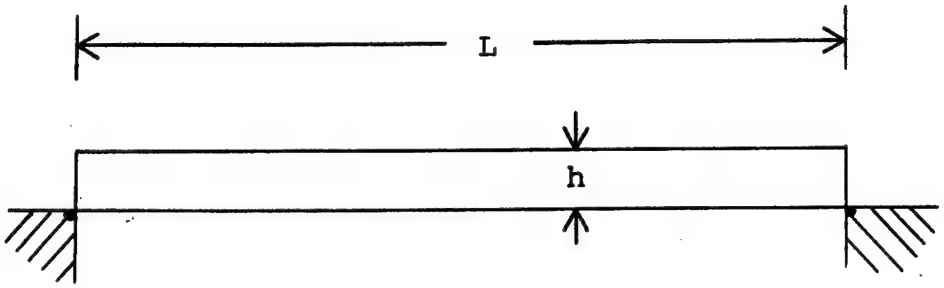


b. Modeshape for $n^{\underline{th}}$ mode

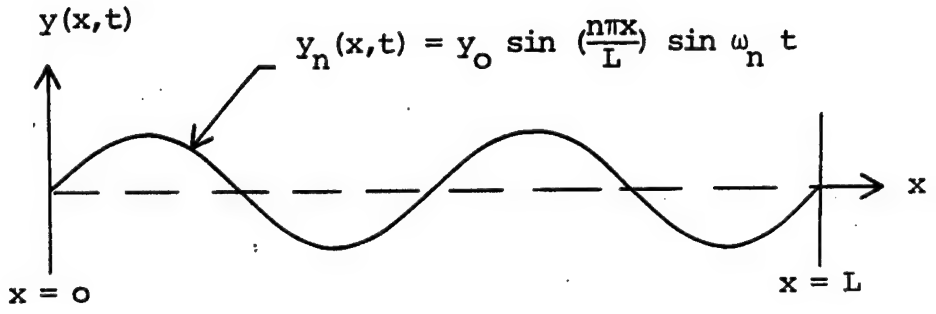


Figure 67. Beam Approximation to MHD Channel Modes.

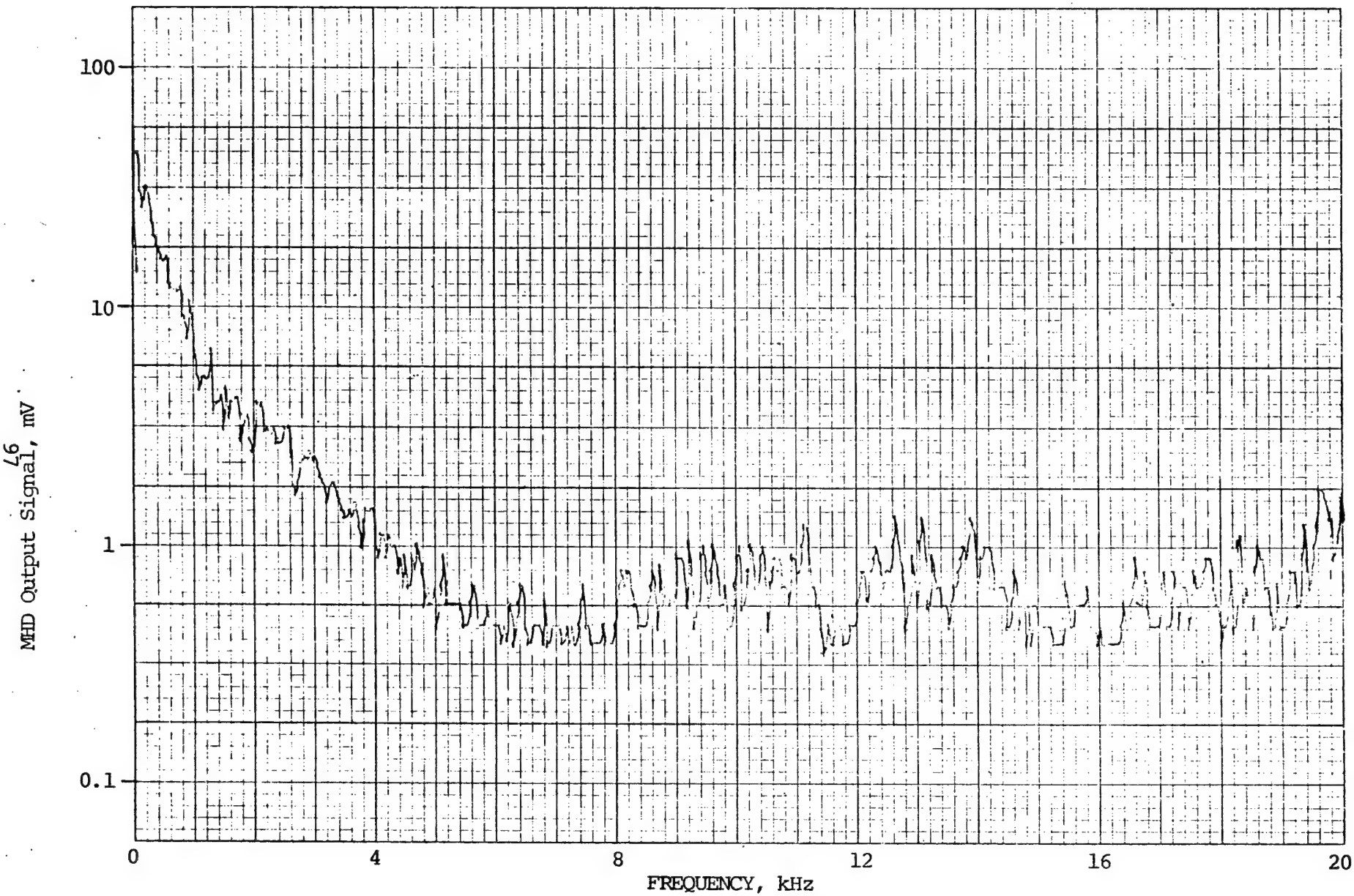


Figure 68. MHD Generator Output Voltage Linear Spectrum, 0-20 kHz.

## APPENDIX C

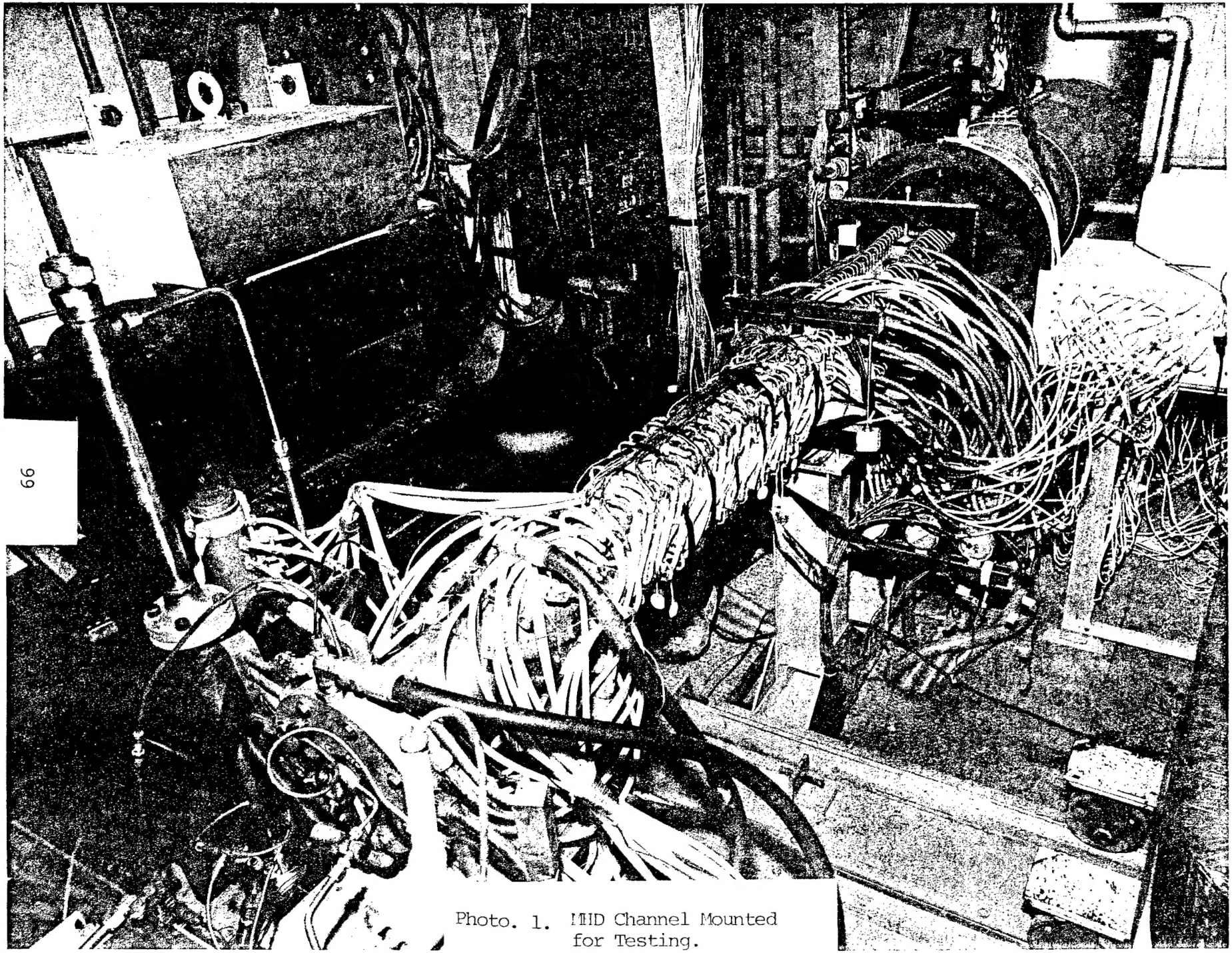

Photo. 1. MHD Channel Mounted for Testing.

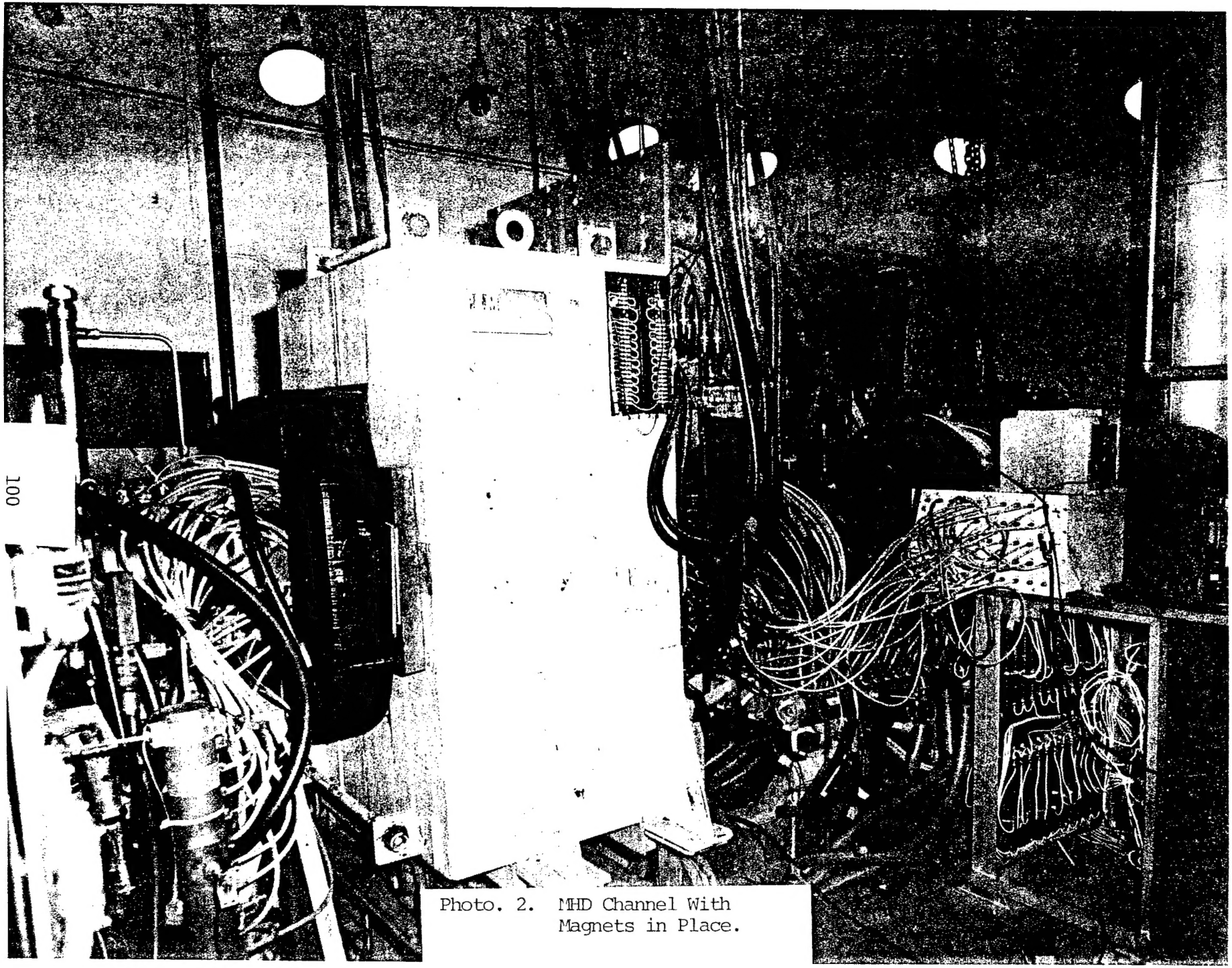

Photo. 2. MHD Channel With Magnets in Place.

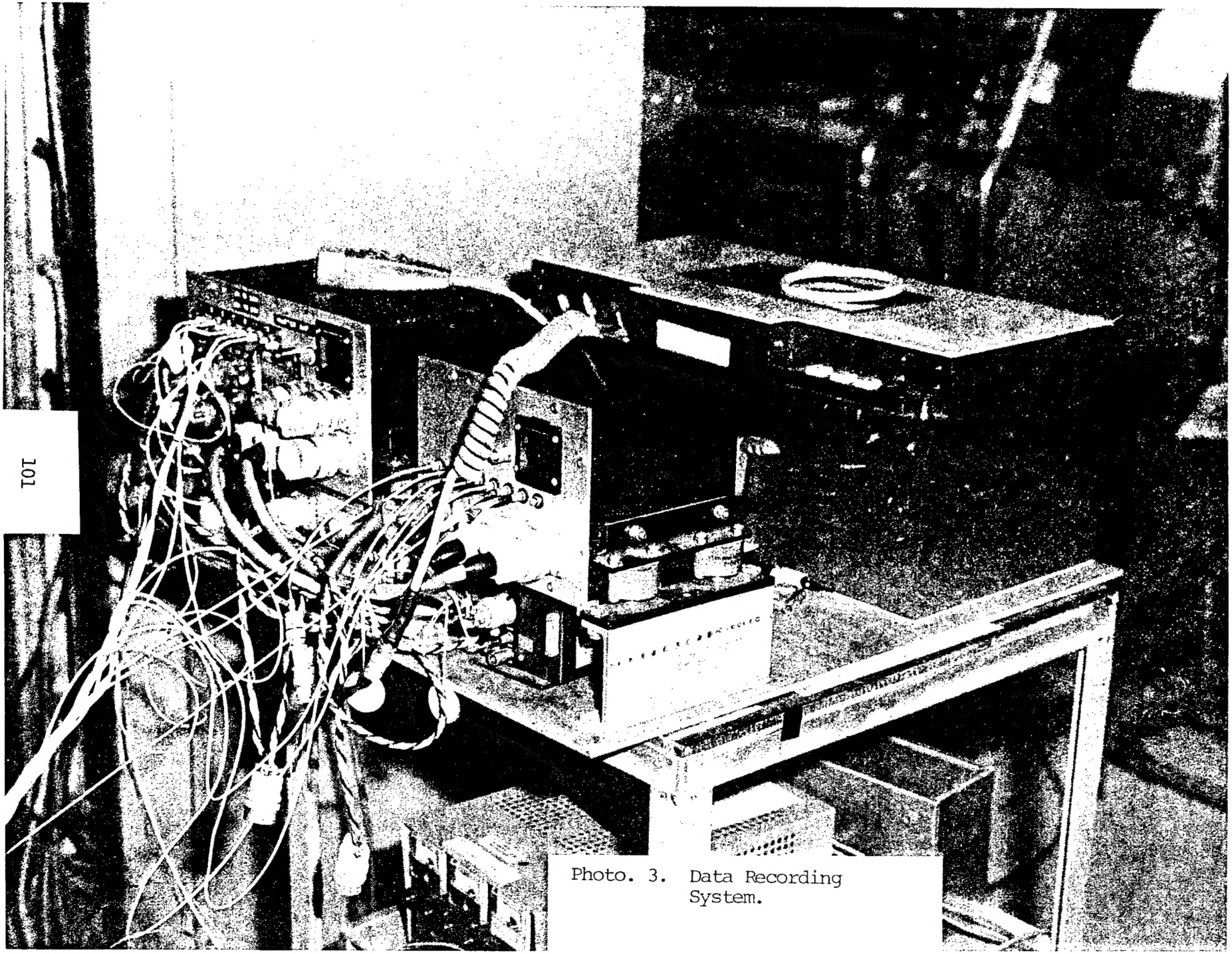

Photo. 3. Data Recording System.